Energie & Umwelt / Energy & Environment
Band / Volume 410
ISBN 978-3-95806-303-7

Mitglied der Helmholtz-Gemeinschaft

JÜLICH Forschungszentrum

Estimate of root water uptake using root dynamics

Energie & Umwelt
Energy & Environment

410

Gaochao Cai

The impact of soil water distribution on root development and root water uptake of winter wheat

Gaochao Cai

Energie & Umwelt / Energy & Environment
Band / Volume 410
ISBN 978-3-95806-303-7

JÜLICH Forschungszentrum

Mitglied der Helmholtz-Gemeinschaft

JÜLICH Forschungszentrum

Schriften des Forschungszentrums Jülich
Reihe Energie & Umwelt / Energy & Environment Band / Volume 410

Forschungszentrum Jülich GmbH
Institut für Bio- und Geowissenschaften
Agrosphäre (IBG-3)

The impact of soil water distribution on root development and root water uptake of winter wheat

Gaochao Cai

Schriften des Forschungszentrums Jülich
Reihe Energie & Umwelt / Energy & Environment — Band / Volume 410

ISSN 1866-1793 — ISBN 978-3-95806-303-7

Bibliografische Information der Deutschen Nationalbibliothek.
Die Deutsche Nationalbibliothek verzeichnet diese Publikation in der Deutschen Nationalbibliografie; detaillierte Bibliografische Daten sind im Internet über http://dnb.d-nb.de abrufbar.

Herausgeber und Vertrieb: Forschungszentrum Jülich GmbH
Zentralbibliothek, Verlag
52425 Jülich
Tel.: +49 2461 61-5368
Fax: +49 2461 61-6103
zb-publikation@fz-juelich.de
www.fz-juelich.de/zb

Umschlaggestaltung: Grafische Medien, Forschungszentrum Jülich GmbH

Druck: Grafische Medien, Forschungszentrum Jülich GmbH

Schriften des Forschungszentrums Jülich
Reihe Energie & Umwelt / Energy & Environment, Band / Volume 410

D 5 (Diss., Bonn, Univ., 2018)

ISSN 1866-1793
ISBN 978-3-95806-303-7

Vollständig frei verfügbar über das Publikationsportal des Forschungszentrums Jülich (JuSER) unter www.fz-juelich.de/zb/openaccess.

Summary

Background and objectives: Root water uptake (RWU) is a key process in the root zone that determines water movement from the soil into roots and transport to the atmosphere via plant stems and leaves. Different RWU models were developed with different assumptions, complexity, and parameters but the description of this process and its parameterization remain challenging in soil hydrology. Due to the difficulty of monitoring of root development and soil states in undisturbed soils, dynamic root distributions and a physically based concept to describe water uptake from soil profiles with vertical variations in soil water availability are often not taken into consideration. Furthermore, the simulated RWU is rarely evaluated by transpiration measurements for different soil water conditions and soil textures. This study aims at 1) introducing two minirhizotron (MR) facilities installed in two different soils with different water treatments that were designed for monitoring dynamic root distribution and spatio-temporal soil state variations *in situ*, 2) parameterizing three RWU models that use different concepts to describe water uptake and investigating the difference in water uptake patterns and the possible links between them, 3) exploring the effect of soil water availability on root development and RWU that were estimated by different RWU models, and evaluating the estimated RWU by measured sap flow data. Although the model approaches and experimental methods are generic and applicable to different crops, only winter wheat was considered in this study.

Methods and materials: Two MR facilities were constructed in two different soils (stony vs. silty) to monitor root growth, root zone processes, and their dependence on soil water availability. Each of the facilities was established with three subplots: sheltered, rainfed, and irrigated. Root dynamics were observed in 7-m-long rhizotubes that were installed horizontally at 10, 20, 40, 60, 80, and 120 cm depth. Time domain reflectometer (TDR) probes, tensiometers, and matrix water potential sensors were installed at the same depths of the rhizotubes to monitor soil moisture, water potential, and soil temperature. The measurements served as input for inversely estimating soil and root-system related parameters of three RWU models: Feddes (without compensation), Feddes-Jarvis (with compensation), and Couvreur (physically based model with compensation) that have been implemented in Hydrus-1D. Sap flow was monitored in the same field for the comparison with simulated RWU.

Results and conclusions: Measurements in the rhizotron facilities demonstrated that soil water content, root density, and crop biomass of winter wheat were higher in the silty than in the stony soil, in which plant and root growth were obviously affected by water treatments and soil types.

Using the data from the sheltered plot of the stony soil, the Feddes, Feddes-Jarvis, and Couvreur models predicted soil moisture equally well and the soil hydraulic parameters optimized by the models with compensation were comparable. The obtained RWU parameters of the Feddes-Jarvis models and root hydraulic parameters for winter wheat were consistent with data reported in the literature. There was no obvious difference between the models in simulated total RWU and other water fluxes. The Feddes-Jarvis and the Couvreur models simulated similar root-system scale stress functions that link total RWU to the effective root zone water potential. The root-system related parameters of the Couvreur model could be constrained but not those of the Feddes-Jarvis model. Simulated RWU profiles differed due to different water redistribution by the root system. But, the impact of these different RWU profiles on soil moisture and soil water potentials was too small to be detected by the sensors.

When broadening the model parameterization and simulations to the different soils and water treatments, the soil hydraulic parameters could be well identified by both the Feddes-Jarvis and Couvreur models. Patterns of crop and root development differed in the plots of the two soil types, which resulted in different RWU due to different soil water availability. The two models simulated similar RWU which was the lowest in the sheltered plot of the stony soil where RWU was also lower than the potential RWU. In the silty soil, RWU was equal to the potential uptake for all treatments. The variation of simulated RWU between the different plots agreed well with measured sap flow. The Couvreur model, which links the relation between maximal RWU and soil water potential to the hydraulic conductance of the root system, which is in turn related to the root density, predicted the ratios of the transpiration fluxes in the two soil types slightly better than the Feddes-Jarvis model. Simulations with the Couvreur model using root system conductances that were observed for a different water treatment and soil indicated that the root system conductance of the plant was adjusted to the soil and water treatment. There was a constant offset between the simulated RWU and the sap flow, which requires further investigation.

Zusammenfasung

Hintergrund und Zielstellung: die Wasseraufnahme von Wurzeln ist ein bedeutender Prozess in der Wurzelzone und kontrolliert den Wassertransport vom Boden in die Wurzeln und von dort über die Leitbündel und Blätter der Pflanze in die Atmosphäre. Es existieren verschiedene mathematische Modelle zur Beschreibung der Wasseraufnahme von Wurzeln, welche sich in ihren Prämissen, ihrer Komplexität und ihren Parameter unterscheiden; dennoch sind die Beschreibung und die Parametrisierung dieses Prozesses nach wie vor eine Herausforderung in der Bodenhydrologie. Auf Grund der Schwierigkeit, die Entwicklung von Wurzeln in ungestörtem Boden zu messen und nachzuvollziehen, werden dynamische Wurzelverteilungen und physikalisch basierte Konzept zur Beschreibung von Wasseraufnahme durch Wurzeln in Bodenprofilen mit vertikal heterogener Wasserverfügbarkeit häufig nicht beachtet. Des Weiteren wurden simulierte Wasseraufnahmen von Wurzeln nur selten mit Transpirationsmessungen unter verschiedenen Bodenwasserbedingungen und Bodentexturen ausgewertet und verglichen. Die vorliegende Studie hat zum Ziel 1) eine Einführung über zwei Minirhizotron (MR) Anlagen zu geben, welche in zwei verschiedenen Böden mit unterschiedlichen Bewässerungspraktiken installiert wurden und konzipiert wurden, um dynamische Wurzelentwicklung und räumlich-zeitliche Bodenzustandsänderungen in situ erfassen zu können, 2) drei Modelle zur Wasseraufnahme von Wurzeln zu parametrisieren, welche sich in ihren Konzepten zur Beschreibung der Wasseraufnahme unterscheiden, um die Unterschiede in den Mustern der Wasseraufnahme und möglichen Verbindungen zwischen denen herauszufinden, 3) den Effekt von Bodenwasserverfügbarkeit auf die Wurzelentwicklung zu untersuchen und die abgeschätzte Quantität der Wasseraufnahme mit Hilfe von Xylemflussmesswerten zu bewerten. Obwohl die Modellansätze und die experimentellen Methoden allgemeingültig und anwendbar auf verschiedene Pflanzen sind, wurde in dieser Studie nur Winterweizen betrachtet.

Methoden und Materialien: zwei MR Anlagen wurden auf zwei unterschiedlichen Böden (der eine steinig, der andere schluffig) konstruiert, um das Wurzelwachstum und andere Prozesse in der Wurzelzone und deren Abhängigkeit von der Bodenwasserverfügbarkeit zu beobachten. Beide Anlagen wurden in drei Areale eingeteilt: eines abgedeckt, eines beregnet und das dritte

bewässert. Die Wurzeldynamiken wurden in sieben Meter langen Plexiglasröhren, welche horizontal in den Tiefen 10, 20, 40, 60, 80 und 120 cm installiert wurden, nachverfolgt.

Um die Bodenfeuchte, das Wasserpotential und die Bodentemperatur nachverfolgen zu können, wurden Zeitbereichsreflektometer (engl.: time domain reflecometer, TDR), Tensiometer und Sensoren für das Matrixpotential in denselben Tiefen wie die Plexiglasröhren eingesetzt. Die Messungen dienten als Input für die Schätzung der von Boden- und Wurzelsystem abhängigen Parameter von drei Modellen zur Wasseraufnahme von Wurzeln: Feddes (ohne Kompensierung), Feddes-Jarvis (mit Kompensierung) und Couvreur (physikalisch basiertes Modell mit Kompensierung), welche in Hydrus-1D implementiert wurden. Xylemflussmessungen wurden auf dem gleichen Feld durchgeführt, um diese mit den simulierten Wasseraufnahmeraten vergleichen zu können.

Ergebnisse und Schlussfolgerungen: mit den Messungen in den Rhizotron-Anlagen konnte gezeigt werden, dass Bodenwassergehalt, Wurzeldichte und Pflanzenbiomasse von Winterweizen auf dem schluffigen Boden höher waren als auf dem steinigen, auf welchem das Pflanzen- und Wurzelwachstum beeinflusst wurden durch die Bewässerungshandhabung.

Betrachtet man die Daten des bedachten Areals in der Anlage mit dem steinigen Boden, dann prognostizieren die Modelle von Feddes, Feddes-Jarvis und Couvreur die Bodenfeuchte gleich gut und auch die bodenhydraulischen Parameter optimiert durch die Modelle waren vergleichbar. Die Parameter für die Wurzelwasseraufnahme des Feddes-Jarvis Models und die wurzelhydrologischen Parameter für den Winterweizen waren übereinstimmend mit Literaturdaten. Es gab keinen eindeutigen Unterschied zwischen den Modellen bezüglich der simulierten gesamten Wasseraufnahme durch Wurzeln und anderen Wasserflüssen. Mit den Modellen von Feddes-Jarvis und Couvreur konnten vergleichbare Stressfunktionen auf Skala des Wurzelsystems simuliert werden, welche die gesamte Wasseraufnahme durch Wurzeln mit dem Wasserpotential der effektiven Wurzelzone koppeln. Die Wurzelsystem-abhängigen Parameter des Couvreur Modells konnten belegt werden, die des Feddes-Jarvis Modells nicht. Die simulierten Profile der Wasseraufnahme durch Wurzeln unterschieden sich auf Grund der unterschiedlichen Wasser-Umverteilung durch das Wurzelsystem. Jedoch war der Einfluss dieser

Unterschiede zwischen den Wasseraufnahme-Profilen auf die Bodenfeuchte und das Matrixpotential zu gering, um von den Bodensensoren erfasst zu werden.

Wenn die Modell Parametrisierung und die Simulationen auf verschiedene Böden und Bewässerungstechniken ausgeweitet wurden, konnten die Bodenhydrologischen Parameter gut mit sowohl dem Feddis-Jarvis Modell als auch mit dem Couvreur Modell identifiziert werden. Die Muster in der Pflanzen- und Wurzelentwicklung unterschieden sich zwischen den Arealen der beiden Bodentypen, was zu unterschiedlichen Raten der Wasseraufnahme bedingt durch verschiedene Bodenwasserverfügbarkeiten führte. Beide Modelle simulierten ähnliche Raten der Wasseraufnahme, welche am niedrigsten für das bedachte Areal im steinigen Boden war, wo die Wasseraufnahme der Wurzeln niedriger war als die potentielle Wasseraufnahme. In dem schluffigen Boden waren die Raten der Wasseraufnahme gleich der potentiellen Aufnahme in allen drei Arealen mit unterschiedlicher Bewässerungstechnik. Die Variationen der simulierten Wasseraufnahmen zwischen den unterschiedlichen Arealen stimmten mit den Xylemflussmessungen überein. Das Couvreur Modell, welches das Verhältnis zwischen der maximalen Wasseraufnahme und dem Bodenwasserpotential mit der hydraulischen Leitfähigkeit des Wurzelsystems verbindet, welches wiederum an die Wurzeldichte gekoppelt ist, prognostizierte die Raten der Trabspirationsflüsse in beiden Bodentypen ein wenig besser als das Feddes-Jarvis Modell. Die Simulationen mit dem Couvreur Modell, bei welchen die Leitfähigkeiten des Wurzelsystems genutzt wurden, welche für unterschiedliche Bewässerungstechniken und Bodenarten beobachtet wurden, zeigten, dass die Leitfähigkeit des Wurzelsystems an den Bodentyp und die Bewässerungstechnik angepasst waren. Ein konstanter Zeitabstand zwischen simulierten Wasseraufnahmeraten und Xylemfluss benötigt weitere Untersuchungen.

Contents

List of Acronyms

C	Couvreur model
CRIM	complex refraction index model
EC	eddy covariance
EMI	electromagnetic induction
ET	evapotranspiration
FJ	Feddes-Jarvis model
GA	genetic algorithm
GPR	ground-penetrating radar
LAI	leaf area index
ME	mean bias error
MPS	matrix water potential sensor
MR	minirhizotron
MRI	magnetic resonance imaging
NRLD	normalized root length density
OF	objective functions
RLD	root length density
RMSE	root mean square error
RWU	root water uptake
SEM	standard error of the sample mean
SWC	soil water content
SWP	soil water pressure head
TDR	time domain reflectometer
ZOP	zero-offset profile

List of symbols

d	index of agreement	-
ET_o	reference evapotranspiration	LT^{-1}
ET_{pot}	potential evapotranspiration	LT^{-1}
h	soil water pressure head	L
h_1	anaerobiosis point	L
h_{3h}	soil water pressure head for high potential transpiration rate	L
h_{3l}	soil water pressure head for lower potential transpiration rate	L
h_4	wilting point	L
h_T	total soil hydraulic head	L
h_{Te}	effective root zone hydraulic head	L
h_{Tleaf}	leaf water hydraulic head	L
h_{Tleaf_crit}	critical leaf hydraulic head	L
k	extinction coefficient	-
K_c	crop coefficient	-
K_{comp}	compensatory RWU conductance of the plant	T^{-1}
K_{rs}	equivalent conductance of the root system	T^{-1}
K_s	saturated conductivity	LT^{-1}
l	empirical model parameter	-
l_z	rooting depth	L
m	empirical model parameter	-
n	a measure of the pore-size distribution	-
S	sink term	$L^3L^{-3}T^{-1}$
S_c	sink term in the Courvreur model	$L^3L^{-3}T^{-1}$
S_e	relative saturation	-
S_{FJ}	sink term in the Feddes-Jarvis model	$L^3L^{-3}T^{-1}$
t	time	T
T_{3h}	high transpiration rate	LT^{-1}
T_{3l}	low transpiration rate	LT^{-1}
T_{act}	actual transpiration (= root water uptake)	LT^{-1}

T_{pot}	potential transpiration	LT^{-1}
z	elevation	L
θ	volumetric soil water content	L^3L^{-3}
θ_r	residual water content	L^3L^{-3}
θ_s	saturated water contents	L^3L^{-3}
α	related to the inverse of the air entry suction	L^{-1}
α_F	water stress response function	-
ω	plant water stress index	-
ω_c	critical water stress threshold	-
γ	compensatory factor	-

List of Tables

List of Figures

Chapter 1

General Introduction and objectives

Feeding more people with limited water is getting more and more challenging since most of the population increase in the following years will be in regions with water scarcity (Borrell et al., 2014; Haub and Kaneda, 2013; Ray et al., 2013; Water, 2012). Because water is an important limiting factor for plant growth (Rost et al., 2008) enhancing the irrigation and crop water use efficiency is one of the important strategies to improve crop yield per unit area (Assouline et al., 2015). Crop yield is highly sensitive to both climatic and soil environmental variations (Brown and Rosenberg, 1997; He et al., 2016; Letey, 1958; Porter and Semenov, 2005; Roncucci et al., 2015). Quantifying root water uptake (RWU) is of great importance to understand water flow in the soil-plant-atmosphere (SPA) system and design efficient irrigation and cultivation practices for yield production for different climate and soil water conditions (Coelho and Or, 1999; Liao et al., 2016). RWU is an important process of the hydrological cycle, transporting water from soil towards into root system of plant and transpiring into the atmosphere. This process does not only bring water for root and plant growth but also determines the transport of nutrients for biochemical reactions.

1.1 Measurement and modeling of root development and root distribution

Plants take up water by their root system and variation in RWU between species and different environmental conditions are related to differences in the root system of different species and on how root systems respond or adapt to environmental conditions. For a given plant, root distribution and development are influenced by climate conditions, soil moisture, soil texture, and nutrient status (Denmead and Shaw, 1962; Jones, 1983; López-Bucio et al., 2003). So as to represent the interactions between root development and soil water status in water uptake process, the dynamics of root distributions need to be properly accounted for (Krounbi and Lazarovitch, 2011; Vereecken et al., 2015). However, root growth and root distribution were simplified in most RWU models, using either a logistic or an empirical growth function (Borg and Grimes, 1986; Hoffman and Van Genuchten, 1983; Šimůnek and Suarez, 1993). They have the advantages of using fewer parameters and being easier to apply in water uptake simulation at large scale. However, when looking at the water uptake at a small scale, for instance, at root system or plant scale, spatial configuration of a root system and the corresponding growth regulation need to be described with more parameters. Complex root architecture models have

been described that explicitly describe root growth and distribution, for instance, RootTyp (Pagès et al., 2004), RootBox (Leitner et al., 2010), ArchiSimple (Pagès et al., 2012), R-SWMS (Javaux et al., 2008), and aRoot (Schneider et al., 2010). All these models simulate root dynamics in 3-D based on different principles and the latter two root models were able to model water transport between soil and root. However, the model complexity, the need for a large number of parameters, and high computational demands make them not easy to apply widespread. Furthermore, the models were described at a single plant scale and not applied for field or region level.

Destructive measurements

A few studies used measured root distribution to simulate RWU but root growth was often not considered (Albasha et al., 2015; De Jong Van Lier et al., 2008). Dynamic root development and distribution from measurements were not often considered in RWU modeling as a result of the difficulty to obtain the continuous information of the "hidden half". Due to the invisibility and inaccessibility, particular techniques, therefore, are required to investigate the development, distribution, and turnover of roots. Soil coring (Fehrenbacher and Alexander, 1955; Schroth and Kolbe, 1994), framed monolith (Weaver and Voigt, 1950), ingrowth core (Raich et al., 1994; Smith et al., 2005), and trench profile (van Noordwijk et al., 2000; Vepraskas and Hoyt, 1988) were traditional methods to acquire accurate estimation of root length density, examine the effect of soil moisture and nutrient on root development and spatial patterns of root distribution. These approaches show precise estimations of roots but have common disadvantages that are either time-consuming or labor-intensive, creating damages to the roots, and not able to apply for long-time observations *in situ*.

Non-destructive measurements

Non-destructive techniques, for instance, computer-assisted tomography (CT) (Heeraman et al., 1997; Mooney et al., 2012), magnetic resonance imaging (MRI) (MacFall et al., 1991; Pohlmeier et al., 2013), and neutron radiography (Zarebanadkouki et al., 2013) were applied to study the root distribution and interactions between root and soil water in the lab. These techniques are

more accurate in the estimation of root growth, root architecture, and water movement. However, the common downside is that they are only suitable for small plants in pots and it takes time for the scanning.

Rhizotrons and minirhizotrons (MR) are minimal-destructive methods to supply direct and repeatable visions of root morphology and the responses of the root system to various ambient conditions along with the time. Large rhizotrons with one- or two-side transparent panel were limited due to the high cost of the installation and setup (Hilton et al., 1969; Taylor, 1969). Small and usually tilt rhizotrons forced roots to preferentially grow along the lower plate and were used to study root system architecture (Alony and Linker, 2013; Luster et al., 2009). MRs were transparent tubes with a diameter around 5 cm for observing spatial-temporal distributions of roots by a portable camera (Box and Ramsuer, 1993). MRs were widely used for root measurements including forest trees (Hendrick and Pregitzer, 1992), shrubs (Brown et al., 2009), crop species (Cai et al., 2016; Garré et al., 2012), and vegetation in wetlands (Iversen et al., 2012). The installation of MRs varied from vertical to horizontal (Fig. 1). Angled ($0 < \alpha < 90°$) and vertical tubes were mostly used for the reason that it is better for collecting information of roots at any given depth and different distances from sparse-planted plants (Johnson et al., 2001). However, the probability of the deepest roots approaching the MRs depends on the root density and grow orientation since the view at any given depth is so limited (Vamerali et al., 2012) and preferential growth along the tubes resulted in underestimation in the shallower layers and overestimation in the deeper layers (Madi and Kangas, 1997; Stadnyk, 2010). Horizontal tubes can only offer images of the specific depth (Dubach and Russelle, 1995) but have the advantages of obtaining quantities of root images and maximizing the view area at each specific depth and minimizing the external influences to the natural soil and the environment of roots growth (Eamus, 2006; Smucker, 1993) .

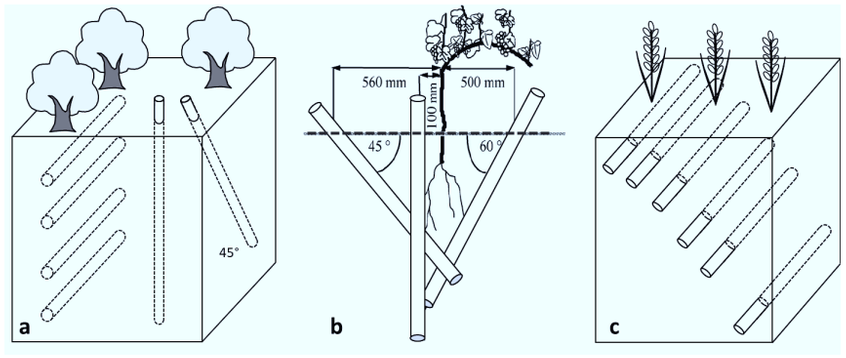

Fig. 1 Orientations of minirhizotrons with the angles of 0°, 45°, 90° off vertical (a) used by Ephrath et al. (1999), angles of 0°, 30°, 45° off vertical (b) by Linsenmeier et al. (2010), and 90° (c) off vertical used by Cai et al. (2016).

1.2 Estimation of root water uptake

Direct measurements

Different technologies have been used to measure RWU based on mass or energy transfer between soil, root, and plant (see reviews by Fernandez et al. (2000), Rana and Katerji (2000), and Orellana et al. (2012)). Lysimeters and sap flow measurements were the main approaches for measuring RWU directly. Using weighing lysimeters all terms of the soil water balance except for the fluxes from the top surface are measured. The evapotranspiration, which is for a crop that fully covers the soil surface nearly equal to RWU, can therefore be derived directly from closing the water balance (Howell et al., 1991; Wegehenkel and Gerke, 2013; Young et al., 1996). However, the representativeness of the isolated soil and limitation of the height and plant density were argued (Grebet and Cuenca, 1991; Rana and Katerji, 2000). Moreover, the installation and maintenance of a lysimeter system are costly (Abdou and Flury, 2004). Sap flow measurements based on heat-pulse or heat-balance principle were conducted in the roots (Brooksbank et al., 2011; Hultine et al., 2004) and plant stems to quantify plant water use (Cohen et al., 1990; Cohen and Li, 1996; Langensiepen et al., 2014; Sakuratani, 1981). This method requires less equipment and does not disturb plant root medium but the uncertainty increases when extrapolating from a single root/stem to a whole canopy or field scale (Chabot et al., 2005). Multiple gauges help to

reduce the estimation error that is resulted from spatial variation in soil-water conditions (Jara et al., 1998; Senock et al., 1996). When using the heat balance approach gauges with different sizes are required to accommodate the stem diameter in the growing season since the gauges were designed with relatively narrow limits for crop stems (Smith and Allen, 1996). Whereas using the heat pulse approach an empirical calibration factor for transpiration conversion should be interpreted with caution since it was species and probe insertion depth dependent (Cohen et al., 1993; Green et al., 2003).

Indirect measurements

Isotopes are widely used to investigate RWU for determining the water source, identifying possible water mixing processes in different depth-rooted vegetation, and partitioning ET into evaporation and transpiration (Ehleringer and Dawson, 1992; Rothfuss et al., 2010; Rothfuss and Javaux, 2017; Smith et al., 1998). Using isotopes has the advantage of non-disturbance to the root system and the ability to distinguish water sources at both lab and field scale for crops and trees (Asbjornsen et al., 2007; Moreira et al., 2000; Sutanto et al., 2012; Wang et al., 2010). Magnetic resonance imaging (MRI) is also a non-destructive and non-invasive technique being used to study RWU patterns by observing changes in water distribution in roots, rhizosphere, and soil (Brown and Johnson, 1989; MacFall et al., 1991; Pohlmeier et al., 2013). However, small plants tend to be used for water flow studies due to the limits of the magnet (Kuchenbrod et al., 1996). Eddy covariance (EC) is a meteorological method to measure ET with a higher temporal resolution without disturbing the monitored surface and it can cover larger surfaces (Wilson et al., 2001). EC is a standardized method that is used in world wide networks of observatories (e.g. Fluxnet) against the disadvantages: the footprint is not constant in time but changes depending on wind speed and direction (Baldocchi et al., 2001; Horst and Weil, 1992). Given the spatial variability in soil properties and vegetation types, this makes that the impact of soil moisture on transpiration and RWU is more difficult to assess and requires that the footprint is well known and soil moisture is monitored with sufficient spatial resolution in a large area. Furthermore, EC measurements may have a bias due to an incomplete closure of the energy balance and it also requires extensive and expensive sensors (Petropoulos, 2013). Similar to eddy covariance, the Penman-Monteith method (Allen et al., 1998) was widely used with the meteorological data to

estimate ET for different objectives, e.g., planning and management of crop production (Smith, 2000), evaluating irrigation efficiency (Blonquist et al., 2006; Grant et al., 2009), and input of RWU models under well-watered conditions (Šimůnek et al., 2016; van Dam et al., 2008; Wu et al., 1999). This approach can be used for a wide range of climatic conditions for RWU estimation.

RWU models

Compared with the direct or indirect measurements discussed above, mathematical models are useful tools to describe the relation between soil moisture, root/plant development, and atmospheric demand in the SPA system, better understand effects of environmental factors on RWU, and estimate RWU for addressing practical problems (Communar and Friedman, 2010; Kandelous et al., 2012; Kumar et al., 2014; Šimůnek and Hopmans, 2009). Numerical RWU models have been developed for estimating plant water use at different scales and investigating the response of the plants to drought and nutrient stress due to complex interactions between root growth and soil heterogeneity (Couvreur et al., 2012; De Jong Van Lier et al., 2008; Feddes et al., 1976; Heinen and De Willigen, 1998; Javaux et al., 2008; Šimůnek and Hopmans, 2009; Vrugt et al., 2001b). RWU is generally described as a sink term in soil water flow models such as the Richards equation:

$$\frac{\partial \theta}{\partial t} = \frac{\partial}{\partial z}\left[K(h)\left(\frac{\partial h}{\partial z} + 1\right)\right] - S_{(z,\,t)} \qquad (1.1)$$

where θ is the volumetric soil water content (SWC) [$L^3\ L^{-3}$], t is time [T], K is the soil hydraulic conductivity [$L\ T^{-1}$], h is the soil water pressure head (SWP) [L], z is the vertical coordinate taken positively upward [L], and S is the sink term [$L^3\ L^{-3}\ T^{-1}$] defined as the volume of water removed from a unit volume of soil due to root extraction.

In order to estimate S, different assumptions were used to describe RWU that can be classified into two categories: functional-structural vs. macroscopic models. The main difference between them is the complexity of root system and interaction between root and soil. The functional-structural models define a root system architectural domain that facilitates the inclusion of explicit root hydraulic properties and related physical concepts to simulate water movement towards individual roots (Doussan et al., 1998; Javaux et al., 2008). Thereunto, root hydraulic

properties are important input in the models since they are responsible for the resistance to water flow of the soil-root-plant continuum and to the evolution of water potential in the plant xylem, which is linked to the regulation of the opening of stomata (Bechmann et al., 2014). The complexity of those models is particularly appropriate to investigate interactions between root development and soil properties (Pagès et al., 2004; Somma et al., 1998), foraging for soil resources (Lobet et al., 2014; Lynch, 2013; Pagès, 2011), and plant responses in heterogeneous environments (Couvreur et al., 2014a; Huber et al., 2014). In macroscopic models, RWU is assumed to be distributed proportionally to root distribution and locally adjusted for water availability. These models integrate RWU with transient soil water flow but did not solve water flow towards and within individual roots. Compared with the functional-structural models, macroscopic models require fewer parameters and lower computational resources for RWU simulation. The simplicity of this effective approach is suitable for applications at larger scales (Baram et al., 2016; Feddes et al., 2001; Oleson et al., 2008). However, the parameters and concepts used in these models are, to a large extent, empirical so that they cannot be linked to directly measurable properties of the root system. Root features and soil moisture availability are not stand-alone elements in water uptake process (Huang and Nobel, 1994), and the interactions between the root system and the soil water status should be considered in the models. Recently, simple 1-D macroscopic expressions of RWU were derived based on small-scale hydraulic principles, respectively, in the soil around roots (De Jong Van Lier et al., 2008) and within the root system (Couvreur et al., 2014b). This allowed a revision of non-physical assumptions in macroscopic RWU models and linking their parameters to properties of the root system (Javaux et al., 2013). There are a number of root architecture models and RWU models available that were developed for different objectives and have therefore different specific strengths and weaknesses. Coupling these models using unifying model languages will improve the understanding of the interaction between root uptake, root development and distribution, and spatial soil water distribution at different scales (Lobet et al., 2015; Vereecken et al., 2016).

Transpiration measured by direct and indirect methods were compared for trees and crops and for different scales (Ford et al., 2007; Fu et al., 2016; Logsdon et al., 2014; Moreno et al., 1996; Wilson et al., 2001). The measured and estimated transpiration by macroscopic RWU models were compared for trees (Gong et al., 2006; Green and Clothier, 1998; Howard et al., 1996), for

which comparison the measurements were also used to validate the model simulation. However, for crops, in particular wheat, such a validation has not yet been performed.

1.3 Model parameterization

The estimation of RWU and associated uncertainties strongly depend on the identification of the parameters. Some parameters of the models, e.g., soil hydraulic properties, can be measured directly by taking samples. However, determining parameters in the laboratory is on the one hand time consuming and labor intensive, and on the other hand not representative for field conditions due to soil heterogeneity (Vereecken et al., 2015; Vereecken et al., 2010). Moreover, the preparation and operation of the experiments may introduce new uncertainty in the model parameters (Sonnleitner et al., 2003). Inverse modeling, as an alternative approach, is usually being used to identify the model parameters based on the measurements *in situ* to overcome that problem. It has the advantage that the estimated parameters are based on the variables that are observed at a longer time- and larger area-scale and under natural boundary conditions (Ritter et al., 2003). Highly increased computational power offers the opportunity to apply inverse modeling to address different practical problems.

Soil hydraulic properties are frequently inversely estimated by reproducing observed SWC and/or soil water potential in the models with different optimization algorithms (Hupet et al., 2003; Ines and Droogers, 2002; Ritter et al., 2003; Scharnagl et al., 2011; Schneider et al., 2013; Simunek and vanGenuchten, 1996; Vrugt et al., 2001b). In the macroscopic models, root distribution (Hupet et al., 2003; Vrugt et al., 2001b; Zuo et al., 2004) and parameters of water stress function (Fujimaki et al., 2008; Vandoorne et al., 2012) were also inversely estimated. Root hydraulic parameters of functional-structural models can either be derived from direct measurement on root segments (Doussan et al., 2006; North and Nobel, 1995) with destructive methods or using inverse modeling. As far as I know, the inverse estimation of root hydraulic parameters was only conducted by Zarebanadkouki et al. (2016) using neutron radiography, deuterated water, and a 3-D RWU model for the root system of lupine and by Meunier et al. (2017) using stable water isotope $^{1}H_2O_{18}$ as a tracer and a root-rhizosphere water flow model for the root system of Italian ryegrass. Both the direct measurements and inverse modeling were

conducted at lab scale. This is because obtaining information of root geometry and root hydraulic parameters, especially for growing plants, is a substantial challenge. The recently developed macroscopic RWU model, Couvreur et al. (2012) with a simplified description of water flow between soil and roots, was upscaled from functional-structural models (Doussan et al., 1998; Javaux et al., 2008) and offers the possibility to obtain root hydraulic properties using inverse approach. This upscaled model reduces the parameters of the single root segments into a function that describes the uptake in case the soil water potential is uniform in the root zone, and an effective root system hydraulic conductance and compensatory conductance parameter. When resistance to axial flow is not very large and the distribution of the radial root conductances of the root segments at a certain depth does not vary a lot with depth, the function for uptake under uniform water potential converges to the root length density.

RWU models with different assumptions were compared (de Willigen et al., 2012; dos Santos et al., 2017) but the simulation quality of the models was not investigated. Inverse modeling combining water uptake or transpiration measurements (e.g., sap flow) offers the opportunities for evaluating model results (e.g., estimated parameters, water uptake profile and cumulative water uptake, and reproduced observed variables) when using different RWU models but same observations, boundary conditions, and model setup.

1.4 Objectives

This study aims at investigating the effect of soil water distribution on root development and RWU simulated by different RWU models using the measured soil moisture and root growth in the field. Five questions are particularly addressed to achieve the objective:

1. How can the dynamics of root development and soil moisture be observed with minimal disturbance in the field?
2. How are root development, crop growth, and RWU affected by different water treatments in different soil types?

3. Are the measurements of root development and soil moisture sufficient to constrain the parameters of the RWU models? Are the values of same parameters (e.g., soil hydraulic parameters) estimated by different RWU models comparable?
4. Are the predicted RWU simulated by different models and for different soil water availability comparable with measured transpiration?
5. Can RWU parameters that were obtained in a certain soil and for certain water treatment be used to predict RWU in other soils and water treatments?
These very generic aims and research questions were applied to a winter wheat in this work.

1.5 Thesis outline

To answer the proposed questions above and achieve the objectives, the thesis is composed of three parts that are based on the published or unpublished manuscripts (chapter 2 to 4).

Chapter 2 introduces the construction of two isolated MR facilities (including sensor installation and calibration) in two different soils (stony vs. silty) using different techniques. The quality of the soil water data measured by different sensors and device was evaluated and the representative of the root distribution was analyzed. The variations of the soil moisture status and root development observed from the two facilities are presented.

Chapter 3 presents the parameterization of three RWU models (Feddes, Feddes-Jarvis, and Couvreur) with different water uptake compensation principles based on the observed data in the sheltered plot of the stony soil. The inversely estimated parameters were compared between the three models and the data from the literature. The response surfaces for the estimated parameters of the models were conducted to show the quality of the inverse modeling. Using the optimized parameters, the variations of RWU profile patterns and the possible links between different models are discussed.

Chapter 4 investigates the effect of different water treatments and soil types on crop and root development and RWU that were estimated by two RWU models (Feddes-Jarvis and Couvreur) and compares the RWU estimated by numerical models and measured sap flow. The differences

in crop growth and root development in the three subplots of the two facilities are discussed first. The inversely estimated parameters of the two models using measurements from the three subplots of each facility are discussed. Then the simulated RWU and measured sap flow obtained from each plot of the two soils was compared. In the end, a sensitivity analysis was done for exploring the effect of different crop and root development on RWU estimation.

Finally, a synthesis is presented in chapter 5 for summarizing the general conclusions from the previous chapters and provides an outlook on future research.

Chapter 2

Construction of horizontal minirhizotron facilities to investigate root development and root zone processes

This chapter is based on a journal article published as:

G. Cai, J. Vanderborght, A. Klotzsche, J. van der Kruk, J. Neumann, N. Hermes, and H. Vereecken. 2016. Construction of Minirhizotron Facilities for Investigating Root Zone Processes. *Vadose Zone J*. 15. doi:10.2136/vzj2016.05.0043

2.1 Introduction

A minirhizotron system supplies direct and repeatable views of root morphology *in situ* in a minimal invasive manner and it measures responses of root development to various ambient conditions over an extended time period (Johnson et al., 2001). Therefore, the method can be used to investigate the interaction between root development, root senescence, and soil conditions. A typical MR system is composed of a computer, a digital camera and a light source mounted on an index handle, and transparent tubes or rhizotubes installed in the soil at a certain angle.

However, the quality and the representativeness of the root observations made in rhizotubes can be strongly influenced by the method of installation. To ensure high quality observations, it is generally important to ensure good contact between the soil and the tubes, minimizing or avoiding scratches on the tube surface, and avoiding soil compression. This might be a great challenge in soils with a heavy texture (silt, clay) or with either a stony or coarse texture. For a heavy-textured soil, Hummel et al. (1989) designed a special auger system with combined soil coring bits of which the outer diameters were 2.8% smaller than that of the 30-degree-angled tubes to ensure a good tube-soil contact while minimizing soil compaction. The excavation afterwards showed that there were generally no gaps, but measurements using a laboratory penetrometer revealed that it caused uniform soil compaction around a tube at a given depth and soil movement along the direction of the tube installation. For a soil with a lot of cobbles and stones, Phillips et al. (2000) used a pneumatic rock-drill, which was fixed on a pneumatic screw-drive guide system to make 30-degree-angled boreholes, and showed that good soil/tube contact was obtained and that there was less soil compaction and disturbance by using this approach in the sandy and rocky soil than using normal techniques (e.g., soil core and auger).

Because of practical reasons, i.e., to avoid the use of heavy machinery, collapse of drilled holes, and tube distortion, MR's are mostly installed either in a vertical manner or with an inclination towards the horizontal surface (vertically inclined). The tubes are usually inclined at 30^{o} or 45^{o}, but other angles are also common in root investigation (Milchunas, 2011; Vamerali et al., 2012). Vertical rhizotubes may lead to artifacts since roots may grow downward preferentially along the tube walls (Bragg et al., 1983). But, also for angled tubes, the root density in the surface soil

layer was seriously underestimated whereas in the deeper layers it was overestimated because roots grew, also as a result of gravitropism, preferentially along the soil-tube interface where conditions for growth were more favorable, e.g., lower penetration resistance, moisture droplets on the tubes due to the gaps between the soil and the tubes (De Ruijter et al., 1996; Madi and Kangas, 1997; Stadnyk, 2010). Another problem with vertically inclined MR's is that root observations at a certain depth can be made in only a small surface surrounding the tube. Because of soil heterogeneity and the spatial structure of the root system, a large number of observations or frames are required to obtain a representative estimate of the root density at a certain depth. This implies that a large number of angled tubes are required. Alternatively, a larger number of frames or root observations at a certain depth can be obtained from a horizontally installed MR (Johnson et al., 2001; Smucker, 1993). Furthermore, horizontally installed rhizotubes minimize external influences on the natural soil and the root environment and avoid that water flows down preferentially along the soil tube interface (Eamus, 2006). However, due to the difficulty of horizontal installation, the use of horizontal rhizotubes was restricted to smaller soil volumes such as lysimeters and outdoor containers (Garré et al., 2011; Meier and Leuschner, 2008) or to large facilities where rhizotubes were installed in repacked soil (Smit et al., 1994; Van de Geijn et al., 1994). Besides, the operation was even more difficult for establishing good contact and minimizing the soil disturbance in the extreme soil textures, e.g., stony or clayey soil (Ephrath et al., 1999).

The objective of this note is to present a construction procedure for rhizotron facilities with long (7-m) horizontal MR's in a stony and a silty soil. We also present the measurement set-up for monitoring the root-root environment using soil moisture, matric potential and soil temperature sensors as well as ground penetrating radar. Soil sensors typically provide local measurements of soil states so that in heterogeneous soils, a large number of sensors may be required to obtain a representative estimate. After presenting the setup, we illustrate datasets that are obtained from the facility. Special emphasis is on the estimation of the spatial variability and the representativeness of the spatial averages of soil moisture and root densities.

2.2 Materials and methods

2.2.1 Field site

The study site is located in Selhausen (50°52'N, 6°27'E) in Germany and is part of the TERENO Eifel-lower Rhine observatory (Zacharias et al., 2011). The field is slightly inclined with a slope of approximately 4°. The main soil type in the field is Luvisol which developed in a layer with a silt loam texture (Weihermüller et al., 2007). The thickness of the silt loam layer varies strongly along the slope of the field. It is up to 3 m thick at the bottom of the slope and not present at the top. This boundary where the sediment layer is present or absent is well indicated by electromagnetic induction (EMI) measurements returning high or low apparent electrical conductivity values, respectively (Rudolph et al., 2015; von Hebel et al., 2014).

The underlying quaternary sediments, which reach to the soil surface at the top of the slope, are fluvial gravel deposits mainly from the Rur river system. The test site is characterized by a strong gradient in stone content with 60% gravel content in the upper part and approximately 4% in the lower part, respectively (Vanderborght et al., 2010). The soil texture is shown in Table 2.1. One facility was constructed at the top and one at the bottom of the slope. Before the facility was constructed, the field was under a winter barley (*Hordeum vulgare L.)* - winter wheat (*Triticum aestivum*) crop rotation. Winter wheat was sown on 31 Oct. 2013, and harvested on 17 July and 31 July 2014 in the upper and lower facility, respectively.

Table 2. 1 Soil texture of the fine soil (<2 mm), mass fraction of stones, field capacity (FC), permanent wilting point (PWP), and porosity in the top- (0–30 cm) and subsoil (30–120 cm) of the upper and lower parts of the field.

		Sand (%)	Silt (%)	Clay (%)	Stone (%)	FC	PWP	Porosity
Upper	Topsoil†	35	52	13	50	0.15	0.07	0.33
part	Subsoil††	37	47	16	69	0.09	0.06	0.25
Lower	Topsoil†	13	70	17	4	0.37	0.25	0.40
part	Subsoil†	11	68	21	2	0.29	0.19	0.40

† the soil texture was from Weihermüller et al. (2007).

†† the soil texture in the subsoil of the upper part was from Stadler et al. (2015).

2.2.2 Setup of the field plots and access trench

Each rhizotron facility was divided into three instrumented plots receiving different water treatments. Each plot was 3.25 m wide and 7 m long and the plots bordered each other along the 7-m-long side. The three plots were bordered by a wooden container (length: 10 m, width: 2.65 m, height: 2.25 m) that was installed in an excavated pit next to the field plots (Fig. 2.1). The wooden container serves as access trench with pre-drilled holes for the rhizotubes and soil moisture sensors. In order to avoid unwanted reflections in the GPR data, the use of metallic objects in the facilities was avoided as much as possible. To minimize the disturbance of the soil thermal regime by the trench, the facility walls were isolated by 50-mm-thick insulation foam sheets.

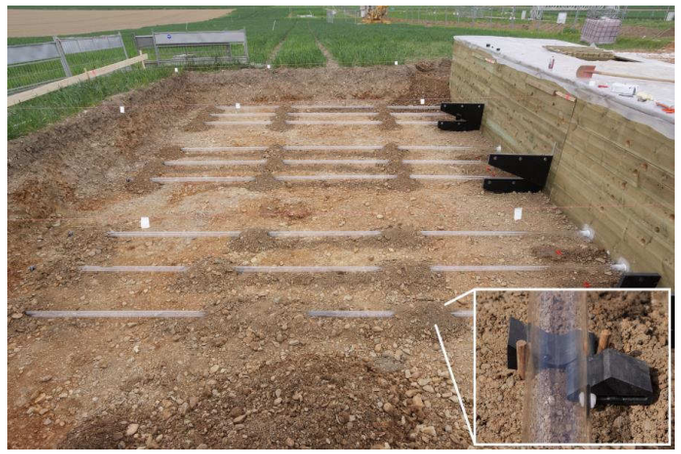

Fig. 2. 1 Installation of the minirhizotron facility in the upper part of the test site. The wood container is the accessible facility. Wedge-shaped fixture blocks shown in the right corner were used to fix the tubes during soil backfill.

One plot was sheltered from rain, one plot was rain fed, and one plot was irrigated with dripper lines. Shelters were installed before the rain started and were removed after the rain stopped. The dripper lines (T-Tape 510-20-500, Wurzelwasser GbR, Münzenberg, Germany) were installed with 0.3-m intervals and parallel to the access trench. A plastic foil was placed down to 1.3 m at the upper facility to separate the three different treatments from each other.

2.2.3 Installation of the rhizotubes

For the installation of the rhizotubes in the upper facility, the high stone content prevented the drilling of horizontal holes (Fig. 2.1). Instead, a pit of 10 m by 10 m was excavated to 1.3 m depth first. For each plot, three replicate minirhizotron tubes, i.e., acrylic glass tubes of 7 m length and with an outer and inner diameter of 64 mm and 56 mm respectively, were installed at 10, 20, 40, 60, 80, and 120 cm depth with a horizontal offset of 10 cm between tubes at different depth levels so that tubes at a certain depth were not overlain by tubes at other depths (Fig. 2.2). Root observations at a certain depth are therefore not expected to be influenced by the presence of MR's at other depths. Acrylic glass was used since it has higher hardness (anti-scratch) and transparency, and less influence on root growth than other plastics, i.e., butyrate, polycarbonate, and last but not least it was less vulnerable than glass (Withington et al., 2003). The tubes were levelled horizontally on the flattened soil surface using a laser measuring device (Javelin-s Leica-geosystems, München, Germany) (Fig. 2.1). To avoid displacement when backfilling the soil, the tubes were fixed by wedge-shaped fixture blocks at three locations and the end was sealed with an inner and an outer cap. The stony soil was backfilled to cover the tubes and sensors carefully. Big stones (>30 mm) were removed when covering the sensors. The backfilled soil was compacted layer by layer to achieve the same bulk density as the undisturbed soil: 1.81 g cm^{-3} in the topsoil layer (0-0.3 m) and 2.02 g cm^{-3} in the subsoil (0.3-1.2 m). The tubes protruded 0.31 m into the access trench to anchor the MR camera. The protruding parts were wrapped up by black tapes and plugged by opaque caps to prevent light, water, and dust entering the tubes (Fig. 2.2). A hole with a diameter of 4 mm was drilled on the topside of each tube at 0.3 m away from the facility wall. This hole was used to fix the camera system on the rhizotube, which consists of an indexing handle that is used to position the camera in the tube. By fixing the camera system to the tube and using the indexing handle, images could be repeatedly taken at the same locations along the tube for every measurement.

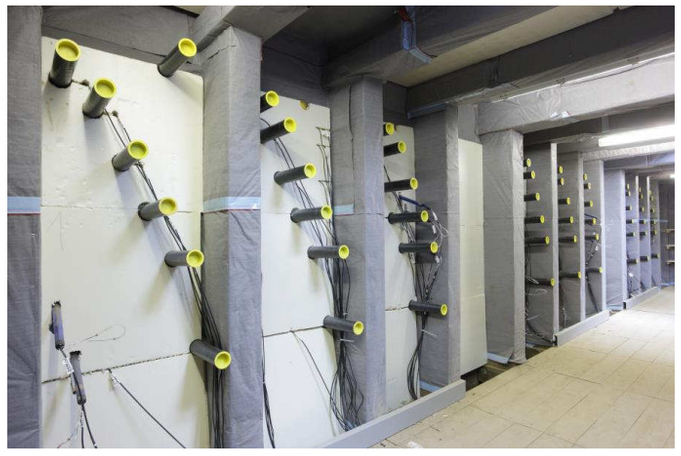

Fig. 2. 2 Interior view of the minirhizotron facility. The rhizotubes were installed perpendicular to the wall profile.

The design of the facility at the lower part of the slope was similar to that at the upper part (same arrangement of MR tubes, soil sensors, and treatment plots) but the soil below 20 cm depth was not excavated to install the MR tubes. Instead, the tubes were inserted in horizontally drilled holes. Therefore, a specialized drilling rig was constructed in the Central Institute for Engineering, Electronics and Analytics (ZEA) of Forschungszentrum Jülich (Fig. 2.3).

Fig. 2. 3 (a) The steel tube, the auger, and the connected drilling bit; (b) the drilling system for boring horizontal holes and installing the rhizotubes in the lower part of the test site.

Steel pipes with an auger inside were pushed into the soil. The pipes were 915 mm long and the outer and inner diameters were 65 mm and 53 mm, respectively. There was a 50-mm-long drilling bit with a diameter of 20 mm in the front of the auger. The auger with an outer diameter

of 51 mm and a length of 910 mm was positioned approximately 50 mm out of the pipe (Fig. 2.3a). Therefore, the drilling unit was used to bore a hole first, and the soil inside the pipe was carried away by the auger. Pipe and auger pieces were screwed together separately with strengthening bolts. The pipes were pushed using a retractable hydraulic cylinder. A maximal force of 127.5 kN could be exerted by the device. The auger rod could withstand a maximal torsion of 190 N m and was connected to other pieces for deeper soil extraction. To keep the direction of the inserted pipes fixed, the drilling rig was suspended in a wheel-equipped frame that was aligned using lasers and fixed to the struts of both sides of the facility (Fig. 2.3b). The distal ends of the steel tubes deviated at most 5 cm in the horizontal and vertical direction. When a steel tube of 7 m length was inserted in the soil, a MR was attached to the distal end of the tube. Therefore, a pit was excavated at the other side of the facility where 7-m-long MR tubes could be laid down. A connector that fixed the MR to the steel tube was constructed using a threaded rod and screws so that it could withstand a tensile force of at least 23.9 kN, which corresponds with the tensile strength of the MR. The MR was subsequently pulled back with the steel pipe through the bored hole using the drilling rig which functioned now as a traction device. Using this procedure, 36 tubes were installed at 40, 60, 80, and 120 cm depth. Two MR tubes could be installed in one day with this technique. The tubes at 10 and 20 cm depth were installed by excavating the top soil layer, which is disturbed anyway by soil tillage. A water tank of 2.6 m^3 was buried in the soil 3 m away from each facility and collected the rainfall from the roof of the wooden container for subsequent irrigation.

2.2.4 Installation and calibration of the soil sensors

At each soil depth in each plot, four own-made TDR soil moisture sensors (3 rods, rod length: 200 mm, spacing between the rods: 26 mm), one tensiometer (T4e, UMS GmbH, München, Germany), and one MPS-2 matrix water potential and temperature sensor (Decagon Devices Inc., UMS GmbH München, Germany) were mounted 0.75 m away from the facility wall. To facilitate the removal of air bubbles in the tensiometers and to improve the filling, the tensiometers were installed with an angle of 15^o upward. The setup of the rhizotubes and soil sensors in one plot is shown in Fig. 2.4. In the lower facility, the TDR and MPS-2 sensors were

refitted with a round base (Fig. 2.5) attached to a plastic pipe and were carefully inserted into the pre-drilled holes from the facility wall. All the sensors in the upper facility and the sensors at 10 and 20 cm in the lower facility were covered by the original soil which was excavated before during the installation (Fig. 2.5). The soil water content (SWC) and soil water potential (SWP) measured by the sensors in each facility was recorded hourly by two data loggers (Model CR3000, Campbell Scientific Inc., Bremen, Germany; DT85M, Cosinus Messtechnik GmbH, Ottobrunn, Germany) with multiplexer peripherals, respectively. The multiplexer (50C81-SDM) that connected TDR probes to the TDR100 cable tester (Campbell Scientific Inc., Bremen, Germany) were constructed with eight different channels. Four cascaded relay levels were used to switch the outer and inner wires of the coaxial cable to make sure that there was no physical connection between different channels during switching and that the travel time of the electromagnetic waves for the eight channels was the same (Weihermuller et al., 2013). This design avoided influences from the electromagnetic noise associated with electric earth currents which are present at the site.

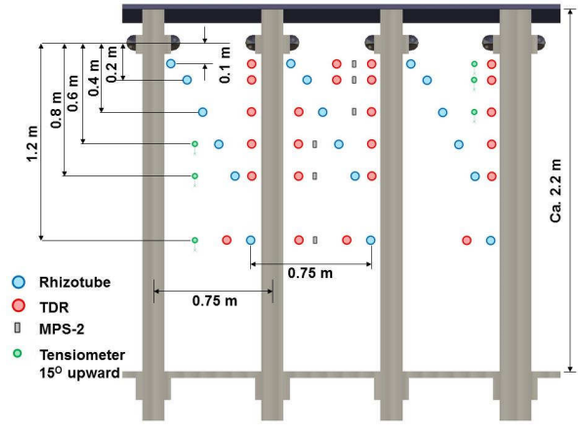

Fig. 2. 4 Setup of the rhizotubes, time-domain reflectometry (TDR) sensors, MPS-2 matrix water potential and temperature sensors, and tensiometers along the transection of the facility wall of one plot.

Fig. 2. 5 Time-domain reflectometry (TDR) sensors in the (a) upper and (b) lower facilities. The bases of the TDR sensors were refitted to a round shape attached to a plastic pipe for inserting into the bored holes in the lower facility.

For lower facility in the silty soil, the Topp's equation (Topp et al., 1980) was used to calculate the water content from the TDR measured dielectric permittivity of the soil. Since the soil of the upper facility has a high stone content, a calibration relation between the TDR measured dielectric permittivity and the SWC was determined in the lab. A set of SWCs was established by mixing air dried soil with a known amount of water. This mixture was subsequently filled in a container with known volume and packed to the same bulk density as the field soil. In this container a TDR probe was installed and the soil was packed around the probes to ensure good contact between the soil and the TDR rods. From the dielectric permittivity that was derived from the TDR waveforms, the water content was calculated using the Topp's equation and the complex refraction index model (CRIM) (Herkelrath et al., 1991; Ledieu et al., 1986).

The relation between the apparent dielectric permittivity measured by TDR and the SWC calculated by the Topp's equation and by the CRIM model are shown in Fig. B1. The parameters of the CRIM model were obtained by fitting the equation to the SWCs. SWC was overestimated by Topp's equation in the stony soil. Hence, the fitted CRIM model was used to calculate the SWC from the dielectric permittivity of the stony soil. The calibration was conducted for the top- and subsoil separately, but the relation between the dielectric permittivity and the SWC for the

two layers did not differ much. So the same calibration relation was used for both top- and subsoil.

The mean of the SWC measured by the four sensors at a certain depth was calculated. However, the measurements by some sensor deviated considerably from the other sensors at the same depth and water treatments. Therefore, we tested whether certain sensor measurements could be considered as outliers using the Grubbs (1950), the Dixon (1950), and the median absolute deviation (MAD) methods (Leys et al., 2013). The description of these tests is given in the supplemental material A.

2.2.5 Root measurements in the rhizotubes

The root development was measured by a minirhizotron system (Bartz Technology Corporation, Carpinteria, CA, USA). A digital camera with a visible frame of 16.5 mm (vertical) × 23.5 mm (horizontal) was used to capture the root images from both left and right sides of the rhizotubes. The camera was positioned using an indexing handle at 20 observation locations in the tubes. Four series of five locations were taken at 1-1.5 m, 2-2.5 m, 3-3.5 m and 4-4.5 m from the access facility wall. Within a series, the centers of the images were located at 0.04, 0.12, 0.26, 0.38, and 0.5 m from the side of the series (Fig. 2.6). Repeatable observations could be carried out at the same locations with fixed intervals on the index handle. The information of rooting depth, root counts, and root length was obtained from the images by using Rootfly (Wells and Birchfield, 2009).

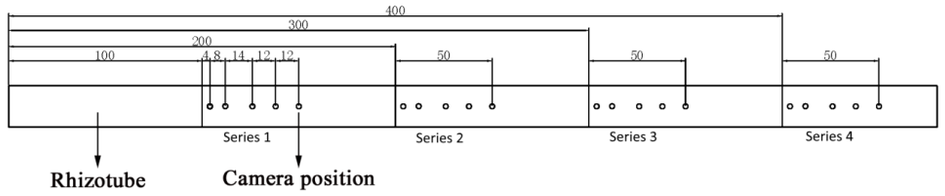

Fig. 2. 6 Measurement locations (circles) distributed in four series along the rhizotube (unit: cm).

2.2.6 GPR measurements in the rhizotubes

GPR is a well-known method to estimate soil water content (Huisman et al., 2003). Two MR tubes can be ideally used to guide a GPR borehole source and receiver to investigate the soil that is present between the two MR tubes. The presence of many horizontal MR tubes at different lateral and vertical positions allows a wide range of possible acquisition setups for borehole GPR measurements and a combination with surface GPR measurements to investigate the soil in horizontal and/or (semi-) vertical planes. Two possible borehole measurement methods are possible: a zero-offset profile (ZOP) where the emitting and receiving antenna are located in two different boreholes and simultaneously moved to the next position with a constant spacing between the measurement points, and a multiple-offset gather (MOG) where the transmitter is fixed at several locations in one borehole, while the receiver is moved through the whole horizontal borehole for each transmitter location. MOG data enable the reconstruction of detailed 2D images between the two boreholes, however the measurement time is significantly larger compared to ZOP measurements. Due to the many MR tubes we mainly performed ZOP measurements in horizontal planes every 5 cm between all pairs of neighboring MR at a given depth (borehole separation of 0.75 m). Because of the presence of the soil sensors and pertaining cables in the first 0.75 m away from the facility wall, GPR measurements were made between 1 m and 7 m away from the facility wall. This resulted in a dataset covering a soil volume of about 1.2 m depth x 1.5 m width x 6 m length for a certain treatment in a facility. The ZOP measurements were acquired using 200 MHz borehole antennae (PulseEKKO PRO system of Sensors & Software Inc.).

Standard ZOP processing is applied to the data which includes correction of the time-zero, applying a dewow filter to reduce low frequency noise, and, accurate and precise picking of first arrival travel times (Oberröhrmann et al., 2013). Because of interferences of the direct wave in the soil and the critically refracted wave traveling in air, the uppermost shallow ZOP results of 0.1 m depth cannot be analyzed with a travel-time analysis and were therefore excluded in the further analysis. A full-waveform inversion approach is currently in development that includes the full waveforms of both the direct wave and the critically refracted air wave to obtain reliable results for these shallow depths. Recently obtained results of full-waveform inversion approaches for cross hole GPR in saturated aquifers (Klotzsche et al., 2014) and surface GPR for agricultural

soils (Busch et al., 2014) indicate that reliable results can be expected when using such an approach.

Due to the known distance between the MR tubes in which the antennas are located and assuming that the electromagnetic wave is traveling on a straight path from the transmitting to the receiving antenna, the electromagnetic velocity of the electromagnetic wave can be estimated from the picked travel time. Using an appropriate petrophysical relationship, the measured velocity or dielectric permittivity can be converted into volumetric water content of the soil, e.g., Steelman and Endres (2011). Similar to the TDR measurements, we used the CRIM model and the Topp's equation for the upper and lower facility, respectively.

2.3 Results and discussion

2.3.1 Installation of the rhizotubes and sensors

We successfully installed 54 rhizotubes, 72 TDR, 18 tensiometers, and 18 MPS-2 in each facility and then did root measurements weekly as listed in Table 2.2. In the upper facility, where the tubes were installed in backfilled soil, we didn't observe tube bending or damage one year after installation. This indicates that compaction of the soil to the same density as the undisturbed soil effectively prevented settling and subsidence of the soil, which was observed to cause tube damage in other studies, e.g., Ephrath et al. (1999).

Table 2. 2 Number of the installed time-domain reflectometry (TDR) sensors, tensiometers, MPS-2 matrix water potential and temperature sensors, and rhizotubes and the measurement frequency of the soil moisture and roots in the two facilities.

Parameter	TDR	Tensiometer	MPS-2	Rhizotube	Images
Number per observation depth of one treated plot in one facility	4	1	1	3	120†
Total number	144	36	36	108	4320
Measurement frequency	1 h^{-1}	1 h^{-1}	1 h^{-1}	1 wk^{-1}	1 wk^{-1}

[†]Images at one observation depth were collected from 40 locations in each of the three replicate rhizotubes.

For a correct estimate of root distribution, the contact between the tubes and the soil is of great importance and is highly related to the installation procedure. Therefore, we collected 240 images (40 images depth^{-1} x 6 depths) from the tubes along the soil profile after the upper facility was constructed. The proportion of the void area in the images showed that approximately 92% of the view window was in contact with soils or stones. Phillips et al. (2000) obtained around 89.5% contact in a site with sandy and rocky soil using angled tubes. Because of the high stone content and the irregular shape of the stones, it is impossible to achieve a 100% contact between the tubes and the soil. For the lower facility, the borehole was clean and straight since much effort was made for the stabilization of the drilling system and it had a diameter that was 1 mm larger than the diameter of the rhizotube. The images collected after the installation of the rhizotubes showed that the contact between the tubes and the soil was approximately 96%. No obvious soil movement and scratches on the tubes were observed. Because of the good contact between the soil and the rhizotubes, root clusters and horizontal preferential growth along the tubes were not observed in the root image analysis.

2.3.2 Root development and distribution

Figure 2.7 shows time series of root images of winter wheat that were collected at the same position along the tubes at 20 cm and 60 cm depth in the two MR facilities. It clearly illustrates that the appearance, downward development, and senescence of the roots in the top- and subsoil can be recorded with time using the MR system.

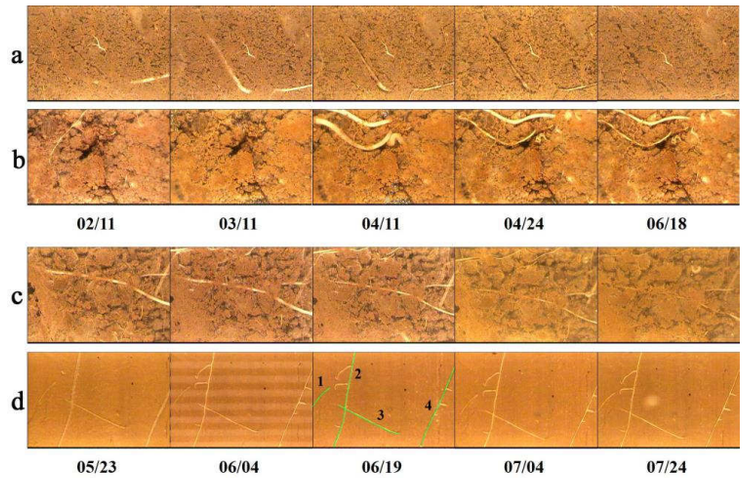

Fig. 2. 7 Time series root images of winter wheat collected from the rhizotubes at (a) 20 cm and (b) 60 cm in the upper facility and at (c) 20 cm and (d) 60 cm in the lower facility. Only single roots were counted and considered in the root analysis but not their laterals. Therefore, there are four roots (green tracks) in the third image of (d).

The measurements were taken at both left and right sides of the tubes, however, large variations in root counts were observed between the two sides along the tubes at each depth (Fig. 2.8). For one observation depth and one treatment, roots were counted in 120 images of 16.5 mm x 23.5 mm. This dataset represents a sample of the population of all possible root counts at this depth. When the root counts in different images are independent, then the standard deviation (or error) of the sample mean (SEM), could be calculated from the standard deviation of the root counts σ_{counts} in the images as:

$$\mathrm{SEM} = \frac{\sigma_{counts}}{\sqrt{N}} \tag{2.1}$$

where N is the number of images. The number of images that are taken per tube directly relates on the reliability of the root estimation. More images result in higher precision but increase the labor in the subsequent process. However, spatial data such as root counts may be spatially correlated so that root counts in images that are close to each other are not independent and the precision of the estimate of the mean will not increase when increasing the number of images. For instance, Dubach and Russelle (1995) found that the precision of the mean root counts of

alfalfa (*Medicago sativa L.*) was not reduced and a single root was less likely to be counted in more than one image when the number of root images reduced from 80 to 40 in a horizontal rhizotube. In order to evaluate the independence of the measurements, we determined the spatial correlation and calculated variograms of the root counts along the tubes exemplarily on May 21 and 23 for each depth of the three water-treated plots in the two facilities (Fig. 2.9). For the calculation of the variogram, the program Vesper (Minasny et al., 2005) was used.

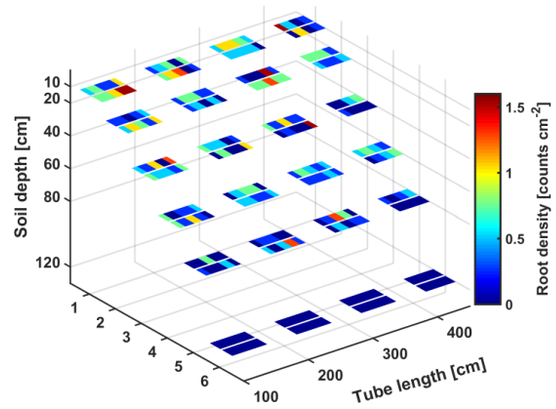

Fig. 2. 8 Root density along the left and right sides of the tubes (one replicate at one soil level) at six soil depths in the rainfed plot of the upper facility. Measurements were taken on 21 May 2014.

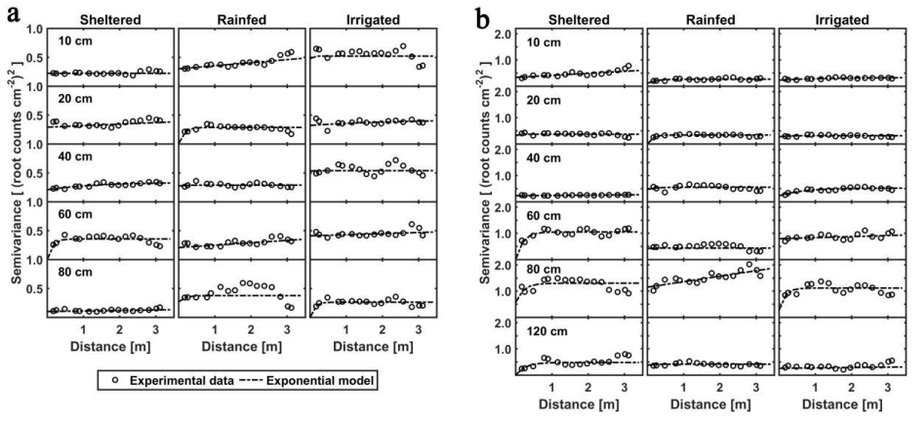

Fig. 2. 9 Variograms for the measured root data in replicate tubes at different soil depths in the (a) upper and (b) lower facilities. Root measurements were taken on 21 and 23 May 2014 for the upper and lower facilities, respectively.

Eighty percent of the variograms did not show spatial correlations. The intercepts on the y-axis were close to the mean variance, which suggested that roots counts in the images were randomly distributed and independent from each other. As a consequence, we calculated SEM and coefficient of the variation (CV) of the sample mean for the 120 images at each depth in each facility (Fig. 2.10). The SEM is around 0.04 counts cm^{-2} in the upper facility and this corresponds to a CV of the sample mean of 8%. The CV increased to 20% at 80 cm due to fewer roots arriving at this depth. In the lower facility, the SEM is larger and reaches up to 0.07 counts cm^{-2} at 60 and 80 cm depth. But, this goes along with the larger root densities at these depths which are about a factor two larger than the maximal root densities in the upper facility. The CV is therefore similar as in the upper facility.

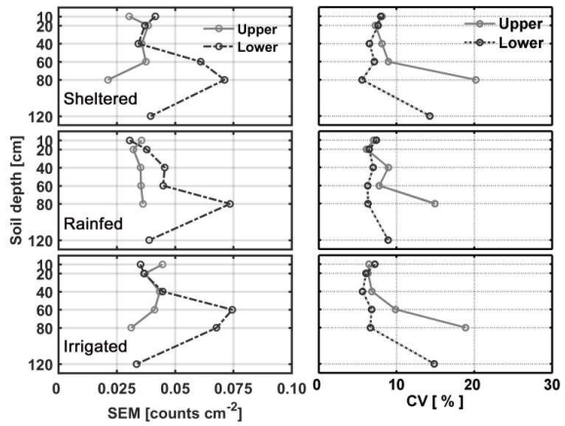

Fig. 2. 10 Standard error of the sample mean (SEM) (left) and the coefficient of the variation (CV) of the sample mean (right) for the measurements from the three replicate tubes (*N* = 120 images) at six observed soil depths in the three water-treated plots of the upper (on 21 May 2014) and lower (on 23 May 2014) facilities.

Before discussing the effects of soil texture, observation depth, and water treatment on root densities in detail, we tested the statistical significance of the effect of different factors, such as soil texture, water treatment, and soil depth on root density by an analysis of variance (ANOVA) in Matlab® 8.6.0. A mixed and nested model was set up for the data measured on 21 May 2014 in the upper facility and on 23 May 2014 in the lower facility, so the effect of measurement date is not included in the analysis. Soil texture, water treatment, and soil depth were the fixed factors whereas the replicated measurement along the horizontal rhizotubes was the random factor, and the random factor was nested to the fixed factors. Root distributions were significantly ($P<0.001$) influenced by the different soil textures, water treatments, and soil depths (Table B1). Overall, the soil texture had the largest effect on the root densities whereas the water treatment had the smallest effect. The effect of the soil depth interacted with that of the soil texture and the water treatment. This implies that in different soil textures the root distribution with depth varies and the impact of the water treatments is different for different depths. However, no statistically significant interaction between the soil texture and water treatment was observed so that the water treatments apparently had similar effects in the different soil textures. The random nested factor ‘tube replicate’ did not explain a significant part of the variability. This implies that root

densities did not differ significantly between replicate tubes which corroborates with the lack of spatial correlation of root densities.

The spatial and temporal distributions of the root density in the three water-treated plots of the two facilities are shown in Fig. 2.11. The lower facility was finished one year later than the upper one and the data logger was ready on 20 May 2014, so the root measurements for this facility were only shown from this date on. The downward root growth and root development in the beginning of the growth stage could be illustrated for all plots in the upper facility.

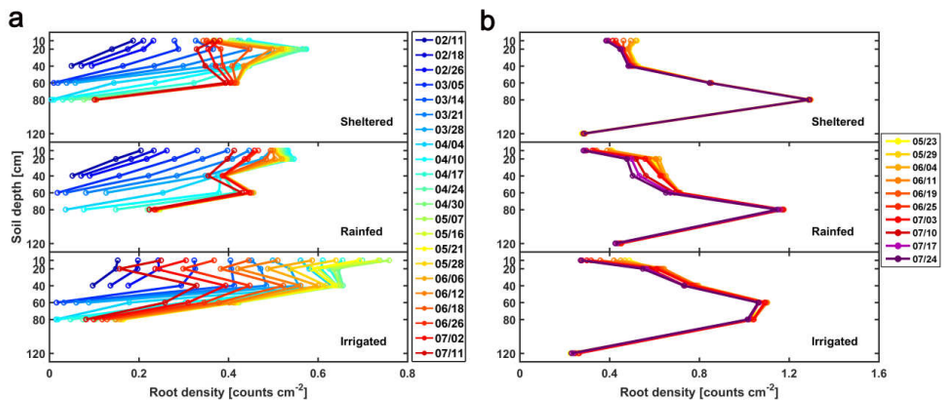

Fig. 2. 11 Time series distributions of root density at six observed soil depths in the sheltered, rainfed, and irrigated plots of the (a) upper and (b) lower facilities.

For the upper facility, most roots concentrated in the shallow soil from 10 to 40 cm before May. The highest root density appeared at 60 cm in the sheltered and rain fed plots, 40 cm in the irrigated plot. Root density from 10 to 40 cm in the irrigated plot was higher than that in other two plots, but decreased significantly with time after the flowering period (21 May). The crops in the irrigated plot ripened earlier (Hossain et al., 2011; Ikeda et al., 1994) and the senescence of the crops resulted in root decay. The maximum observed rooting depths in the three plots were the same, being 80 cm. For the lower facility, roots were detected at the deepest rhizotubes at 1.2 m depth. The first observations at the lower facility were made on May 23. After May 23, root senescence was also observed in the lower facility (except for 120 cm depth). In contrast to the upper facility, root densities increased with depth until 80 cm depth (60 cm depth in the irrigated plot) where the highest root densities were observed. At 80 cm depth, the highest densities were

observed in the sheltered plot. The rainfed and irrigated plots showed higher root densities at 20 and 40 cm depth than the sheltered plot. This could be anticipated based on the higher amount of water that these plots received from rainfall and irrigation than the sheltered plot leading to drier top soil conditions in the sheltered plot. The drier upper soil layer in the sheltered plot apparently promoted root development in the deeper soil layers more strongly than in the other plots.

When comparing the lower with the upper facility, the maximal root densities that were observed at 80 cm (60 cm in the irrigated plot) were about twice as high as the maximal root densities that were observed in the upper facility. The higher SWC in the silty deep soil layers of the lower facility may account for the high root density in the deep soil layers (see the following section). The root densities that were observed in the upper MR's of the lower facility (10-40 cm depth) were however similar to their counterparts in the upper facility (around 0.45 counts cm^{-2} in the sheltered and rainfed plots and 0.66 counts cm^{-2} in the irrigated plot).

2.3.3 Soil water content and water potential measurements

The variations of the SWC monitored by TDR sensors at six soil depths in the three water-treated plots of the two facilities are shown from May, 23 until August, 2 in Fig. 2.12. The SWC in the lower facility was higher, especially in the subsoil (40 cm and deeper), compared to the corresponding plots of the upper facility reflecting the difference in stone content and soil texture between the two facilities. Generally, the standard deviation of the SWC in the lower facility was larger than that in the upper one, especially in the deeper soil layers. This may be because soil water movement was quite heterogeneous in the non-disturbed silt soil.

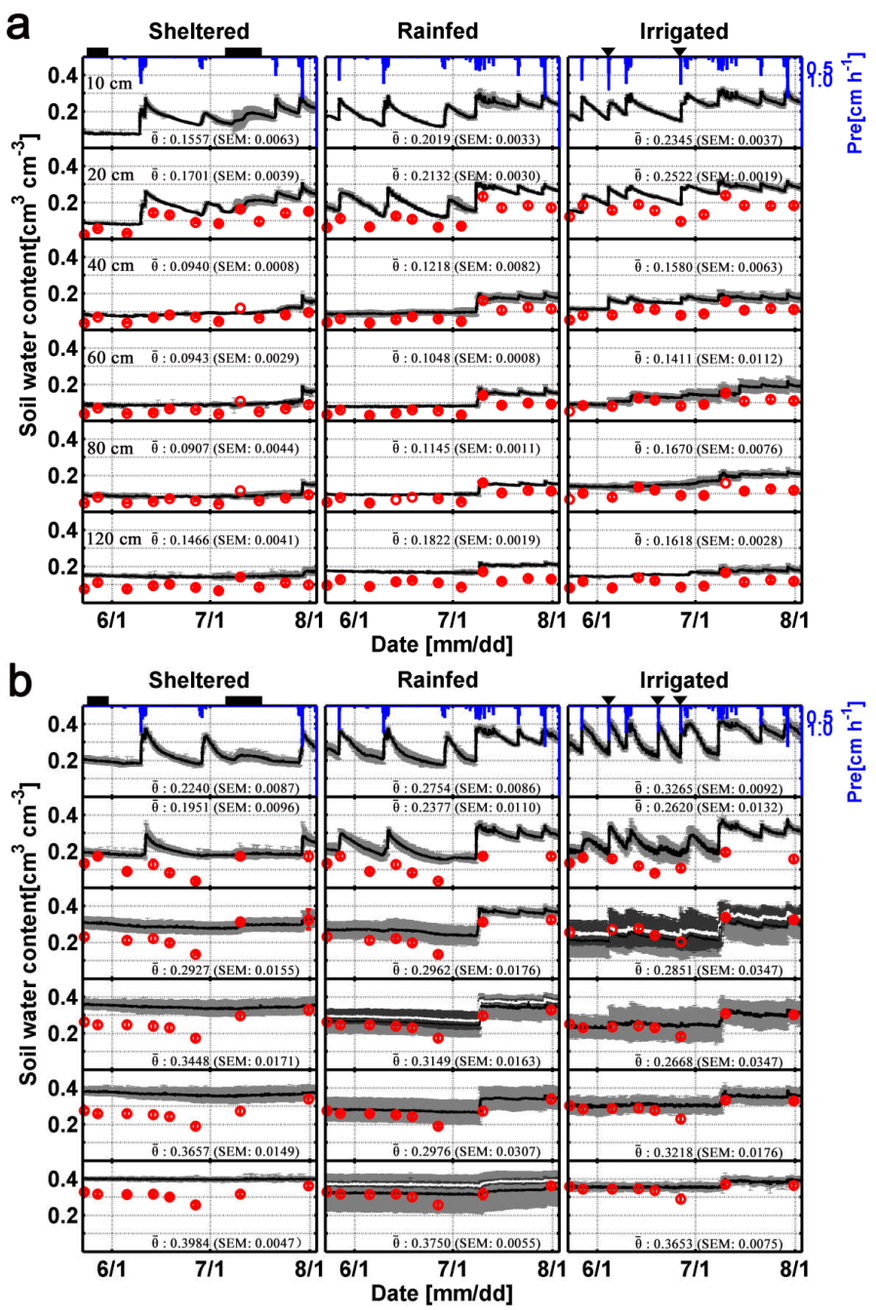
a
Sheltered
Rainfed
Irrigated
Soil water content[cm3 cm-3]
Pre[cm h-1]
10 cm
20 cm
40 cm
60 cm
80 cm
120 cm
θ̄ : 0.1557 (SEM: 0.0063)
θ̄ : 0.2019 (SEM: 0.0033)
θ̄ : 0.2345 (SEM: 0.0037)
θ̄ : 0.1701 (SEM: 0.0039)
θ̄ : 0.2132 (SEM: 0.0030)
θ̄ : 0.2522 (SEM: 0.0019)
θ̄ : 0.0940 (SEM: 0.0008)
θ̄ : 0.1218 (SEM: 0.0082)
θ̄ : 0.1580 (SEM: 0.0063)
θ̄ : 0.0943 (SEM: 0.0029)
θ̄ : 0.1048 (SEM: 0.0008)
θ̄ : 0.1411 (SEM: 0.0112)
θ̄ : 0.0907 (SEM: 0.0044)
θ̄ : 0.1145 (SEM: 0.0011)
θ̄ : 0.1670 (SEM: 0.0076)
θ̄ : 0.1466 (SEM: 0.0041)
θ̄ : 0.1822 (SEM: 0.0019)
θ̄ : 0.1618 (SEM: 0.0028)
6/1
7/1
8/1
Date [mm/dd]
b
Sheltered
Rainfed
Irrigated
Soil water content[cm3 cm-3]
Pre[cm h-1]
θ̄ : 0.2240 (SEM: 0.0087)
θ̄ : 0.2754 (SEM: 0.0086)
θ̄ : 0.3265 (SEM: 0.0092)
θ̄ : 0.1951 (SEM: 0.0096)
θ̄ : 0.2377 (SEM: 0.0110)
θ̄ : 0.2620 (SEM: 0.0132)
θ̄ : 0.2927 (SEM: 0.0155)
θ̄ : 0.2962 (SEM: 0.0176)
θ̄ : 0.2851 (SEM: 0.0347)
θ̄ : 0.3448 (SEM: 0.0171)
θ̄ : 0.3149 (SEM: 0.0163)
θ̄ : 0.2668 (SEM: 0.0347)
θ̄ : 0.3657 (SEM: 0.0149)
θ̄ : 0.2976 (SEM: 0.0307)
θ̄ : 0.3218 (SEM: 0.0176)
θ̄ : 0.3984 (SEM: 0.0047)
θ̄ : 0.3750 (SEM: 0.0055)
θ̄ : 0.3653 (SEM: 0.0075)
6/1
7/1
8/1
Date [mm/dd]

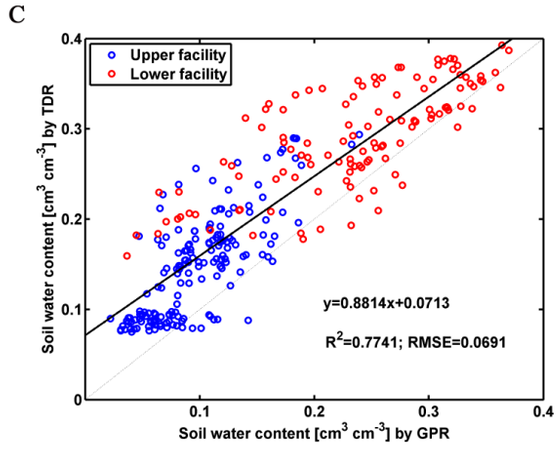

Fig. 2. 12 Time series soil water content (SWC) at different soil depths in the sheltered, rainfed, and irrigated plots of the (a) upper and (b) lower facilities measured by time-domain reflectometry (TDR) (solid line, SWC; light gray bars, standard deviation of SWC measured by four replicate TDR sensors; white line in b, SWC after removing the outliers; dark gray bars, standard deviation of SWC after removing the outliers) and by ground-penetrating radar (GPR) (red circles). Numbers in the plots refer to the temporal means ($\bar{\theta}$) and the standard error of the sample mean (SEM) of the TDR-measured water contents (outliers removed); ■: sheltered period, ▼: irrigation, Pre: precipitation; and (c) the correlation between the SWC measured by TDR and GPR.

Especially the standard deviations of the SWC at 40, 60, 80, and 120 cm in the rainfed plot, and at 40 cm, and 60 cm in the irrigated plot of the lower facility were larger than the standard deviations at other depths (Fig. 2.12a). Therefore outlier tests were conducted for those depths using Grubbs' approach as it is usually used for small sample sizes (Fig. B2a). It shows that the Grubbs' values of 84% of the SWC measurements from suspected sensors at 60, and 120 cm depth in the rainfed plot, and approximately 50% of the values at 40 cm in the irrigated plot were higher than the significance level of 0.05 since July 9. However, the Grubbs' values at the other three depths were much lower than the critical value, which means that the data were in the reasonable and acceptable range. We also found that the water contents measured by the suspected sensors were 0.1 to 0.2 cm^3 cm^{-3} lower than water contents measured by the three sensors. Also the Dixon and median absolute deviation approach, which are more robust for smaller sample sizes since they do not use the outlier values to calculate the mean or standard deviation, identified the same suspected sensors as outliers (Fig. B2b and B2c). Therefore, the SWCs at those three depths were removed for the subsequent analysis.

When comparing the water contents between different treatments, the time averaged water contents at 10 and 20 cm depth decreased, as expected, from the irrigated, rainfed to sheltered plots and were higher in the lower than in the upper facility (Fig. 2.12a and b). The temporal variations of soil moisture, especially in the topsoil responded quickly to the water treatments: increasing values were observed due to irrigation and rainfall and decreasing values because of root water uptake, evaporation, and drainage. For 40 and 80 cm depth, the water contents were also lower in the non-irrigated than in the irrigated plots of the upper facility. For the lower facility, the difference in temporally averaged water contents in the subsoil (40 cm and deeper) between the treatments was not consistent with the different amount of water that the treatments received. The water content in the subsoil of the irrigated plot was for instance lower than that in the sheltered plot even after removing the measurements of the suspected sensor. However, the difference must be compared with the SEM of the four (three when the suspected sensor was removed) soil water sensors, which is larger in the lower facility. Despite the fact that the temporal averages of the water contents in the different plots of the lower facility could not be linked to the water treatment of the plots, the observed temporal dynamics were consistent with the water treatments. The irrigation and larger rainfall events influenced the dynamics of the soil moisture in the deeper soil layers. In the non-irrigated plots, the water contents at 60 cm and deeper soil depth did not respond to the rain events until July 9 when the rainfall lasted for a week.

The weekly GPR ZOP measurements show lateral SWC changes along the MR tubes for different depths (not shown). To compare the obtained results with the TDR data, the data were averaged along the 6-m measurements to obtain one mean SWC value for each depth and plotted in Fig. 2.12 with red circles. Note that the TDR volume of investigation that was within one meter away from the facility wall could not be sensed by the GPR measurements obtained between 1 and 7 m away from the facility wall due to the interfering reflections of TDR cables. Despite the fact that TDR and GPR data cannot be compared directly, they show a similar trend but with GPR SWC being lower (Fig. 2.12c) than SWC derived from TDR.

SWP was monitored both by tensiometers and MPS-2(s). Tensiometers are usually used for measuring SWP for wet conditions whereas MPS-2(s) are employed for drier conditions. The measuring range of the tensiometers and MPS-2(s) are from 0 to -85 kPa and from -9 to -10^5 kPa,

respectively (Decagon Devices, 2016; UMS, 2011). The accuracy of the two sensors was ± 0.5 kPa and ± (25% of reading + 2 kPa) from -9 to -100 kPa, respectively. The values between -9 and -85 kPa measured by the two types of sensors at different depths were not always correlated as a result of the accuracy of MPS-2 in this range and the soil heterogeneity. When the water potential continuously decreased to -70 kPa without precipitation or irrigation, the values monitored by tensiometers levelled off. Therefore, the values between 0 to -70 kPa were chosen from tensiometers whereas the values lower than -70 kPa were picked from MPS-2 measurements for the subsequent analysis. The temporal variations of SWP in the different plots of the two facilities are shown in Fig. 2.13. For the topsoil, the SWP in the two facilities increased quickly to a high value (approximately -10 kPa or even higher) after the rain or irrigation events and then decreased subsequently. The decreases of the SWP in this soil layer of the lower facility were larger than those in the upper facility after each precipitation event due to the different soil properties. For the subsoil, the SWP decreased more in the non-irrigated than in the irrigated plot since less water infiltrated from the topsoil. The SWP at 120 cm, similar to the SWC, was not influenced by the different water treatments. SWP in the subsoil of the non-irrigated plots in the upper facility decreased to considerably lower values than in the subsoil of the lower facility. This indicates that plants in lower facility were less subjected to water stress since the water potential in the subsoil, where also the root density observed in the MR's was the largest, was not so low.

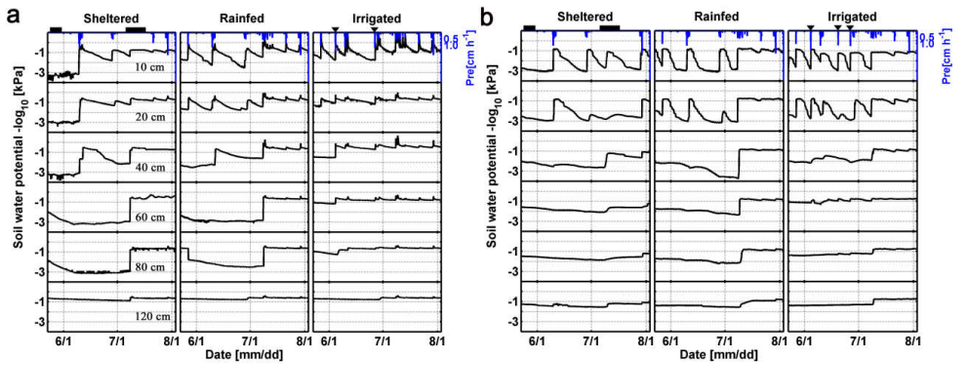

Fig. 2. 13 Time series soil water potential (SWP) at six soil depths in the sheltered, rainfed, and irrigated plots of the (a) upper and (b) lower facilities: sheltered period (■), irrigation (▼), precipitation (Pre).

Subsequently, the measured SWC and SWP in the three water-treated plots of the two facilities that covered a large range, from near saturated to wilting point, were used to describe the water retention characteristic of the soil. Figure B3 shows the soil water retention curves fitted by the van Genuchten (1980) model for the top- and subsoil of both facilities. The predicted saturated water contents for different soil layers were generally close to the highest water contents observed in the winter and the periods with frequent rain events. The fitting for the subsoil was not as good as that in the topsoil which might be mainly due to soil heterogeneity and the smaller range of measured water contents.

2.3.4 Soil temperature

The spatial and temporal variations of soil temperature at six depths in the three water-treated plots of the two facilities are shown in Fig. B4. The soil temperature and the amplitude between daytime and night decreased with increasing soil depths in both facilities. For the upper facility, the soil temperature at each depth of each plot was 1-2 ºC higher than that at the corresponding depths in the lower facility. The high stone content and lower SWC may account for the difference in temperature though the soil was exposed to the same weather conditions. High stone content changed the soil thermal conductivities and heat capacities (Nobel et al., 1992). Stones or rocks affect the heat in the immediate vicinity of the surrounding soil and act as heat sources at night. The different water treatments had furthermore a clear effect on the soil temperature and daily temperature fluctuations in the upper facility which were larger in the sheltered than in the irrigated plot.

2.4 Summary and conclusions

We presented two MR facilities that were constructed to investigate the effect of soil moisture and soil type on root development of agricultural crops under field conditions. Different soil moisture treatments were established by setting up sheltered vs rainfed vs irrigated plots in a stony and in a silty soil plot. Root development can be monitored in the facilities in horizontally

installed rhizotubes at 10, 20, 40, 60, 80, and 120 cm depth. A method to install these rhizotubes without excavating the soil so that the root development can be monitored in naturally structured soil was developed. Besides for monitoring root development, we demonstrated that the rhizotubes can also be used to map soil water distributions using crosshole GPR. Also four TDR sensors were installed in each water/soil treatment to measure soil moisture locally at the depths where the rhizotubes were installed. The local soil measurements within a treatment and depth varied considerably between the different TDR probes and for three out of the 36 soil texture/water treatment/depth combinations, outliers that were identified using statistical outlier detection method were excluded. The three replicates of 7-m-long rhizotubes that were installed in a soil treatment/depth combination allowed obtaining root observations at a large number of locations so that differences in root development between different treatments can be tested for statistical significance and spatial correlation. Root density was observed to be larger in the wet treatments and in the silty than in the stony soil. In the silty soil, the highest root densities were observed at 60-80 cm depth but not in the topsoil layer and the drier treatments showed higher root densities at greater depths than the irrigated treatment. No spatial correlation of root densities in the horizontal direction was observed for the investigated winter wheat crop. But, we anticipate that spatial correlations in root densities in a row crop (e.g., maize) could be observed in the rhizotubes.

Plant water stress depends rather on the soil water potentials in the root zone than on the water content. In order to measure soil water potentials also in the range when soil water potentials create water stress we installed two types of soil water potential sensors: classical tensiometers that measure water potential until -85 kPa and MPS sensors that can measure until -10^5 kPa. Especially in the upper part of the root zone, very low soil water potentials were measured. In order to evaluate whether this leads to a reduction in root water uptake, additional measurements that deliver direct or indirect information about the transpiration (e.g., sap flow and canopy surface temperature) are required and planned. It should finally be noted that soil temperatures were higher in drier treatments. To what extent this can be related to different soil thermal properties of the drier soil or to a smaller transpiration and hence smaller evaporative cooling requires further investigation.

Chapter 3

Parameterization of root water uptake models considering dynamic root distributions and water uptake compensation

This chapter is based on a journal article published as:

G. Cai, J. Vanderborght, V. Couvreur, C. Mboh, H. Vereecken. 2017. Parameterization of root water uptake models considering dynamic root distributions and water uptake compensation. *Vadose Zone J*. doi: 10.2136/vzj2016.12.0125

3.1 Introduction

Numerous root water uptake (RWU) models have been developed with different assumptions, complexity, and parameters but the description of this process and its parameterization remains challenging in soil hydrology (Kumar et al., 2014; Vereecken et al., 2015). Though it is commonly acknowledged that RWU is defined by water potential gradients and hydraulic resistances in the soil-plant system (Steudle and Peterson, 1998; Van den Honert, 1948), this principle is seldom included in models.

RWU models can be classified into two main classes: functional-structural vs. macroscopic models. The former class defines a root system architectural domain facilitating the inclusion of explicit root hydraulic features and associated physical concepts to simulate water flow towards individual roots (Doussan et al., 1998; Javaux et al., 2008). Their complexity is particularly appropriate to address questions of interactions between root growth and soil properties (Pagès et al., 2004; Somma et al., 1998), foraging for soil resources (Lobet et al., 2014; Lynch, 2013; Pagès, 2011) and plant responses in heterogeneous environments (Couvreur et al., 2014a; Huber et al., 2014).

In macroscopic models, RWU intervenes as a sink term in the soil water flow equation, without solving flow towards individual roots. Water uptake is typically assumed to be distributed proportionally to rooting densities and locally adjusted for water availability. The simplicity of this effective approach and the lower computing time are particularly suitable for applications at larger scales (Baram et al., 2016; Feddes et al., 2001; Oleson et al., 2008). However, the parameters and concepts used in these models are to a large extent empirical so that they cannot be linked to directly measurable properties of the root system. Recently, simple 1-D macroscopic expressions of RWU were derived based on small-scale hydraulic principles, respectively, in the soil around roots (De Jong Van Lier et al., 2008) and within the root system (Couvreur et al., 2014b). This allowed a revision of non-physical assumptions in macroscopic RWU models and linking their parameters to properties of the root system (Javaux et al., 2013).

The parameters of a functional-structural RWU model can be derived from direct measurements (e.g., root architecture, root hydraulic properties). However, these measurements are impractical

in the field and hence typically carried out in the lab on young plants (Doussan et al., 2006; Lobet and Draye, 2013; Steudle et al., 1987) that may not be representative of field conditions. Similarly, soil hydraulic properties can be directly measured or derived from measurements on relatively small soil samples following prescribed experimental protocols. But, soil heterogeneity makes it challenging to get representative properties of larger soil volumes, for instance, to describe processes at the field scale (Vereecken et al., 2015; Vereecken et al., 2010). Hence the interest in simpler approaches that rely on fewer parameters. These parameters are hardly measurable directly but can be fine-tuned so that models effectively behave like the real system, as commonly done in water management-oriented simulations (Asseng et al., 1998; Deb et al., 2011; Freundl et al., 1998; Hupet et al., 2002). In this context, inverse modeling is adequate to infer soil and root properties from *in-situ* measurements of soil water status (water contents and potentials) and fluxes (Šimůnek and Hopmans, 2009; Vrugt et al., 2001b; Wöhling et al., 2013). With optimization algorithms, inversion approaches search for effective parameter values that optimally reproduce field observations.

The distribution of RWU in the soil profile is greatly affected by the spatial-temporal root distribution. More specifically, RWU is generally assumed to be a direct function of root length densities (RLD) (Feddes et al., 2001; Heinen, 2014; Molz, 1981). So as to represent the interactions between root development and soil water status, the dynamics of root distributions need to be properly accounted for (Krounbi and Lazarovitch, 2011). However, most simulations of RWU use simplified descriptions to represent root growth and root distributions. Either a logistic or an empirical growth function (Borg and Grimes, 1986; Hoffman and Van Genuchten, 1983; Šimůnek and Suarez, 1993) is used to simulate the root development. A few studies simulated RWU using the measured root distribution obtained from soil cores in lysimeters or in field plots at the end of the crop cycle (Albasha et al., 2015; De Jong Van Lier et al., 2008). An important problem with observations of root distributions is that they often require destructive sampling so that the dynamics of root distributions are difficult to observe. Root length density distributions may be estimated from dynamic soil moisture measurements (Hupet et al., 2003; Hupet et al., 2002; Musters and Bouten, 1999; Musters and Bouten, 2000; Vrugt et al., 2001a) using inverse modeling. But, these studies also pointed at uncertainties that may arise when the soil hydraulic parameters are not well known. Therefore, direct measurements of RLD

distributions and their temporal dynamics are important additional information that can be used to constrain other parameters related to stress and water uptake compensation functions in RWU models. To monitor the evolution of root density profiles non-invasively, the rhizotube or minirhizotron method (Johnson et al., 2001; Rewald and Ephrath, 2012; Smucker et al., 1987; Volkmar, 1993) has been introduced. The observations from minirhizotrons helped to improve the understanding of root dynamics and functions (Garré et al., 2012), however, few studies used minirhizotron observations to estimate RWU and RWU model parameters (Wu et al., 1999).

The distribution of the RWU depends, besides on the root distribution, also on the water availability in the soil profile, which is linked to the soil water potential. When the soil dries out and the water potential decreases and becomes closer to the wilting point, the difference in water potential between the soil and the plant and consequently the RWU decreases. The relation between RWU, soil water potential, and transpiration demand is described by so-called stress functions (Feddes et al., 1978). It should be noted that more precise formulations, which are based on the matric flux potential and account for the difference between the bulk soil water potential and the water potential at the soil-root surface and in the root xylem, have been derived (De Jong Van Lier et al., 2008; de Jong van Lier et al., 2013).

Since the root system is a connected network, this reduction of RWU can be compensated by a higher uptake from wetter soil layers with a higher water potential, i.e., RWU compensation (Huang et al., 1997; Jarvis, 1989; Pang and Letey, 1998; Šimůnek and Hopmans, 2009). Skaggs et al. (2006) reviewed compensatory RWU mechanisms and simulations suggested that compensation can be of great importance when water potentials vary within the root zone. Actual RWU may be underestimated if compensation is not considered (Kuhlmann et al., 2012). However, the physical basis for the water stress and compensation functions that are currently used in macroscopic models, e.g., the Feddes-Jarvis functions (Feddes et al., 1978; Jarvis, 1989), and that are implemented in the unsaturated zone simulation model Hydrus-1D (Simunek et al., 2013), can be debated e.g., Javaux et al. (2013). For instance, the compensation term was defined in terms of the local water stress function whereas compensation represents the non-local nature of RWU, i.e. RWU at one location also depends on the water potential at other locations, and compensation may occur independently of water stress. Alternatively, physically based macroscopic stress and compensation functions can be derived from an analysis and upscaling of

functional-structural soil-root architecture models (Couvreur et al., 2014b; Couvreur et al., 2012; Javaux et al., 2013). Studies that tested and parameterized these different stress and compensation functions using field measurements are, however, scarce (Dong et al., 2010; Li et al., 2001) and have not been performed yet for the physically-based macroscopic model.

In this study, we focus on the Feddes-Jarvis (Šimůnek and Hopmans, 2009) and the Feddes (Feddes et al., 1978) models, which are often used for RWU simulations, and the physically-based macroscopic model, the Couvreur model (2012). The objectives of this paper are (1) to parameterize the soil hydraulic properties, water stress, and compensation functions of the three models, from time series of soil water status that were measured at six depths under growing winter wheat and using data of root distributions obtained from rhizotubes; and (2) to compare the transpiration fluxes and RWU profiles that are predicted by the calibrated models. We test whether the time series of water status can be described equally well by the different models and whether differences in RWU models can be compensated by a different parameterization of the soil hydraulic properties. We hypothesize that the inversely estimated parameters are consistent with literature data (Feddes-Jarvis model) and with parameters that are directly derived from a root architecture model (Couvreur model).

3.2 Theory

Spatial-temporal distributions of the water content in the soil are obtained from numerical solutions of the Richards equation which describes the water fluxes in the water balance equation using the Buckingham-Darcy equation and uses a sink term to represent RWU:

$$\frac{\partial \theta}{\partial t} = \frac{\partial}{\partial z}\left[K(h)\left(\frac{\partial h}{\partial z} + 1\right)\right] - S(z,t) \quad (3.1)$$

where θ represents the volumetric soil water content (SWC) [L^3L^{-3}], t is time [T], z is the elevation [L], h is the soil water pressure head (SWP) [L], K is the hydraulic conductivity function [LT^{-1}], and S is the sink term [$L^3L^{-3}T^{-1}$] defined as the volume of water removed from a unit volume of soil per unit time due to root extraction.

According to the van Genuchten–Mualem constitutive model (Mualem, 1976; Van Genuchten, 1980), the soil water retention and soil hydraulic conductivity functions are given by

$$\theta(h) = \begin{cases} \theta_r + \frac{\theta_s - \theta_r}{[1 + |\alpha h|^n]^m} & h < 0 \\ \theta_s & h \geq 0 \end{cases} \quad (3.2)$$

$$K(S_e) = K_s S_e^l [1 - (1 - S_e^{\frac{1}{m}})^m]^2 \quad (3.3)$$

where θ_r and θ_s are the residual and saturated water contents [L^3L^{-3}], respectively, S_e is the relative saturation: $S_e = \frac{\theta - \theta_r}{\theta_s - \theta_r}$ [-], and K_s is the saturated hydraulic conductivity [LT^{-1}]. The parameters α (L^{-1}), n, m (m = 1 - 1/n, n > 1), and l are empirical coefficients affecting the shape of the hydraulic functions.

3.2.1 Feddes and Feddes-Jarvis models

In the RWU model defined by Feddes et al. (1978), the sink term is a function of potential transpiration, the vertical root distribution, and the pressure head and is expressed as follows:

$$S_F(z) = \alpha_F(h)\, T_{pot}\, \mathrm{NRLD}(z) \quad (3.4)$$

$$\alpha_F(h) = \begin{cases} 0 & h \geq h_1, h \leq h_4 \\ \frac{h - h_1}{h_2 - h_1} & h_2 \leq h < h_1 \\ 1 & h_3 < h \leq h_2 \\ \frac{h - h_4}{h_3 - h_4} & h_4 < h \leq h_3 \end{cases} \quad (3.5)$$

$$T_{pot} = ET_{pot}\,(1 - e^{-kLAI}) \quad (3.6)$$

$$\mathrm{NRLD}(z) = RLD(z) / \int_0^{l_z} RLD(z)\,dz \quad (3.7)$$

where $\alpha_F(h)$ is the water stress response function ($0 < \alpha_F < 1$) [-], h_1 and h_4 the anaerobiosis and the wilting points above and below which RWU is null, respectively, h_2 and h_3 the pressure

heads between which RWU keeps the maximum rate, T_{pot} the potential transpiration [LT^{-1}], ET_{pot} the potential evapotranspiration [LT^{-1}], k a constant representing the extinction coefficient per unit leaf area (0.6 was used in this study) (Allen et al., 1998; De Faria et al., 1994; Mo and Liu, 2001), and LAI the leaf area index, NRLD the normalized root length density [L^{-1}], RLD root length density [LL^{-3}], and l_z the rooting depth [L]. Note that α_F depends also on T_{pot} since the critical point (h_3) is a piecewise linear function of T_{pot} (Simunek et al., 2013; Wesseling and Brandyk, 1985):

$$h_3 = \begin{cases} h_{3h} & T_{pot} > T_{3h} \\ h_{3h} + \frac{(h_{3l} - h_{3h})(T_{3h} - T_{pot})}{(T_{3h} - T_{3l})} & T_{3l} < T_{pot} < T_{3h} \\ h_{3l} & T_{pot} < T_{3l} \end{cases} \quad (3.8)$$

where h_3 is smaller (h_{3l}, more negative) for lower potential transpiration rates (T_{3l}) and higher (h_{3h}) for higher transpiration rates (T_{3h}). The dependency of h_3 on T_{pot} can be considered to effectively represent the higher pressure drop in the plant from the root system to the shoot under higher than under lower transpiration rates. Assuming that the pressure head in the shoots regulates stomatal closure and the stomatal closure will be triggered for higher SWPs when the transpiration rate is higher.

The stress function α_F, which reduces the water uptake at a certain depth, is a local function which only depends on the pressure head at that depth. However, since the root system is a connected network, RWU at a certain depth is influenced by pressure heads and uptake at other depths. To account for these non-local effects, a plant water stress index ω was introduced in the Feddes-Jarvis model which integrates the stress function over the root zone using the normalized root density function as a weighing function (Jarvis, 1989; Šimůnek and Hopmans, 2009):

$$\omega = \int_{l_z} \alpha_F(h)\, \mathrm{NRLD}(z) dz \quad (3.9)$$

It is assumed that as long as this plant stress index is above a certain threshold value, ω_c, the total RWU is equal to the T_{pot} and it decreases linearly with decreasing ω when ω is below ω_c:

$$\frac{T_{act}}{T_{pot}} = \begin{cases} 1 & \omega_c < \omega \leq 1 \\ \frac{\omega}{\omega_c} & \omega < \omega_c \end{cases} \quad (3.10)$$

where T_{act} is the actual RWU [LT^{-1}]. Therefore, RWU at a certain depth in the Feddes-Jarvis model is obtained by combining Eq. 3.4 and 3.10:

$$S_{FJ}(z) = \alpha_F(h)\,\mathrm{NRLD}(z)\,T_{pot}\,\frac{1}{max(\omega,\ \omega_c)} \quad (3.11)$$

The parameter ω_c controls the ability of the plant to compensate reduced water uptake at a certain depth by increasing water uptake in the root profile. For $\omega_c < 1$, water uptake is, in fact, increased in all depths compared to the case when no uptake compensation is considered, which corresponds to $\omega_c = 1$. However, the increase is larger in the wetter parts of the root zone where $\alpha_F(h)$ is larger.

3.2.2 Couvreur model

A new 3-D macroscopic RWU model based on root system hydraulic architecture and the analytical solution of the flow equation in the root network was developed by Couvreur et al. (2012), in which parameters were not defined at root segment scale but at the soil element or the plant scale. For densely sown crops such as wheat, the 3-D high-resolution model can be upscaled to a 1-D model (Couvreur et al., 2014b). The 1-D model describes gradient-based water flow in the coupled soil-root architecture considering the hydraulic conductance of the soil-root system and is expressed by the following equations:

$$S_C(z) = K_{rs}\,(h_{Te} - h_{Tleaf})\,\mathrm{NRLD}(z) + K_{comp}\,(h_T(z) - h_{Te})\,\mathrm{NRLD}\,(z) \quad (3.12)$$

$$\text{where } \begin{cases} K_{rs}\left(h_{Te} - h_{Tleaf}\right) = T_{pot} & when\ h_{Tleaf} > h_{Tleaf\_crit} \\ K_{rs}\left(h_{Te} - h_{Tleaf\_crit}\right) = T_{act} & else \end{cases} \quad (3.13)$$

$$h_{Te} = \int_0^{l_z} h_T(z)\,\mathrm{NRLD}(z)\,dz \quad (3.14)$$

where K_{rs} is the 1-D equivalent conductance of the root system [T^{-1}], K_{comp} the compensatory RWU conductance of the plant [T^{-1}], h_T the total soil hydraulic head (pressure head plus elevation head: h + z) [L], h_{Te} the effective root zone hydraulic head sensed by the plant [L], h_{Tleaf} the leaf water hydraulic head [L], which can be obtained from Eq. 3.13: $h_{Tleaf} = h_{Te} - T_{pot}/K_{rs}$, h_{Tleaf_crit} a critical leaf hydraulic head that is constant by stomatal regulation in isohydric plants (Tardieu and Simonneau, 1998). Coupling to a leaf stomotal model, the anisohydric behaviour could also be properly accounted for in this macroscopic model (Huber et al., 2015).

According to Eq. 3.12, RWU is split into two components: an uptake component that corresponds to the uptake from a profile in hydrostatic equilibrium with a homogeneous hydraulic head and a compensatory component that describes the increase/decrease of local water uptake due to a locally higher/lower hydraulic head than the effective hydraulic head h_{Te}. In contrast to the original models of Couvreur et al. (2012), we used the normalized RLD functions, NRLD(z), to describe the RWU in a soil profile with uniform hydraulic head and to weigh the local h_T for the calculation of h_{Te}. Couvreur et al. (2014b; 2012) demonstrated that the weighting function used in Eq. 3.12 and 3.14 might deviate from NRLD(z) depending on the hydraulic parameters (radial conductivity, axial conductance, etc.) of the root segments.

3.3 Materials and methods

3.3.1 Measurements

Root distributions, SWC, and soil water potential were measured in a cropped field in Selhausen (50°52'N, 6°27'E), Germany. The field is slightly inclined with a slope less than 4°, and the soil is characterized by a strong gradient in soil texture with 60% gravel content at the upper slope and 4% in the down slope, respectively (Vanderborght et al., 2010). At the site, two minirhizotron facilities were constructed, one at the upper and one at the lower site of the field. In each facility, three 7 m by 3 m plots: a rain sheltered, a rainfed and an irrigated plot were established. The construction of the facilities and the technical details of the instrumentation were described in a technical note (Cai et al., 2016). Since the objective of this paper is to compare the performance of different RWU models and to evaluate a procedure to determine

their parameters by inverse modeling, we focus in this paper on data from the sheltered plot in the upper facility with the stony soil. In later work, we will evaluate the effect of the treatments and the soil types on root development and parameters of RWU models. Winter wheat (*Triticum aestivum*) was sowed with a seed density of 300 – 320 grains m^{-2} on 30 Oct. 2013 and harvested on 17 July 2014. The fertilizer rate of 120 kg N ha^{-1} (KAS 27) was applied on 21 Mar., and 60 kg N ha^{-1}, 30 kg P ha^{-1} (P_2O_5), and 116 kg K ha^{-1} (K_2O) were applied on 6 May 2014. After completion of stem extension, plots were covered at four times during rainy periods (6 May – 15 May, 21 May – 23 May, 25 May – 28 May, and 4 July – 15 July) and approximately 197.2 mm of rainfall was sheltered out. One irrigation event with 14.7 mm was applied on 9 June 2014.

Soil water content and soil water potential were monitored hourly by the own-made time domain reflectometer (TDR) probes (Cai et al., 2016; Weihermuller et al., 2013), tensiometers (T4e, UMS GmbH, München, Germany), and dielectric water potential sensors – MPS-2 (matrix water potential and temperature sensor, Decagon Devices Inc., UMS GmbH München, Germany), respectively. The sensors were installed at 10, 20, 40, 60, 80, and 120 cm depth. Soil water content was presented as the mean of the data that were monitored by the four TDR sensors at each depth. Root development was observed in 7-m-long rhizotubes (clear acrylic glass tubes with outer and the inner diameter of 64 mm and 56 mm respectively) of which three replicates were horizontally installed at the same depths as the SWC sensors. Soil water potential was converted to soil water pressure head (SWP) in the later simulation. There was a horizontal offset of 0.1 m between rhizotubes at different depth levels to make sure that rhizotubes at a certain depth were not overlain by rhizotubes at other depths. Root measurements were carried out repeatedly from both left and right sides of the rhizotubes at 20 locations along each tube by a digital camera (Bartz Technology Corporation, Carpinteria, CA, USA). The images with the size of 16.5 mm by 23.5 mm were analyzed with Rootfly (Wells and Birchfield, 2009).

Generally, RLD is expressed as root length per unit volume of soil (LL^{-3}) but in the rhizotubes the number of roots or the root length in an observation window is observed. This corresponds with a root length per surface or root number per surface. These observations can be translated into a root length per volume by multiplying the root length per surface with a soil depth factor that represents the ‘observation depth’ from the tube surface. Upchurch (1987) indicated that the observed soil depth from the tube surface ranged from 1 to 3 mm according to the soil texture.

Steele et al. (1997) used 2 mm for coarse sand soil and Garré et al. (2011) used 1 mm for loamy sand. However, this depth of view from the tube is arbitrary. Machado et al. (2003) used root intensity instead, being root length per unit area (LL^{-2}) that was observed from rhizotubes. However, a problem with root length observations around rhizotubes is that root growth may be affected by disturbances at the rhizotube surface and therefore not representative for root length densities in the bulk soil. Therefore, Garré et al. (2012) used root impacts (total primary root counts per observed area) on the rhizotubes. The relation between root impacts and RLD depends on the geometry of the root system (Vansteenkiste et al., 2014) but is not influenced so strongly by the presence of the rhizotubes. In order to relate the impacts to RLD, we assumed that RLD and impact are proportional and that the proportionality factor does not depend on the observation depth, which is an approximation. The proportionality factor cancels out when calculating the normalized root length density (NRLD) so that it does not need to be defined.

Root measurements were carried out 22 times weekly from 11 Feb. (tillering period) until 14 July 2014 (ripening period). Weekly measurements were frequent enough to capture the behavior of root development (Vamerali et al., 2012). Figure 3.1 shows the distribution of the normalized root length densities. At the beginning of the observation, roots reached the tubes at 40 cm and the RLD decreased with increased soil depths. The value of NRLD decreased at the shallow depths (e.g., 10 and 20 cm) and increased at deeper depths (e.g., 40 cm) as roots developed. It must be noted that the decrease in NRLD in the upper soil layers (10 – 20 cm depth) was not only due to an increase in root density in lower layers but also due to root decay.

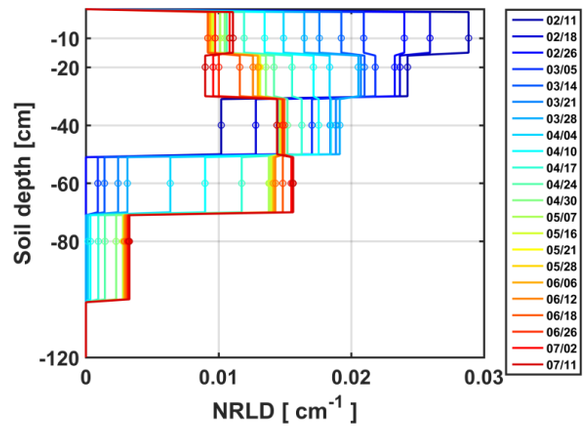

Fig. 3. 1 Spatial and temporal distribution of normalized root length density (NRLD) along the soil profile for 22 weekly measurements. The circles are the measurement locations.

Leaf area index was measured by a plant canopy analyzer (LAI-2200, LI-COR, Inc. USA) (Fig. 3.2). The meteorological data, e.g., global and net radiation, precipitation, air temperature, wind speed, and relative humidity were monitored at 2 m above the soil level at a 10-minute interval in the mini-weather station that was 140 m away from the test site. During the experimental period from 11 Feb. 2014 until 14 July 2014, the amount of precipitation was 312.6 mm. The potential crop evapotranspiration was obtained using the Penman-Monteith equation (Allen et al., 1998):

$$ET_{pot} = K_c * ET_o \tag{3.15}$$

where ET_o is the reference evapotranspiration [LT^{-1}], and K_c the crop coefficient [-]. The K_c's for the different plant development stages with corrections for wind speed, the minimum daily relative humidity, and the crop height were obtained from Allen et al. (1998). The potential transpiration and potential evaporation (E_{pot}) were separated by Eq. 3.6 and Eq. 3.15, and the hourly variations during the measurement period are shown in Fig. 3.2.

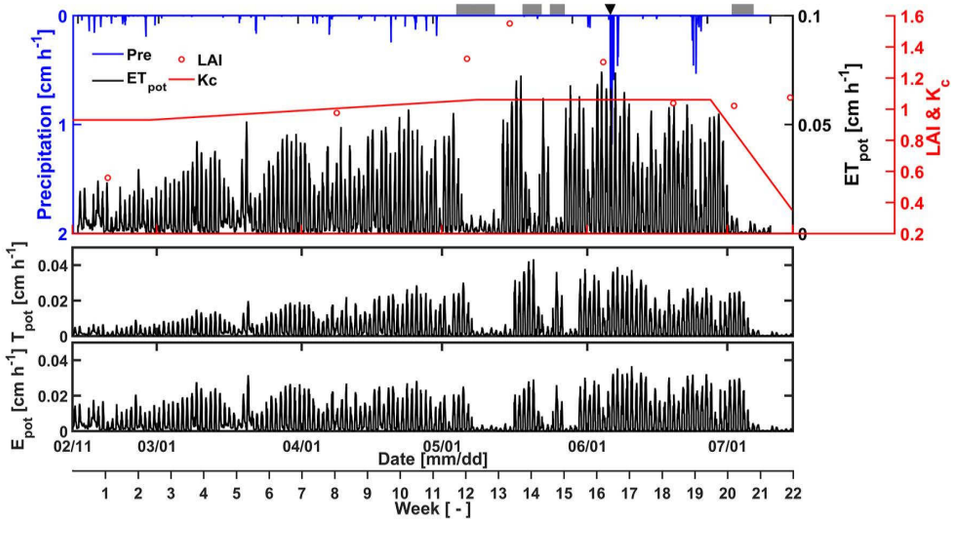

Fig. 3. 2 Variations of precipitation (blue), potential evapotranspiration (ET_{pot}: black), leaf area index (LAI: red dots), and crop coefficient (K_c: red line). ■: sheltered periods, ▼: irrigation (14.7 mm)

3.3.2 Model setup and simulation runs

For the numerical simulations, we considered a 145 cm deep soil profile which was discretised into the 1-cm-thick intervals. Two soil layers with different soil hydraulic parameters: 0 – 30 cm (the tillage layer) and 30 – 145 cm were considered. The parameters of the water retention curve θ_r, θ_s, α, and n were obtained from fitting Eq. 3.2 to observed SWC and SWP in the two soil layers and are listed in Table 3.1 (see Cai et al., 2016).

Table 3. 1 Hydraulic parameters of the Mualem-van Genuchten functions: residual soil water content, θ_r, saturated soil water content, θ_s, curve fitted parameters, α and n.

Depth (cm)	θ_r ($cm^3\ cm^{-3}$)	θ_s ($cm^3\ cm^{-3}$)	α (cm^{-1})	n (-)
0-30	0.0430	0.3256	0.0361	1.3860
30-120	0.0534	0.2286	0.0495	1.5340

Other parameters (e.g., K_s, l) were obtained by inverse modeling. Therefore, the Hydrus model (Šimůnek et al., 2016) was used to solve the Richards equation and simulate the water potentials and water contents that were compared with measured values to derive the parameters in the three models. An atmospheric boundary with surface layer and free drainage were used as upper and lower boundary conditions, respectively. For the upper boundary, the parameter *hCritA*, which defines the minimal pressure head that can be reached at the soil surface, was estimated using inverse modeling. The value of *hCritA* could be obtained from the air humidity (Feddes et al., 1974) but this would lead to values much lower than the permanent wilting point. It has been suggested that *hCritA* ranges from -150 m to -1000 m for different soil textures (Simunek et al., 2013). For the evaporation from a soil surface on which a crop is growing, the resistance for vapor transfer from the soil surface into the air also contributes to the reduction of evaporation, which is not considered in the splitting of the evapotranspiration into evaporation and transpiration (Eq. 3.6). Therefore, we considered optimizing *hCritA* in the simulations.

The parameters K_s and l of the two soil layers were obtained using inverse modeling. To avoid the physically unrealistic behavior with $dK/d\theta < 0$, we constrained the lower boundary for l by the criterion given by Lambot et al. (2002):

$$l > -2 \frac{(1-S_e^{\frac{1}{m}})^{m-1} S_e^{\frac{1}{m}}}{1-(1-S_e^{\frac{1}{m}})^m} \tag{3.16}$$

For the RWU parameters, the following parameters were kept fixed: $h_1 = 0$, $h_2 = -1$ cm, $h_4 = -16000$ cm (Wesseling, 1991), $h_{Tleaf\_crit} = -16000$ cm (we set z = 0 at the soil surface and defined the critical collar hydraulic head). We decided not to fit h_{Tleaf_crit}, T_{3h}, and T_{3l} since these parameters are generally assumed not to vary between different crops (Kropff and Van Laar, 1993; Nelsen et al., 1978; O'Toole and Moya, 1981; Shimshi, 1979). T_{3h} and T_{3l} were set to 0.02 cm h^{-1} and 0.004 cm h^{-1}, respectively (Groh et al., 2016; Yang et al., 2009).

We considered three different inverse modeling setups: case 1, Feddes-Jarvis Model with inverse estimation of ω_c, h_{3h}, and h_{3l}; case 2: Feddes model (no compensation, ω_c =1) with inverse estimation of h_{3h} and h_{3l}. For the Couvreur model, case 3, K_{rs} and K_{comp} were optimized. However, K_{rs} and K_{comp} depend on the root architecture and increase when the root system grows

(Doussan et al., 2006; Pierret et al., 2006). We assumed that K_{rs} and K_{comp} were proportional to the total root length so that their values at the ith week could be calculated from the initial K_{rs_ini} or K_{comp_ini} and the integrated root lengths (IRL) at the ith week and at the start of the observations as:

$$K_{rs,i} = K_{rs\_ini} \frac{IRL_i}{IRL_{ini}} \tag{3.17}$$

where IRL is:

$$IRL = \int_{Lr} RLD(z)dz \tag{3.18}$$

We optimized K_{rs_ini} and K_{comp_ini} of the first week.

The simulations were run with hourly boundary conditions for 154 days from 11 Feb. to 14 July 2014. As initial conditions, the pressure heads measured at the start of the simulation period were used. We assumed that the root distribution in every soil layer was constant over 7 days. Since only one root distribution can be used as input in Hydrus-1D, 22 input files (each covering a time span of one week) were created for 22 successive Hydrus-1D simulations. The simulated SWP profile at the end of each week was used as initial condition for the simulation of the next week.

The procedure of the inverse modeling and simulations is depicted in Fig. 3.3. Before performing the simulations of RWU, candidate values for two soil hydraulic parameters $K_{s(1,\,2)}$ and $l_{(1,\,2)}$ of the top- and subsoil, h_{3h}, h_{3l}, ω_c, K_{rs_ini}, and K_{comp_ini} were sampled by the optimizer (described in the following paragraph) at the beginning of the 1st week. The simulations were performed separately in Hydrus for the Feddes-Jarvis, the Feddes, and the Couvreur models. Note that executable Hydrus files for the Feddes and the Couvreur models are different (a modified H1D contains the Couvreur model). For each newly started simulation, new candidate parameters $K_{s(1,\,2)}$, $l_{(1,\,2)}$, ω_c, h_{3h}, h_{3l}, K_{rs}, and K_{comp} were sampled from uniform distributions with the boundaries given in Table 3.2.

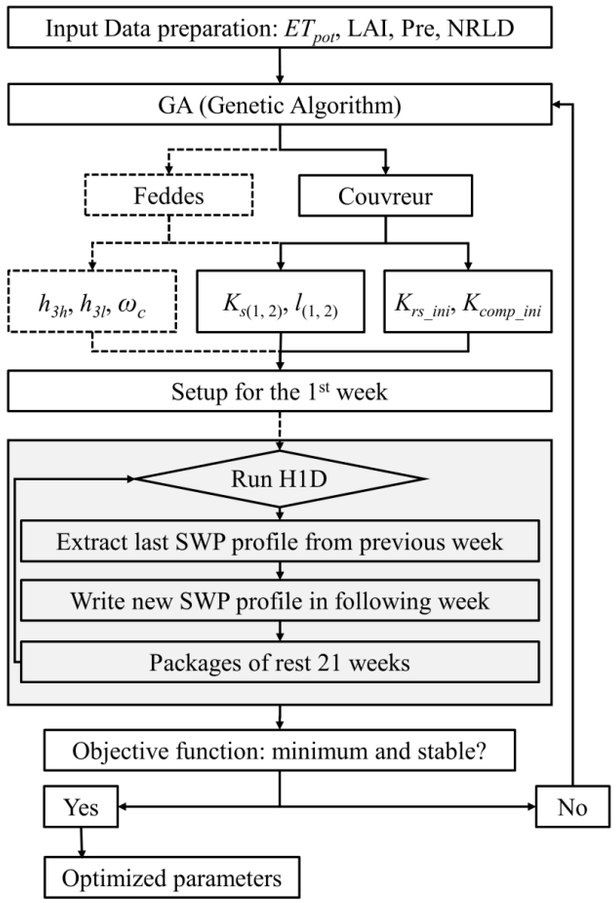

Fig. 3. 3 Procedure of optimizations of soil hydraulic parameters by the Feddes-Jarvis /Feddes (dashed lines) model and K_{rs}, K_{comp} by the Couvreur model (solid lines) in Hydrus-1D framework, and sequential simulations of RWU with observed dynamic root distributions. ET_{pot}, potential evapotranspiration; LAI, leaf area index; Pre, precipitation; NRLD, normalized root length density; h_{3h} and h_{3l}, water potential at high and low transpiration; ω_c, root adaptability factor; K_s, saturated conductivity; l, pore-connectivity; 1, 2: top- and subsoil; K_{rs_ini}, equivalent conductance of the root system in the 1st week; K_{comp_ini}, compensatory RWU conductance of the roots in the 1st week; H1D, Hydrus-1D.

Table 3. 2 Boundaries of the soil hydraulic parameters in the top- and subsoil, pressure heads at high and low transpiration rates in the Feddes model, and root system / compensatory root water uptake conductance in the Couvreur model.

Parameters	unit	Lower bound	Upper bound
†$\log_{10}(K_{s1,2})$	cm h^{-1}	-1.8802	0.9198
$l_{1,2}$	-	-4.000	6.000
†$log_{10}(\|hCritA\|)$	cm	2	4.5
h_{3h}	cm	-700	-200
h_{3l}	cm	-1500	-600
ω_c	-	0	1
†$\log_{10}K_{rs}$	h^{-1}	-6.480	-4.880
†$\log_{10}K_{comp}$	h^{-1}	-7.880	-5.380

†The $\log_{10}$-transformed values were transformed back to the normal form in the subsequent inverse modeling and simulations.

In the inverse modeling steps, the optimum parameters were obtained by systematically minimizing the deviations between the observed (*Obs*) and simulated (*Sim)* variables. The considered variables were: SWC, difference of SWC over a time period (*d*SWC); SWP, difference of SWP over a time period (*d*SWP); Sto, water storage (integration of SWC from 0 to 125 cm); *d*Sto, difference of water storage between each time and the first time; cumT ($cumT_{pot}$: Obs, $cumT_{act}$: Sim; note that T_{act} is actual RWU). To avoid the impact of noise on the variables that represent changes over time, differences between observations (*d*SWC and *d*SWP) were calculated over 4, 10, and 25 days to represent the short-, medium-, and longer-term changes. The deviations between measured and simulated values were evaluated using the following objective function (OF) that aggregates normalized root mean squared errors of the different considered variables (Baram et al., 2016):

$$\mathrm{OF} = \sum_{j=1}^{J} \frac{\sqrt{\sum_{i=1}^{N_j} (Sim_{i,j} - Obs_{i,j})^2 \, w_{i,j}}}{\overline{obs_{i,j}}} \, p_j \qquad (3.19)$$

where j refers to the number of variables and i to the number of the measurement in the dataset of variable j that contains N_j measurements. The weights w were defined as:

$$w_{i,j} = \begin{cases} \frac{1}{N_j} & \text{variable (SWC, SWP, Sto, cumT)} \\ \frac{|Sim_{i,j}|+|Obs_{iEj}|}{\sum_{iE}^{N_j}(|Sim_{i,j}|+|Obs_{i,j}|)} & \text{changes of the variable (} d\text{SWC}, d\text{SWP}, d\text{Sto)} \end{cases} \quad (3.20)$$

For the variables SWC, SWP, Sto, and cumT, equal weight was given to each measurement whereas *d*SWC, *d*SWP, and *d*Sto were weighted proportionally to the amplitude of the variables so that large variations (e.g., a jump in SWC after a precipitation event) were attributed more weight. In contrast, small fluctuations (e.g., scattering in monitoring) contributed less to the OF. For instance, when neither measurements nor simulations fluctuate at a particular depth, extra weight is attributed to other depths and times in order to focus on most informative parts of the signal (Baram et al., 2016). The weighted root mean square errors of each variable were normalized by the mean absolute values of the corresponding variable, $\overline{Obs}$, so as factor out the impact of the different dimensions of the terms in the aggregated objective function. The weights of the different variables in the aggregated objective function (p) were chosen somewhat arbitrarily as: SWC: 10%, *d*SWC: 10%, SWP: 30%, *d*SWP: 15%, Sto: 15%, *d*Sto: 15%, cumT: 5%. The total weight attributed to soil moisture measurements (50%) was partitioned between local (SWC and *d*SWC) and integrated observations (Sto and *d*Sto). While the former aims at minimizing absolute differences in individual layers, they do not suffice at minimizing absolute deviations from the overall soil water balance, which is the role of the latter variables in the OF. The variable cumT was included in the objective function with a minor weight in order to limit deviations between potential and actual cumulative transpiration. This was necessary to avoid the undesired drift of the optimizer towards parameter sets predicting extreme water stress events during the whole simulation period (even at spring time when rainfall was abundant).

To minimize the OF, the forward simulations were combined with genetic algorithm (GA) from the global optimization toolbox of Matlab 2015b (main functions: ga, gaoptimset) (MathWorks, 2015) with 100 parameter sets as initial population. To test the matches between the measured and predicted parameters by the three models, the comparisons were evaluated by root mean square error (RMSE), the mean bias error (ME) (Shen et al., 1998), and an index of agreement (d, dimensionless) (Willmott et al., 1985). They are defined as follows:

$$\text{RMSE} = \sqrt{[\sum_{i=1}^{N}(Sim_i - Obs_i)^2]/N} \quad (3.21)$$

$$\text{ME} = [\sum_{i=1}^{N}(Sim_i - Obs_i)]/N \quad (3.22)$$

$$d = 1 - [\sum_{i=1}^{N}(Sim_i - Obs_i)^2]/[\sum_{i=1}^{N}(|Sim_i - \overline{Obs}| + |Obs_i - \overline{Obs}|)^2] \quad (3.23)$$

To evaluate the uniqueness of the inversely estimated parameters, Bayesian statistics can be used to derive posterior probability distributions of the optimized parameters (Vrugt and Ter Braak, 2011). However, because of computational limitations, we were not able to apply these methods. In order to get an appraisal of the confinement of the parameters, response surfaces of the objective function (Eq. 3.19) were generated using possible combinations of two selected parameters while keeping the other parameters at their optimized values (Simunek et al., 1998; Toorman et al., 1992). The response surfaces illustrate the sensitivity and the correlations between parameters and whether the estimated values are in a local or global minimum. The range of each parameter was subdivided into 50 intervals so that response surfaces were constructed from a grid of OF values with 2500 grid points.

3.3.3 Scenarios investigated

In order to evaluate the effect of RWU compensation on the simulated transpiration, we considered a scenario in which parameters were equal to the optimized parameters of the Feddes-Jarvis model but with $\omega_c = 1$. The difference between this scenario (F_{w1}) and the simulations with the optimized Feddes-Jarvis (FJ) model better represents the effect of RWU compensation than the difference between the optimized Feddes-Jarvis and Feddes (F) models. RWU compensation could be partly accounted for in the Feddes model by adapting stress and soil hydraulic parameters.

The soil at the test site is quite stony and has a low water holding capacity (see the low θ_s in Table 3.1, especially in the subsoil). The saturated conductivity K_s of such a soil depends strongly on the stone content (Novák et al., 2011). To evaluate the effect of K_s on the simulated

transpiration, we carried out a second sensitivity analysis. The transpiration was simulated using optimized root parameters of the different water uptake compensation models for a range of K_s values obtained from the literature and representing soil textures from sandy loam to silty clay (Carsel and Parrish, 1988).

3.4 Results and discussion

3.4.1 Simulation of soil moisture and water fluxes using optimized parameters

The time courses of observed and simulated SWC and SWP that were simulated by the Feddes model with (FJ) and without compensation (F and F_{w1}) and by the Couvreur model using the optimized parameters are depicted in Fig. 3.4 at six soil depths and at daily time scale for the observation period. Using the time series of measured root distributions, SWCs, and SWPs simulated by both models responded well to the hydrologic changes: gradual decreases during dry spells and rapid increases due to the precipitation and irrigation events. However, discrepancies also exist. The absolute values of SWPs at 10 cm from mid-April to mid-May and at 80 cm during June were underestimated. The SWC in the topsoil and the SWP in the whole soil profile was not well described after the last rain event (on the right side of the vertical dashed line in Fig. 3.4) when the shelter was partly uncovered because of a thunderstorm, likely causing an offset between measured and actual infiltration rates. In the inverse modeling, this part was thus not considered (the vertical dashed line marks the end of the optimization period). Visually, there was no obvious difference between the simulations that were modeled by the Couvreur and the Feddes models with and without compensation. The different models simulated also similar differences *d*SWC and *d*SWP (see for instance *d*SWC and *d*SWP over a 4-day period in Fig. C1).

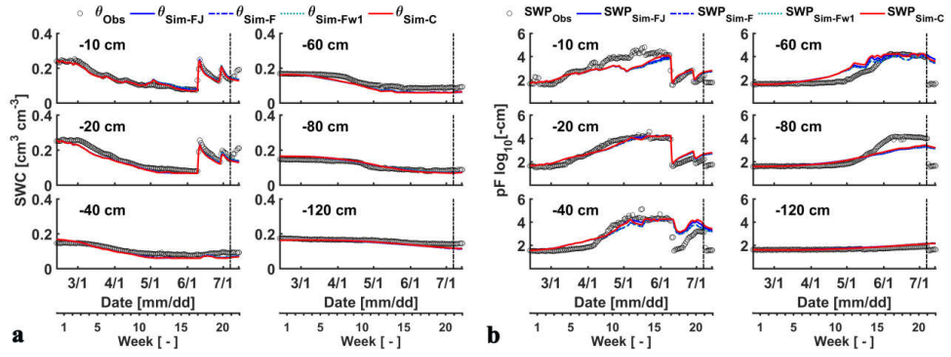

Fig. 3. 4 Comparison of soil water content (SWC) (a) and soil water pressure head (SWP, absolute value in cm) (b) over a day at six soil depths between observation (θ_{obs}, SWP_{obs}) and simulation (θ_{Sim}, SWP_{sim}) by the Feddes model with and without compensation, and without compensation, and by the Couvreur model. FJ: Feddes-Jarvis, F: Feddes without compensation, F_{w1}: Feddes-Jarvis but $\omega_c = 1$, C: Couvreur.

The cumulative RWU and the water flux that were simulated by the Feddes (FJ, F, and F_{w1}) and the Couvreur models with the optimized soil hydraulic parameters, pressure heads in the Feddes stress function, and root related parameters in the Couvreur model are illustrated in Fig. 3.5. Until the early May, the actual RWU rate simulated by the models equaled the potential rate, gradually increasing from 0.05 cm d^{-1} to 0.2 cm d^{-1} (Fig. 3.5a). Then the potential RWU rate increased continuously in the period without sheltering (in the middle of May) and decreased in the middle of June. The actual RWU simulated by the Feddes model with compensation was not able to meet the atmospheric demand from week 12 (Fig. 3.5a), whereas without compensation the RWU was constrained one week earlier. There was no water stress in RWU simulated by the Couvreur model until week 12. The delayed water stress in models with compensation is due to the fact that a local water limitation in soil implies a redistribution of water uptake, but not necessarily a reduction of transpiration (as it would in F and F_{w1}). In the Couvreur model, any soil water potential variation with depth generates redistribution, as in a hydraulic network, which tends to equilibrate soil water potential and thus delays the occurrence of water stress more than FJ. The estimated RWU by the Feddes model with (FJ) or without (F, F_{w1}) compensation followed the daily (or hourly, data not shown in the plots) variations of the T_{pot} during the water stressed and non-stressed periods, whereas for the Couvreur model transpiration under water stress (e.g., from week 14 to 18 in Fig. 3.5a) was higher before noon as typically

observed experimentally (Dodd et al., 2008). The cumulative actual RWU simulated by the Feddes model with and without compensation, and by the Couvreur model accounted for, respectively, 78.84 %, 78.81% (75.08% for F_{w1}), and 81.11% of the cumulative potential water uptake in the whole observation period (Fig. 3.5b). The estimated cumulative soil evaporation matched the cumulative potential soil evaporation until March 9, when the falling rate phase started. At the end of the observation, the cumulative evaporation simulated by the Couvreur model equaled that by the Feddes model with compensation, but both were slightly (4 mm) lower than that by the Feddes model without compensation. The drainage simulated by the Couvreur model was slightly (2 mm) lower than that by the Feddes model from middle of April to middle of May, but there was no difference at the end of the simulation period. Water storage derived from SWC measurements and from simulations is shown in Fig. 3.6. The water storage derived from observed SWC and simulations corresponded well except for the short time at the beginning with 1.7 cm higher storage for the simulations. At the end of the optimization period, the simulated storage was 1 cm lower than that derived from the measurements. It should be noted that the observed storage is derived from interpolation of soil moisture measurements at 6 depths in the soil profile, which might be the reason for the deviations between the storage derived from simulations and measurements.

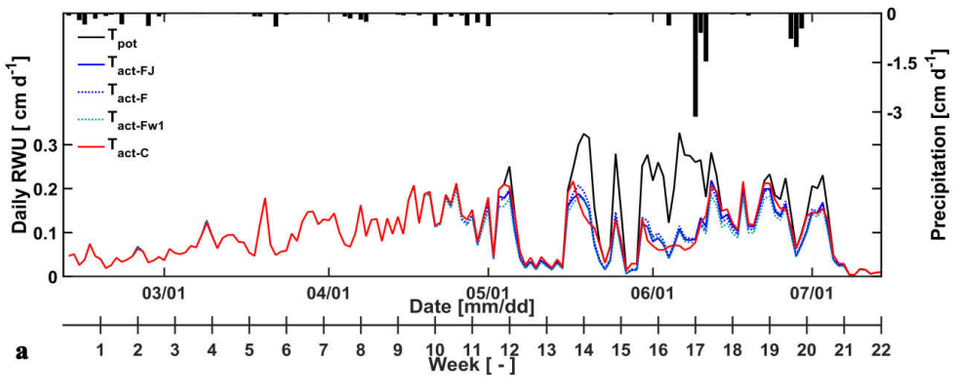

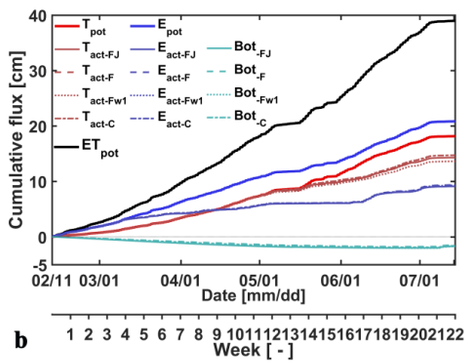

Fig. 3. 5 (a) Comparisons between potential daily transpiration (T_{pot}), actual root water uptake (T_{act}) simulated by the Feddes (FJ, F, and F_{w1}) and the Couvreur (C) models; (b) Comparisons between cumulative ET_{pot}, T_{pot}, T_{act}, E_{pot}, E_{act}, and bottom flux (Bot) simulated by the Feddes (FJ, F, and F_{w1}) and the Couvreur (C) models in the whole period. The gray rectangle and the triangle are sheltering periods and irrigation event, respectively.

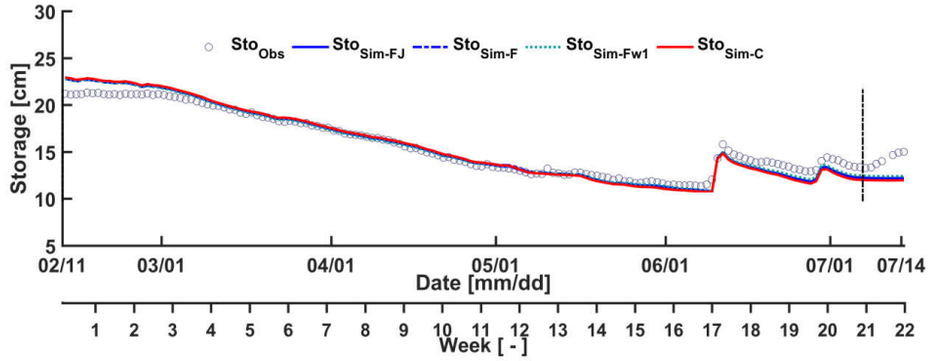

Fig. 3. 6 Time evolution of the water storage (Sto) that was calculated from soil moisture measurements and simulated by the Feddes (FJ, F, and F_{w1}) and the Couvreur (C) models.

Overall, the measured and simulated data matched well for both models at the six soil depths. We did not observe systematic differences between the Feddes (with and without compensation) and the Couvreur models. This can be seen in Fig. C2 which shows the RMSE, ME, and *d* for the Feddes (FJ, F, and F_{w1}) and the Couvreur models. The RMSE of SWC and SWP were no larger than 0.02 cm^3 cm^{-3} and 0.6 in pF ($\log_{10}$ (|h| cm)) units respectively, indicating that the simulation errors were quite small. The distribution of ME depicted that SWC at 20, 40, 60, and 120 cm was

slightly ($\leqslant$ 0.02 cm^3 cm^{-3}) underestimated (SWP was overestimated $\leqslant$ 0.4 in pF units), and that the water storage was slenderly ($\leqslant$ 1 mm) overestimated. Also, the difference of water content (*d*SWC), water potential (*d*SWP), and water storage (*d*Sto) were well predicted by all the models. The smaller coefficients of agreement, *d*, at greater depths are due to the small temporal changes at these depths.

3.4.2 Optimized parameters of the two root water uptake models

The optimized parameters of the Feddes (both Feddes-Jarvis and Feddes) and the Couvreur models are listed in Table 3.3. The optimized soil hydraulic parameters that were obtained using the Feddes-Jarvis model with compensation and using the Couvreur model were very similar but deviated from the soil parameters that were obtained when using the Feddes model without compensation. The value of K_s was much smaller in the subsoil than in the topsoil. This may due to the high stone content with non-uniform size (Thoma et al., 2014) and the compaction of the soil during the construction of the plot (Cai et al., 2016). This soil condition creates heterogeneity and strongly affects soil hydraulic properties. Hydraulic conductivity decreased when the stone content increased (Novák et al., 2011). The parameter *l* was positive in the upper and negative in the lower soil layers. To some extent, negative *l* may be considered to be 'unphysical' because it implies that tortuosity decreases when the soil dries out. Negative *l* was also obtained for other soils (e.g., Schaap and Leij, 2000; Yates et al., 1992), which shows that this parameter is rather a shape factor than a physically based parameter.

Table 3. 3 Optimized soil hydraulic parameters, including saturated hydraulic conductivity ($K_{s1,2}$) and empirical coefficient ($l_{1,2}$) in the top- and subsoil, minimum pressure head at the soil surface (*hCritA*), pressure heads at high (h_{3h}) and low (h_{3l}) transpiration rates, and the critical water stress threshold ω_c and initial root system (K_{rs_ini}) or compensatory (K_{comp_ini}) root water uptake conductance in the Feddes (F), Feddes–Jarvis (FJ), and Couvreur (C) models.

Model	K_{s1} (cm h^{-1})	l_1 (-)	K_{s2} (cm h^{-1})	l_2 (-)	*hCritA* (cm)	h_{3l} (cm)	h_{3h} (cm)	ω_c (-)	K_{rs_ini} (h^{-1})	K_{comp_ini} (h^{-1})
FJ	3.417	1.470	0.026	-2.797	-7434	-1172	-648	0.8	-	-
F	2.529	1.084	0.015	-3.274	-5633	-1194	-685	1(fixed)	-	-
C	3.853	1.472	0.021	-2.892	-9120	-	-	-	3.792×10^{-7}	1.125×10^{-7}

The obtained values of *hCritA* differed considerably between the different models but were considerably less negative than the commonly used values of -15000 or -16000 cm in RWU simulations. Pang et al. (2000) indicated that this value is soil texture related, being lower for fine materials and higher for coarse materials (around -5000 cm for sand or gravel). A sensitivity analysis showed that the simulation results were not affected when lower values of *hCritA* than the values in Table 3.3 were used.

The root uptake parameters h_{3l} and h_{3h} that were obtained using the Feddes-Jarvis and the Feddes models were very similar and about 30% lower than the values suggested for wheat by Wesseling et al. (1991) (-500 cm and -900 cm). The critical water stress threshold ω_c in the Feddes-Jarvis model was 0.8, which is consistent with the speculation of Šimůnek and Hopmans (2009) that ω_c is relatively high for cultural plants compared with natural plants as the cultural plants have limited ability to compensate stress. For the Couvreur model, the optimized K_{rs_ini} is about a factor 4 larger than K_{comp_ini} (Fig. 3.7), which is also indicative of a relatively small RWU compensation. Both K_{rs} and K_{comp} increased by a factor of 6.3 (which is the ratio of maximum to the initial root length) during the growth period, at the end of which the values decreased slightly due to root senescence.

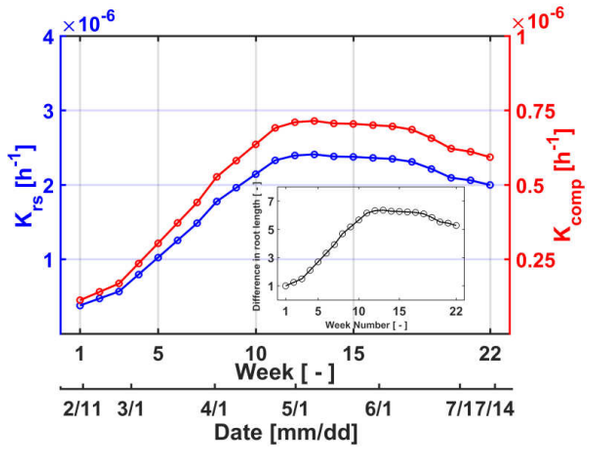

Fig. 3. 7 Estimated equivalent conductance of the root system (K_{rs}) and compensatory RWU conductance (K_{comp}) in the 22 weeks. The inner plot shows the relative difference of root length between the first week and the following weeks.

To evaluate the uniqueness of the parameters found by the GA optimization and whether the GA algorithm found the global optimum, selected response surface are shown in Fig. 3.8. Considering the soil hydraulic parameters, the response surfaces showed clear minima indicating that the parameters were identifiable (Fig. 3.8a-c). Also, the parameters of the Couvreur model were identifiable (Fig. 3.8d-f). However, for the parameters h_{3h} and h_{3l} of the Feddes and Feddes Jarvis (Fig. 3.8g-h) model, the response surface did not show a distinct minimum whereas a minimum could be observed for ω_c (Fig. 3.8i) in the response surface.

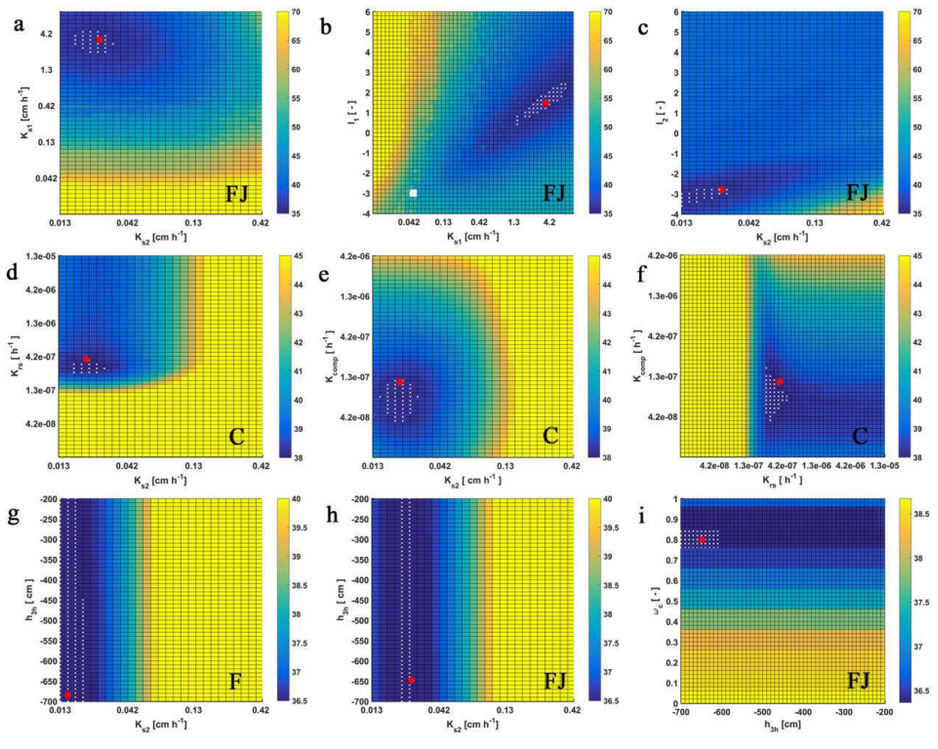

Fig. 3. 8 Response surface for K_{s2} - K_{s1} (FJ), K_{sl} - l_1 (FJ), K_{s2} - l_2 (FJ), K_{s2} - K_{rs} (C), K_{s2} - K_{comp} (C), K_{rs} - K_{comp} (C), K_{s2} - h_{3h} (F), K_{s2} - h_{3h} (FJ), and h_{3h} - ω_c (FJ) parameter panes. FJ: Feddes-Jarvis, F: Feddes without compensation, C: Couvreur. Color bar: range of the objective function; white dot: area within 0.5% range of OF minimum; red dot: optimum value obtained from the inverse modeling.

The root system hydraulic conductance, K_{rs}, can also be measured directly in the lab or in field experiments by a high-pressure flow meter (Judd et al., 2016; Tyree et al., 1995) or a pressure chamber (Miyamoto et al., 2001). However, the measurements were restricted to extracted root systems and for crops the measurements were mostly carried out for young roots of seedlings. The values obtained from those studies could therefore not be compared with the inversely estimated values in this study due to different root development. Alternatively, K_{rs} and K_{comp} can be calculated directly from the root architecture and the hydraulic properties of root segments. Couvreur et al. (2014b) calculated K_{rs} and K_{comp} of winter wheat by virtually reconstructing its hydraulic architecture using literature data. The architecture was generated with the model RootTyp (Pagès et al., 2004), accounting for plant-specific root traits and reproducing RLD

profiles observed in early spring. Radial and axial conductivities changing with root segment age were also accounted for. The conductances derived from these calculations represent the conductance of a single plant whereas K_{rs} used in the 1-D model represents the conductance of the root systems per unit area of the upper soil surface. To match the units, K_{rs} obtained from calculations was divided by the root length of the virtual plant and K_{rs} obtained from inverse modeling was divided by the total root length under a horizontal unit surface area, which corresponds to the depth integral of the RLD (Fig. 3.9a). Therefore, observations of root numbers or root lengths in the rhizotubes had to be transformed to RLDs.

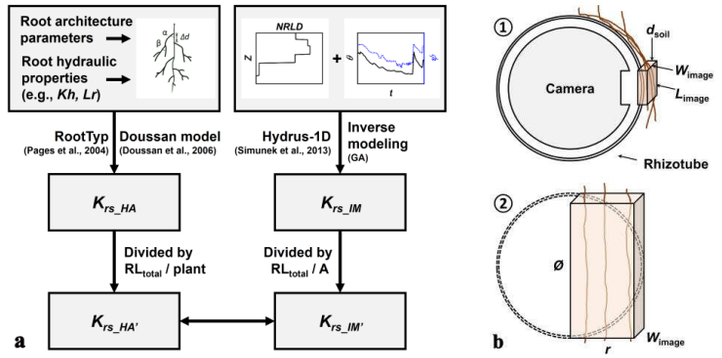

Fig. 3. 9 (a) Deriving root hydraulic conductance from the architecture model and the inverse modeling, and (b) options for calculating root length density from the rhizotube: (1) uses the root length that is observed in the images and an empirical soil thickness of 2 mm and (2) uses the root counts from the images; *Kh* and *Lr* are root axial conductance (cm^3 d^{-1}) and radial conductivity (d^{-1}), NRLD is normalized root length density, K_{rs_HA} and K_{rs_IM} are root hydraulic conductance derived from the architecture model (cm^2 d^{-1}) and inverse modeling (h^{-1}), RL_{total} is root length of a single plant (cm), A is the horizontal soil area per plant (cm^2), d_{soil} is the observed soil thickness (cm), W and L are width and length of the effectively observed volume (cm), and Φ and r are diameter and radius of the rhizotube (cm).

We considered two approaches which make different assumptions about the distribution of roots in the soil around rhizotubes (Fig. 3.9b). The first one uses the root length that is observed in the images and an empirical soil thickness of 2 mm. This approach assumes that the volume of the rhizotube has no impact on the RLD that is observed in a small soil volume at the lateral sides of the rhizotubes. The second option uses the root counts from the images. It assumes that all roots that impact on the walls of the rhizotube grow along the rhizotube surface and are detected at the

lateral sides. When it is further assumed that roots would grow nearly vertically in absence of the rhizotube, the projected root length equals the number of intercepted roots times the diameter of the rhizotube. Considering a planting density of 310 plants m^{-2}, the calculated total root length per plant in week 8 when roots were firstly observed at 80 cm was, respectively from observed lengths and observed impacts, 37.76 and 4.62 m. This range represents an uncertainty range of the actual root length of a plant that is estimated from rhizotube images. This range could be narrowed down when using a calibration of the rhizotube observations against direct observations of RLD. With the root architecture model, a root length of 43.56 m per plant and a rooting depth of 95 cm was obtained (data was from Couvreur et al., 2014b). The K_{rs} derived from the architecture model was 0.0152 cm^2 d^{-1} (data was from Couvreur et al., 2014b) for a single plant and K_{rs} obtained in this study was 1.8×10^{-6} h^{-1} in week 8. Consequently, the root hydraulic conductance per unit root length was 1.54×10^{-8} and 1.26×10^{-7} cm h^{-1} for week 8, and 1.48×10^{-7} cm h^{-1} for the root architecture model.

When comparing the root conductances obtained from the inverse modeling and the root architecture model, it must be considered that the root architecture model was not calibrated for this specific soil with a high stone content and for the water stress conditions in the experiments but used root-related parameters from literature. Furthermore, there is uncertainty about the translation of the inverted root conductances to a root conductance per unit root length that is related to the interpretation of the rhizotube measurements. As a consequence, the fact that the order of magnitude of the derived parameters corresponds indicates that the inversely estimated root conductances are consistent with properties of the root system that can be measured directly.

Different from what was obtained in the numerical modeling, K_{comp} was much lower than K_{rs} in this study. The smaller K_{comp} limited compensatory RWU though it remained quite significant as shown by the changing shape of the RWU profile (discussed in section 4.4). The value of K_{comp} could be equal to K_{rs} if axial resistance is much lower than radial resistance, however, the difference between the two parameters becomes larger when the root axial conductance decreases (Couvreur et al., 2012). Roots may lose contact with the soil when the soil dries out, which will lead to a lower redistribution to drier soil layers (Carminati et al., 2009), which also accounts for the lower K_{comp}. Besides, we assumed that the uptake is proportional to the RLD. However, the radial conductance of root segments decreases when they grow older. Therefore,

the sink term and compensatory uptake may be smaller in regions where the roots are on average older. Given the complexity of realistic root hydraulic properties, these two parameters should best be considered as two independent variables for other crop species in future investigations in order to grant an extra degree of freedom to the model, especially when the root axial conductance is relatively low (Couvreur et al., 2012).

3.4.3 Effect of soil hydraulic parameters

For a saturated conductivity in the lower soil layer of 0.02 cm h^{-1}, which was close to optimized K_{s2} of the Couvreur model, the F_{w1} model predicted about 7% less uptake than the Couvreur model and 5% less than the Feddes-Jarvis model (Fig. 3.10). These results demonstrate the effect of considering RWU compensation on the cumulative RWU in this study. For all models, the simulated uptake increased with increasing K_{s2} up to 0.45 cm h^{-1} when the simulated uptake equaled the potential uptake. These results indicate that the amount of water retained in the soil profile was sufficiently large to satisfy the potential uptake but the uptake in this soil was limited by the soil hydraulic conductivity that prevented water redistribution in the soil profile. The root system could compensate only partly this limited redistribution.

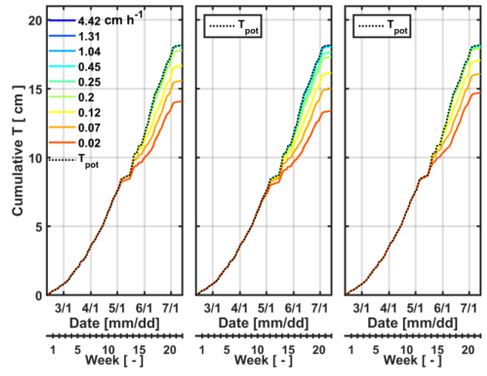

Fig. 3. 10 The cumulative root water uptake simulated by the Feddes-Jarvis (left: FJ, ω_c = 0.8, right: F_{w1}, ω_c = 1) and the Couvreur (right: C) models with different K_s values in the subsoil.

3.4.4 Simulated RWU profiles by the different models

Similar soil moisture distributions and cumulative uptake were estimated by the Feddes (with and without compensation) and the Couvreur models. In this section, we investigate whether simulated RWU distributions differ between the different models. Figure 3.11 shows the RWU distributions simulated by the Feddes (FJ and F_{w1}) and the Couvreur models and the root distributions along the soil profile during a 24-hour period in week 11 (no water stress in the Couvreur model but stress started in the Feddes model), 15 (in the stress period), and 18 (a day before water stress ended and after a rainfall event). The spatio-temporal variations of RWU that were simulated by the Feddes (FJ and F_{w1}) and the Couvreur models along the soil profile were similar in week 11. The water uptake profile simulated by the models followed the spatial root distribution: when there was no water stress RWU was higher in the soil layers where NRLD was higher as observed by Adiku et al. (2000) and de Willigen et al. (2012). The water uptake simulated by the Feddes (FJ and F_{w1}) model stopped at night, however, for the Couvreur model, the soil water was taken from 40 to 70 cm depth and released from 10 to 40 cm between 22:00 and 5:00. For the Couvreur model, compensation is considered as the internal adjustment of water uptake and happens even when there is no water stress but with non-uniform distribution of water potentials within the root zone (Couvreur et al., 2012; Javaux et al., 2013).

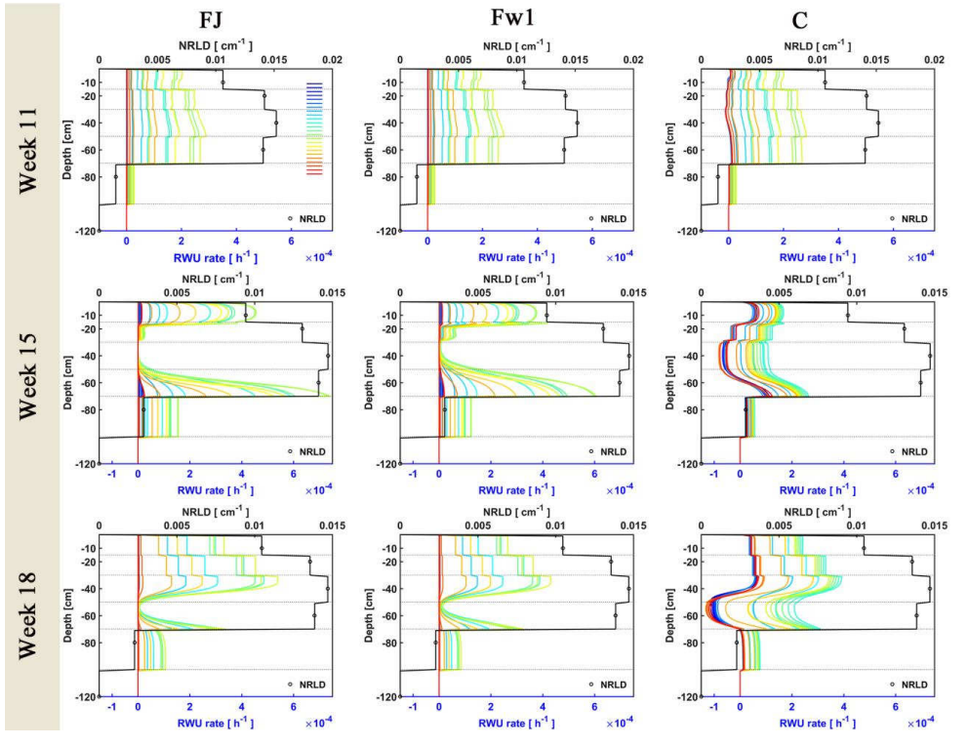

Fig. 3. 11 Normalized root length density (NRLD, black lines) and root water uptake rate (RWU, colored lines) simulated by the Feddes (FJ and F_{w1}) and the Couvreur (C) models in 24 hours of week 11, 15, and 18 along the soil profile. The corresponding dates are 22 Apr., 20 May, and 13 June 2014. The legend for the 24h is represented by the color from blue (1h) to red (24h).

Water depletion and a reduction in water uptake occurred first in the layers from 15 to 50 cm depth. It should be noted that also in the layer from 50 to 70 cm depth the uptake rate was high before the onset of stress (or at the early stage of water stress, e.g., week12). But, this layer could be replenished by water from deeper soil layers, as is also evidenced by the higher uptake at the bottom of this layer during week 15. After the irrigation and rainfall events during week 18, the water uptake rate increased again and became equal to the potential uptake rate in the upper soil layer from 0 to 40 cm depth whereas uptake was still reduced from 40 to 70 cm. The dry conditions in the deeper soil layers prevented that the crop transpiration returned immediately after irrigation and precipitation back to the potential transpiration rate (see also Fig. 3.5a).

Comparing the simulated RWU by the Feddes-Jarvis and the Feddes (F_{w1}) models when RWU from the layer between roughly 15 and 50 cm depth was reduced, RWU compensation in the Feddes-Jarvis model resulted in a higher RWU from the deeper soil layers but also from soil layer between 0 and 15 cm. Despite these differences, the RWU profiles simulated by the Feddes-Jarvis and Feddes (F_{w1}) models were very similar and differed considerably from the uptake profiles simulated by the Couvreur model (Fig. 3.11). The Feddes (FJ, F_{w1}) models did not simulate RWU at night whereas in the Couvreur model, uptake from wetter regions in the root zone continues at night and the absorbed water is released again in drier soil layers. This process is called hydraulic lift when water is released in shallow layers (Caldwell et al., 1998; Neumann and Cardon, 2012; Richards and Caldwell, 1987). Interestingly, the Couvreur model also simulated absorption from shallower layers after a rainfall event and a release in deeper drier layers (week 18). Such an inverse hydraulic redistribution was also reported in both woody and grass plant root systems (Bleby et al., 2010; Leffler et al., 2005). The redistribution of water through the root system at night also had an impact on the simulated RWU profiles during the day. Water that was released in dry soil layers during the night was taken up during the next day so that the water uptake during the day was more equally distributed over the root profile than in the Feddes (FJ and F_{w1}) models.

In order to evaluate the effects of the difference in diurnal dynamics of RWU that is simulated by the different models, simulated transpiration rates and soil water contents during week 15 are shown in Fig. 3.12. The Couvreur model simulated smaller peak RWU rates but larger RWU rates, which equaled the potential ones, during the morning and evening than the Feddes models. The Couvreur model simulated largest water release at night at 40 cm, the release and subsequent uptake of water (7.7×10^{-5} h^{-1} at 22:00 in Fig. 3.11) was quite small and the corresponding variation of SWC was 0.002 cm^3 cm^{-3} that was too small to be detected by soil moisture sensors (Fig. 3.12b). This small variation of SWC due to the water redistribution from roots to the dry soil was also indicated by other researches. Zegada-Lizarazu and Iijima (2004) investigated 16 food crops using deuterium labeling and the results showed that for wheat crop the deuterium concentration (delta notation) was increased by 0.003% during night in the topsoil (up to 25 cm) through hydraulic lift. Shen et al. (2011) indicated that SWC increased 0.01 to 0.02 cm^3 cm^{-3} in the dry and upper soil (up to 15 cm) in the night during the blooming stage of winter wheat

through hydraulic lift. Guderle and Hildebrandt (2015) simulated an increase of SWC around 0.003 cm^3 cm^{-3} using an exponential root growth model and synthetic data. The changes in SWC and SWP during the compensatory process were too small to be detected using soil moisture sensors. However, water isotope tracing techniques could be applied to determine the magnitude of hydraulic lift and RWU compensation, and deliver relevant information to parameterize RWU models (Rothfuss and Javaux, 2016). This information could be supplemented by information about the diurnal transpiration dynamics obtained from sap flow measurements (Langensiepen et al., 2014).

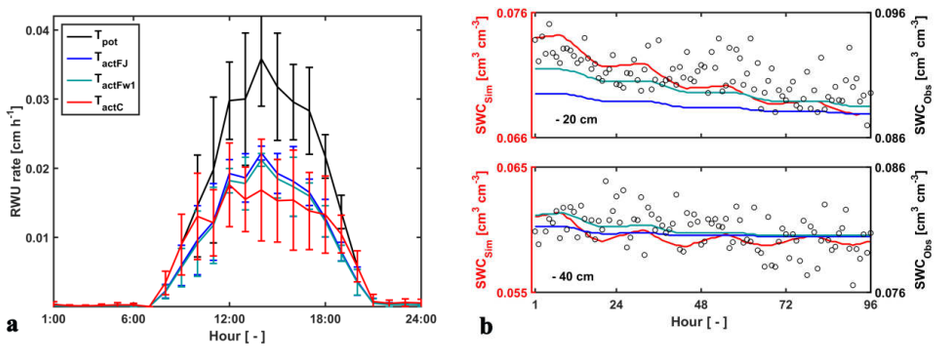

Fig. 3. 12 (a) Variations of diurnal averaged root water uptake (RWU = T_{act}), and (b) hourly soil water content (SWC) simulated by the Feddes (FJ and F_{w1}) and the Couvreur (C) models at 20 and 40 cm depths from 17 May to 20 May 2014 (week 15).

3.4.5 Relation between root water uptake and soil water pressure head

Figure 13 shows how the simulated ratio of actual to potential transpiration (Fig. 3.13a) and the actual transpiration during stress periods (Fig. 3.13b) are related for the different models to the effective soil water potential in the root zone, h_{Te}. Only actual transpiration rates at 12:00 p.m. are shown. These functions represent a root-system or plant-scale stress functions that relate the total RWU to an effective water potential in the root zone, h_{Te}. Since the potential transpiration rates at 12:00 were mostly above 0.02 cm h^{-1} (Fig. 3.2), the h_3 parameter for the Feddes reduction function α_F was mostly equal to h_{3h}. This explains why for the Feddes-Jarvis model, all points in the T_{act}/T_{pot} versus h_{Te} plot fall nearly on a line. For the Feddes model without RWU

compensation (F, F_{w1}), the line is equal to the α_F function for the high transpiration rate. However, RWU compensation shifts the line towards more negative h_{Te} values demonstrating that compensation leads a lower reduction in actual transpiration for a given h_{Te} and to a more negative h_{Te} when stress onset occurs than the threshold h_3 in the α_F function (which was -648 cm for the Feddes-Jarvis model, see Table 3.3). This demonstrates that when root water compensation occurs, the local stress function α_F cannot be derived from a plant scale stress function that could be derived directly from measuring plant transpiration and pressure heads in the root zone. In the Couvreur model, during water limitation the relation between T_{act}/T_{pot} and h_{Te} is linear but with a slope that is proportional to K_{rs}/T_{pot} (see Eq. 3.13), which explains the scatter in Fig. 3.13a (in which red lines corresponding to different T_{pot} values). It is interesting to note that for T_{pot} = 0.03 cm h^{-1} and K_{rs} = 2.5 × 10^{-6} h^{-1}, which are representative for, respectively, the maximal T_{pot} and the root system conductance during the considered period, the relation between T_{act}/T_{pot} and h_{Te} predicted by the Couvreur model is similar to the one obtained for the Feddes-Jarvis model (Fig. 3.13a). This suggests that proxies of Couvreur model parameters may be inferred from Feddes-Jarvis model parameter libraries (Couvreur et al., 2014a). When T_{act} during stress periods is plotted versus h_{Te}, a linear relation is obtained for the Couvreur model (Fig. 3.13b). For the Feddes-Jarvis and the Feddes models, the points are scattered. In the Feddes models, the relation between T_{act}/T_{pot} and h_{Te} can be made a function of T_{pot} by making h_3 a function of T_{pot}. However, the maximal value of T_{pot} for which h_3 varied (0.02 cm h^{-1}) was smaller than the T_{pot} values at 12:00 pm that was considered so that there was, in fact, no dependence on T_{pot} in the relation between T_{act}/T_{pot} and h_{Te} shown in Fig. 3.13a. This led to the scatter in the relation between T_{act} and h_{Te} for the Feddes models in Fig. 3.13b. However, for the Feddes-Jarvis model, the points scattered around the relation that was obtained for the Couvreur model so that both models simulated on average the same relation between T_{act} and h_{Te}.

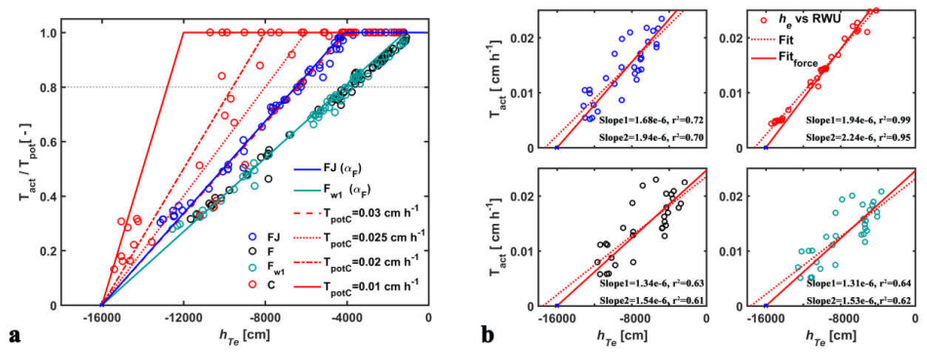

Fig. 3. 13 (a) The relation between effective soil hydraulic head (h_{Te}) and relative root water uptake (RWU) that was simulated by the Feddes (FJ, F_{w1}, and F) and the Couvreur (C) models (circles), calculated by the Feddes stress function (α_F) using the optimized h_{3h} and h_{3l}, and calculated by the Couvreur model using the mean K_{rs} (from week 11 to 21) and different T_{pot} values. (b) The relation between h_{Te} and actual root water uptake (T_{act}) simulated by the Feddes (FJ, F, and F_{w1}) and the Couvreur (C) models in water stress periods. h_{Te} was selected at 12:00 p.m. and the data in the sheltered periods were not included. Slope 1 (dashed line) and slope 2 (solid line) denote the slope of the fitted curve and the fitted curve with forcing through the point (-16000, 0), respectively.

3.5 Summary and conclusions

This study compared the soil moisture prediction and the performance of RWU with different compensation by the coupled Feddes-Jarvis, the Feddes, and the Couvreur RWU models in Hydrus-1D framework with *in situ* observations from a minirhizotron facility. Soil hydraulic parameters and RWU parameters of three different models could be estimated using observations of soil water content, potential, and root distribution. The three models could describe the observations equally well. The same soil hydraulic properties were obtained for the two models that considered RWU compensation. The Feddes model without considering compensation could describe the observation data but slightly different soil parameters were obtained. If the same soil hydraulic parameters were used in the Feddes model as in the models that considered RWU compensation, less RWU was simulated by the Feddes model (F_{w1}). But RWU compensation increased the total water uptake only to a small extent and was not able to avoid water stress. A sensitivity analysis demonstrated that the amount of water in the soil profile would be sufficient

to avoid water stress but the hydraulic conductivity of the soil profile limited the redistribution of water in the root zone that would be necessary to avoid water stress.

The obtained RWU parameters were consistent with data reported in the literature. Response surfaces of the objective function showed that the root-related parameters of the Couvreur model could be identified using inverse modeling. Furthermore, these parameters were consistent with simulations using root architecture models and hydraulic parameters of roots. However, for the Feddes and Feddes-Jarvis models, the RWU parameters that define the onset of water stress as a function of the soil water pressure, h_{3l} and h_{3h}, could not be uniquely identified.

The obtained root parameters were indicative of limited RWU compensation. The Couvreur and the Feddes-Jarvis models simulated similar (the Couvreur was 2.8% more) total RWU, however, they predict different diurnal dynamics of local RWU. The Couvreur model predicted water exudation at night in dry soil layers (hydraulic lift or hydraulic redistribution). The exuded water was taken up during the next day so that the net water uptake from the dry layers was zero and equal to the uptake predicted by the Feddes-Jarvis model. The amount of water that was released at night was however too small to be detected by soil moisture sensors. Although there is evidence from isotope trace studies that this process is taking place, it remains questionable whether this process is relevant for RWU for longer periods.

Although the RWU compensation functions of the Feddes-Jarvis and Couvreur models arise from different approaches and the nature of their parameters differs, they predicted similar plant or root-system scale stress functions, which opens possibilities of parameter transfer between both models. The root-system scale stress functions deviate due to RWU compensation from the local stress functions that are used in the Feddes-Jarvis model. The close agreement in root-system scale stress functions between the Couvreur and the Feddes-Jarvis models was due to the more or less constant root system conductance during the period when the stress occurred. The Couvreur model links the stress function to the root system conductance which in turn depends on the development of the root system. As a consequence, this model will predict different root-system scale stress functions at different stages during the growing season and will also predict different stress functions for plants growing in different soils in which the root system development is different. Similarly, Vandoorne et al. (2012) indicated that the parameters, h_{3l}

and h_{3h}, which are assumed to remain constant during the growing season (Feddes et al., 1978), in the Feddes stress function, were “not unique for a given plant” and differed between different periods in the growing season of Chicory (*Cichorium intybus L.*). This implies that the stress function parameters in the Feddes-Jarvis model should be a function of the crop development stage and root system status. As a consequence, these parameters should be adapted depending on the development of the root system. But, a function that links the stress parameters to root system parameters is lacking.

Chapter 4

Root growth, water uptake, and sap flow of winter wheat in response to different soil water availability

This chapter is based on a journal article in preparation:

G. Cai, J. Vanderborght, M. Langensiepen, H. Hüging, H. Vereecken. 2017. Root growth, water uptake, and sap flow of winter wheat in response to different soil water availability. *Submitted to Hydrol. EarthSyst.Sci. doi.org/10.5194/hess-2017-711*

4.1 Introduction

Root water uptake (RWU) is a vital process for plant functioning since it conditions nutrient transport and balances transpiration. Estimating RWU is needed to make predictions of crop water use, to assess water and nutrient use efficiency in function of root architecture and environmental controls, and to design efficient water and nutrient resources management in agricultural practices (Molz, 1981). However, quantifying RWU for water and nutrient management in different regions and climates continues to be a challenge due to the lack of knowledge of key RWU parameters and appropriate description of the RWU process (Vereecken et al., 2016). Typically, RWU is estimated from the transpiration demand, which is calculated from the canopy energy balance under the assumption that the crop is well-watered. Different soil water balance models have been developed that allow estimating RWU using different parameterizations of the root system and water uptake mechanisms. However, the availability of field plot scale experiments in different soil textures and for different soil water regimes that are needed to validate and improve these models is very limited.

In many soil water balance models that are used to predict RWU Richards equation is used for calculating water flow in unsaturated soils and a sink term is defined that describes RWU:

$$\frac{\partial \theta}{\partial t} = \nabla(K(h)\nabla(h + z)) - S \qquad (4.1)$$

where θ represents the volumetric soil water content (SWC) [L^3 L^{-3}], t time [T], K the soil hydraulic conductivity [L T^{-1}], h the soil water pressure head (SWP) [L], z the elevation [L], and S the sink term [L^3 L^{-3} T^{-1}] defined as the volume of water removed from a unit volume of soil due to root extraction. A popular macroscopic RWU model that has been used to quantify the sink term is the Feddes model (Feddes et al., 1976) because of its simplicity and low data requirement (Luo et al., 2003; Peters et al., 2017; Skaggs et al., 2006). It uses the normalized root length density distribution and stress functions to determine the distribution of the sink term in the root zone. Piecewise linear stress functions define how the sink term at one location in the root zone is reduced as a function of the SWP and this function depends in turn on the potential transpiration rate. This model was refined later to the Feddes-Jarvis model by adding a factor to

account for increased water uptake, i.e. uptake compensation, from moister soil layers when uptake from drier layers is reduced (Jarvis, 1989; Šimůnek and Hopmans, 2009).

Besides transpirational demand and soil water pressure head (SWP), RWU is also influenced by root hydraulic properties (i.e. root hydraulic conductance) which may vary over time due to root development and growth (Doussan et al., 1998; Javaux et al., 2008; Steudle, 2000). Root hydraulic properties determine the resistance to water flow within the plant and define the water potential losses along the sap flow from the roots to the shoot and the leaves (Bechmann et al., 2014). The relation between soil water and leaf water potentials, and sap flow depends on root hydraulic properties which therefore should be considered in RWU models (Vadez, 2014; Vereecken et al., 2015). Physically-based macroscopic RWU models were developed that describe water fluxes in the soil-root (or soil-root-plant) system based on water potentials and conductivities or conductances of the soil and the root system. Nimah and Hanks (1973) characterized water uptake as a function of root density, axial root conductance, and water potential at the root collar. Heinen (2001) considered root hydraulic properties and water pressure head at the root-soil interface in the RWU model but without considering water uptake compensation. De Jong Van Lier et al. (2008) developed a 1-D water flow model in which RWU rate was a function of root surface water potential and root radius. This model considered implicitly lateral flow from soil to root with implicit compensation mechanism but did not include the information of axial root hydraulic conductances.

In order to present a mechanistic description of the RWU process that contains physically defined parameters, Couvreur et al. (2012) developed a 3-D model based on the approach of root system hydraulic architecture (Doussan et al., 2006; Javaux et al., 2008). In this model, RWU is dependent on root system hydraulic conductance (K_{rs}), the root distribution, and the difference between the local soil water potential and the water potential at the root collar. Variations of this potential difference with depth in the root zone lead to water uptake compensation. For crops with small lateral variations in root length density (RLD), this 3-D model could be upscaled to a 1-D model (Couvreur et al., 2014b) which shows similarities to the models of Nimah and Hanks (1973) and of Amenu and Kumar (2008). Cai et al. (2017) obtained the root hydraulic parameters of the 1-D upscaled Couvreur model for winter wheat (Couvreur et al., 2014b) by inverse modeling using time series of soil water potential, water content, and root length density

measurements in the field. Since the upscaled root hydraulic parameters have physical meaning, the upscaled parameters obtained from inverse modeling could be compared to and were found to be consistent with parameters that were derived from direct measurements of hydraulic properties of root segments and models of the hydraulic root architecture (Couvreur et al., 2014b).

Another way to validate the inversely estimated parameters is to evaluate whether the model is able to predict the RWU and its reduction when SWP decreases. For crops with a small water capacity, the RWU corresponds closely with the transpiration rate. Measurements of crop transpiration can therefore be used to parameterize or validate RWU models.

Many techniques have been used to investigate transpiration ranging between the single plant and catchment scale (Allen et al., 1989; Jaeger and Kessler, 1997; Twine et al., 2000). At the field plot scale, weighing lysimeters allow to measure transpiration (e.g., Garré et al., 2011; Groh et al., 2016). A disadvantage of lysimeters is that they are costly and, although possible (e.g., Garré et al., 2011; Vandoorne et al., 2012), root distributions are difficult to measure in lysimeters and their spatial growth is influenced by the confined soil space which also frequently causes undesired boundary effects (e.g. high root length densities at lysimeter walls). Measuring sap flow with the thermoelectric method is a direct and *in situ* technique which was discovered by Huber (1932). It was used to estimate transpiration for different trees species (Cermak et al., 2004; Granier et al., 1996; Massai and Remorini, 2000) and crops (Chabot et al., 2005; Cohen et al., 1993; Langensiepen et al., 2014). Due to limitations of sensor installation on small and vulnerable crop stems, sap flow measurements on crops with small stem diameters of less than 5 mm are practically challenging. Senock et al. (1996) provided first sap flow measurements for wheat under field conditions but the values were within 10 % of gravimetric measurements and the experimental verification of a high sap flow rate (up to 5 g h^{-1}) is not available. Applying an empirical method for calculating sap flow from standard stem heat sensor outputs, Langensiepen et al. (2014) obtained close agreements between measured sap flow and transpiration rates measured with a standard eddy covariance system. Continuous sap flow measurements can be carried out with modern logging techniques (e.g. multiplexer and data logger), providing insight into the temporal dynamics of transpiration and how for instance RWU changes when SWP decreases over time. The use of sap flow measurements to validate theories of RWU was

demonstrated for trees (Gong et al., 2006; Green and Clothier, 1998; Howard et al., 1996), but for crops, in particular wheat, such a validation has not yet been performed under field conditions.

The main objective of this study is to investigate whether a physically-based model for RWU can simulate the effect of different soil water availability on wheat RWU resulting from differences in soil water application and differences in soil water retention characteristics. This includes testing whether parameters of such a model can be calibrated using measurements of soil water content, water potential, and root density and validating the calibrated model against sap flow measurements. Second, we investigated whether differences in crop shoot and root developments between treatments with different soil water availability lead to different model parameter estimates and whether these parameters estimates can be linked to directly observable properties of the root system.

Therefore, water potentials and contents, root distributions, crop development and sap flow were monitored in six plots (two soil types and three water application treatments) and used to parameterize two RWU models: the empirical Feddes-Jarvis model (FJ model) and the physically-based Couvreur model (C model).

4.2 Materials and methods

The experimental set up of the plots was described in detail in Cai et al. (2016) and the model setup and the inverse modeling procedure that was used to determine the parameters by Cai et al. (2017). For more detailed information on the setup and the inverse modeling procedure, we refer the reader to these publications.

4.2.1 Setup of the test site

Two instrumented rhizotron facilities were constructed in the upslope and the downslope of a cropped field in Selhausen (Germany, 50°52'N, 6°27'E). The field is on a west-facing slope

(smaller than 4°) and characterized by a high stone content (up to 60%) in the upslope and silty texture in the downslope. Each facility was divided into three plots of 7 m length × 3.25 m width. To produce a gradient in soil water availability, one plot was sheltered from rain, one plot was rainfed, and one plot was irrigated by drip-irrigation. A sketch of the facilities with the location of the sheltered, rainfed and irrigated plots and the wooden framed trenches is shown in Fig. 4.1.

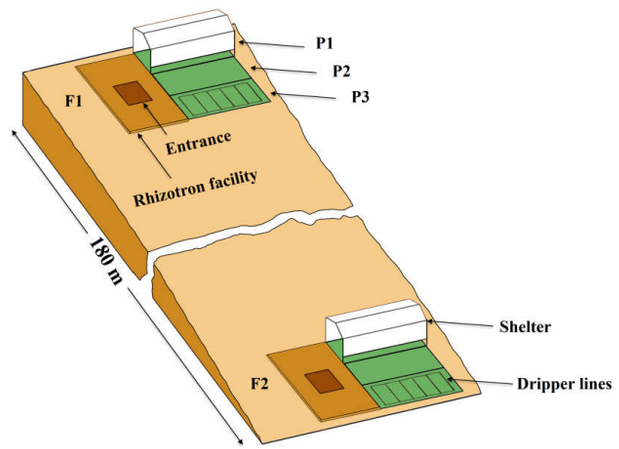

Fig. 4. 1 Sketch map of the location and the setup of the upper (F1, stony soil) and lower (F2, silty soil) rhizotron facilities. P1, P2, and P3: the sheltered, rainfed, and irrigated plots.

Precipitation and other meteorological data for the calculation of the reference evapotranspiration (ET_o) using the FAO56 Penman-Monteith equations (Allen et al., 1998) were obtained from a weather station located in close proximity to the two facilities. The average annual precipitation for the past 50 years in this area was 699 mm (Knaps, 2016).

Winter wheat (variety Ambello) was sown at a density of 300 – 320 seeds m^{-2} on 31 Oct. 2013 in all plots and harvested on 17 July 2014 in the stony soil (upper facility) and on 31 July 2014 in the silty soil (lower facility) as the contrasting soil-water regimes in the two soils affected ripening times. Total shoot biomass was harvested in an area of 7.31 m^2 (3.25 m × 2.25 m) in each plot and weighed after oven drying. Leaf area index (LAI) was measured using a plant canopy analyzer (LAI-2200, LI-COR, Inc. USA) and ranged from 0.8 to 2.5 in the stony soil and from 0.8 to 4.0 in the silty soil between 8 Apr. and 14 July 2014 (Fig. 4.2a). Precipitation depth between the seeding and harvest was 434.49 mm for the stony and 495.89 mm for the silty soil,

the difference resulting from different growth period lengths in both facilities. Fig. 4.2b shows the cumulative amount of water received by the three plots in both soils.

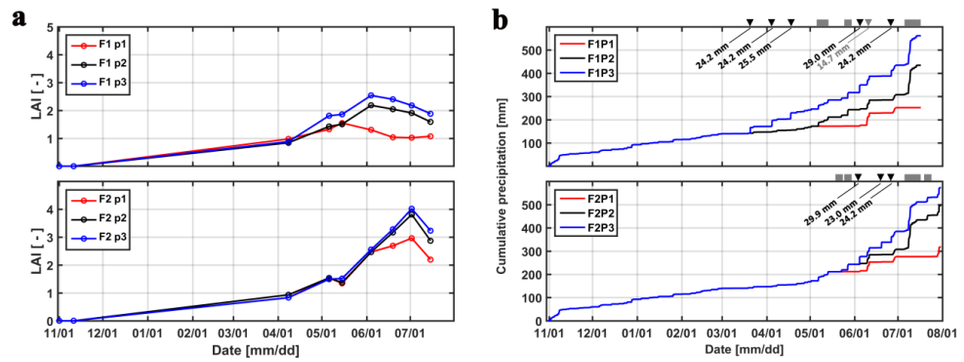

Fig. 4. 2 (a) Measured leaf area index in the three plots (P1: sheltered; P2: rainfed; P3, irrigated) of the stony (F1) and silty (F2) soils. (b) Cumulative precipitation and irrigation applied to the three plots of the stony (F1) and silty (F2) soils. ■: sheltered period, ▼: irrigation in P3, ▼: irrigation in P1.

4.2.2 Measurements of soil moisture, root distribution, and sap flow

Soil water content and potential

Time domain reflectometers (TDR), tensiometers (T4e, UMS GmbH, München, Germany), and matrix water potential sensors (MPS-2, Decagon Devices Inc., UMS GmbH München, Germany) were installed in each plot at 0.1, 0.2, 0.4, 0.6, 0.8, and 1.2 m depth in the vertical walls of the facilities to monitor hourly SWC and soil water potential.

Root observation

Root distributions were measured non-destructively at weekly intervals from 11 Feb. 2014 to 11 July 2014 in the stony soil and from 14 Mar. to 24 July 2014 in the silty soil with a minirhizotron camera (Bartz Technology Corporation, Carpinteria, CA, USA) in 7-m-long horizontally installed rhizotubes. Three replicates of rhizotubes were installed at the same depths as the soil moisture sensors. Root images with the size of 16.5 mm × 23.5 mm were taken from left and

right sides at 20 fixed locations along each tube and were analyzed subsequently using the software Rootfly (Wells and Birchfield, 2009) to determine the length of roots per area of the image. Root length densities were therefore expressed in units of length per surface. To calculate the total root length below a unit surface area, both root length and root counts per image surface were considered in Cai et al. (2017). We assumed that root lengths in the images were proportional to root counts. Using root counts has the advantage of avoiding to use the empirical soil thickness (e.g. 2 mm) viewed by the camera in the estimation of absolute total root length. The root counts were associated with a soil volume that corresponds with the diameter (height, 64 mm) and the radius (width, 32 mm) of the tube, and the image width (depth, 16.5 mm) to obtain an estimate of root length density (Cai et al., 2017). The root densities were subsequently integrated over depth to obtain the total root length below a unit surface area.

Sap flow

Sap flow was determined with SGA3 Dynagage sap flow sensors (Dynamax Inc., Houston, USA) in five randomly selected wheat tillers located in the center of each plot. They were continuously operated from 23 May 2014 to 6 July 2014. Signals of the sap-flow sensors were scanned every 60 seconds with Dynamax control units consisting of voltage regulators, AM 16/32B multiplexers and CR1000 dataloggers (Dynamax Inc., Houston, USA; Campbell Scientific, Logan, Utah). The readings were averaged every 10 minutes, stored in a text file and processed with an R script containing the standard calculation procedures for computing sap-flow from Dynagage files (Dynamax, 2009) and an improved post-processing method for removing the noise from standard calculations (Langensiepen et al., 2014). Tiller density was determined in a fixed area of 1 m^2 for each plot and used for converting average sap flow rate (g d^{-1} $tiller^{-1}$) to an area-based transpiration rate (cm d^{-1}).

4.2.3 Root water uptake models and parameterizations

Model description

We used two 1-D RWU models: the coupled FJ model (Šimůnek and Hopmans, 2009) and the physically-based C model (Couvreur et al., 2014b; Couvreur et al., 2012), both of which considered water uptake compensation. The two models have been implemented in Hydrus-1D (Šimůnek et al., 2016). The sink term in the two models is calculated with following equations:

$$S_{FJ}(z) = T_{pot}\,\alpha_F(h)\mathrm{NRLD}(z)\gamma \tag{4.2}$$

$$S_C(z) = min(T_{pot},\, T_{act})\ \mathrm{NRLD}\ (z) + K_{comp}(h_T(z) - h_{Te})\ \mathrm{NRLD}\ (z) \tag{4.3}$$

where S_{FJ} and S_C are the sink term accounting for RWU rates in, respectively, the FJ and C models [$L^3L^{-3}T^{-1}$], z elevation [L], T_{pot} and T_{act} the potential transpiration and transpiration under water stress condition [LT^{-1}], α_F the water stress function [-], h the measured soil water pressure head (SWP) [L], NRLD the root distribution that was identical to normalized root length density [L^{-1}], γ the compensatory factor [-], K_{comp} the compensatory RWU conductance of the root system [T^{-1}], h_T the total hydraulic head (sum of pressure head and elevation head) [L], and h_{Te} the effective root zone SWP [L]. h_{Te} is the integration of soil hydraulic head and root distribution along the rooting depth (l_z, [L^{-1}]) profile:

$$h_{Te} = \int_0^{l_z} h_T(z)\ \mathrm{NRLD}(z)\ dz \tag{4.4}$$

T_{pot} is given by:

$$T_{pot} = ET_oK_c\ (1 - e^{-k*LAI}) \tag{4.5}$$

where K_c is the crop coefficient [-] that accounts for changes in evapotranspiration with crop development (Allen et al., 1998) (Table 4.1), LAI the leaf area index [-], and k an extinction coefficient (0.6 was used (Mo and Liu, 2001)). In the C model, the leaf water hydraulic head, h_{Tleaf} [L] is related to T_{pot}, the equivalent root system hydraulic conductance, K_{rs} [T^{-1}], and the effective root zone SWP, h_{Te} [L], by

$$T_{pot} = K_{rs}(h_{Te} - h_{Tleaf}) \tag{4.6}$$

as long as h_{Tleaf} [L] is larger than a critical leaf hydraulic head, h_{Tleaf_crit} (-16000 cm was used in this study (Wesseling, 1991)). When the leaf water potential equals h_{Tleaf_crit}, the transpiration rate is reduced and the actual transpiration rate T_{act} is obtained from:

$$T_{act} = K_{rs}(h_{Te} - h_{Tleaf\_crit}) \tag{4.7}$$

Table 4. 1 Crop coefficients (K_c) of winter wheat in the stony (F1) and silty (F2) soils in different growing periods. K_c was calculated according to Allen et al. (1998).

	Initial period	Mid-season	Late stage
	31.10.13 – 27.02.14	08.05 – 27.06.14 (F1) 08.05 – 09.07.14 (F2)	17.07.14 (F1) 31.07.14 (F2)
F1	0.93	1.26	0.27
F2	0.93	1.26	0.29

For the FJ model, the RWU under water stress condition was constrained by a piecewise function (α_F) that is dependent on SWP:

$$\alpha_F(h) = \begin{cases} 0 & h \notin [h4, h1) \\ \frac{h - h_1}{h_2 - h_1} & h \in (h2, h1] \\ 1 & h \in [h3, h2] \\ \frac{h - h_4}{h_3 - h_4} & h \in [h4, h3) \end{cases} \tag{4.8}$$

where $h_{1,4}$ and $h_{2,3}$ are the thresholds of SWP where RWU is completely constrained ($S = 0$), and arrives the maximum, respectively. The value of h_3 is a function of T_{pot} (Brandyk and Wesseling, 1985):

$$h_3 = \begin{cases} h_{3l} & T_{pot} \in [0, T_{3l}] \\ h_{3h} + \frac{(h_{3l} - h_{3h})(T_{3h} - T_{pot})}{(T_{3h} - T_{3l})} & T_{pot} \in (T_{3l}, T_{3h}) \\ h_{3h} & else \end{cases} \tag{4.9}$$

where T_{3h} and T_{3l} were set to 0.02 cm h^{-1} and 0.004 cm h^{-1} (Yang et al., 2009).

The water uptake compensation in the C model is described by the second term on the right-hand side of Eq. 4.3. For the FJ model it is controlled by an empirical factor (γ) that is water stress related:

$$\gamma = 1/\max(\omega, \omega_c) \tag{4.10}$$

$$\omega = \int_{l_z} \alpha_F(h)\ \mathrm{NRLD(z)}\ dz \tag{4.11}$$

where ω is the plant water stress [-], ω_c is the critical water stress threshold [-] and the value is between 0 and 1 which correspond to, respectively, full compensation and no-compensation (Jarvis, 1989; Šimůnek and Hopmans, 2009).

The soil hydraulic properties were described by the combined Mualem-van Genuchten equations (Mualem, 1976; Van Genuchten, 1980):

$$\theta(h) = \begin{cases} \theta_r + \frac{\theta_s - \theta_r}{[1 + |\alpha h|^n]^m} & h \in (-\infty, 0) \\ \theta_s & else \end{cases} \tag{4.12}$$

$$K(S_e) = K_s S_e^l [1 - (1 - S_e^{1/m})^m]^2 \tag{4.13}$$

where θ_r and θ_s are the residual and saturated water content [L^3L^{-3}], α [L^{-1}], n (n > 1), m (m = 1 - 1/n), and l are model empirical parameters, K and K_s are the unsaturated and saturated hydraulic conductivity [LT^{-1}] , S_e is the effective saturation [-]: (θ - θ_r)/(θ_s - θ_r).

Inverse Modeling and model setup

The parameters of the van Genuchten (1980) soil water retention function were fitted using the measured SWC and soil water head (Cai et al., 2016) (Table 4.2). The parameters, K_s, l, h_{3h}, h_{3l}, and ω_c of the FJ model, K_{rs}, and K_{comp} of the C model were inversely estimated by fitting simulated to hourly measured SWP and SWC. For the stony soil, a time series from 11 Feb. to 14 July 2014 and for the silty soil from 22 May to 30 July 2014 was used. Besides the time series of the SWP and SWP, also other variables that were derived from these time series, such as changes in SWP and SWC over time and water storage in the soil profile were included in the objective function that was minimized in the fitting procedure as described in Cai et al. (2017) and we

refer for the details to that paper. In the current study, observations and simulations of soil moisture dynamics for the three treatments per soil type (i.e. stony and silty soils) were lumped into one objective function whereas Cai et al. (2017) used only data from the sheltered plot in the stony soil. Hence, for each soil type, the same soil and RWU parameters were used to simulate RWU for the three treatments. But, since the two objective functions with data from the two different soil types were optimized independently, different soil and RWU parameters were obtained for the two different soils.

Table 4. 2 Parameters of soil hydraulic properties at the top- (0 – 30 cm) and subsoil (30 – 120 cm) of the stony (F1) and silty (F2) soils. θ_r and θ_s are residual and saturated soil water content, respectively. α and n are curve-fitting parameters.

	θ_r	θ_s	α	n
	$cm^3\ cm^{-3}$	$cm^3\ cm^{-3}$	cm^{-1}	
F1 topsoil	0.0430	0.3256	0.0361	1.3860
F1 subsoil	0.0543	0.2286	0.0495	1.5340
F2 topsoil	0.1392	0.4089	0.0231	1.2920
F2 subsoil	0.1304	0.4119	0.0050	1.1920

The 1-D Richards equation was numerically solved using Hydrus in a 145 cm deep soil profile for the stony soil and a 300 cm deep profile for the silty soil using a spatial discretisation of 1 cm. Two soil layers with different hydraulic properties, the topsoil (0 – 30 cm) and the subsoil (30 – 145 cm for the stony soil and 30 – 300 cm for the silty soil), were considered at both facilities. An atmospheric boundary condition was used at the top and a free drainage boundary condition at the bottom (Simunek et al., 2013). The soil water pressure heads measured at the start of the simulation period were used as initial conditions. In order to consider the root development during the growing period, the simulation period was split up in one-week periods during which a constant RLD profile was assumed. The parameters K_{rs} and K_{comp} of the C model, which were assumed to depend on the total root length, were hence adjusted at weekly intervals. One set of parameters: K_{rs_ini} and K_{comp_ini} that correspond with the RWU parameters from the sheltered plot during the first week of the simulation period were estimated using inverse modeling. K_{rs} and K_{comp} during the ith week of a certain water treatment were obtained by scaling K_{rs_ini} and K_{comp_ini} with the ratio of the integrated root length (integration of RLD over the soil profile) in

week *i* in that water treatment to the integrated root length during the first week in the sheltered plot. The initial conditions of a one-week period were derived from the simulated SWP profile at the end of the previous one-week simulation period.

The model results were evaluated in terms of root mean square error (RMSE), mean bias error (ME), and an index of agreement (*d*):

$$\text{RMSE} = \sqrt{[\sum_{i=1}^{N}(Sim_i - Obs_i)^2]/N} \quad (4.14)$$

$$\text{ME} = [\sum_{i=1}^{N}(Sim_i - Obs_i)]/N \quad (4.15)$$

$$d = 1 - [\sum_{i=1}^{N}(Sim_i - Obs_i)^2]/[\sum_{i=1}^{N}(|Sim_i - \overline{Obs}| + |Obs_i - \overline{Obs}|)^2] \quad (4.16)$$

where *Sim* and *Obs* are simulated and measured variables, *i* is the index of a given variable, and *N* is the total number of observations.

4.3 Results and discussion

We first discuss the effect of water treatments and soil textures on crop and root development. In the second part, we discuss the inverse estimation of RWU parameters of the FJ and C models from measured SWC and SWP. In the third part, simulated RWU by the two models in the different soils and water treatments are discussed and compared with sap flow measurements. In the last part, we discuss a sensitivity analysis that was carried out to evaluate the effect of the different development of the wheat crop in the different soils and water treatments on the simulated water uptake.

4.3.1 Effect of water treatment on crop and root development

Tiller densities and crop biomass in the three different water treatments in the two soils are shown in Table 4.3. Contrasting soil water availability affected crop biomass growth and yield.

Less water application (sheltered plot received 55.13% and 44.52% of the water received by the irrigated plots in the stony and silty soil, respectively, Figure 4.2b) reduced the tiller density in the sheltered plot with respect to the irrigated plot by 38.4% in the stony and 11.3% in the silty plots, and reduced the biomass by 58.8% in the stony and 40.8% in the silty plots. The biomass of wheat in the treatments that received less water was reduced stronger than the tiller density as was also reported by Musick and Dusek (1980). The tiller density and biomass were generally higher in the silty than in stony soil, especially for the sheltered plots. The higher water holding capacity of the silty soil supplying more available water in the subsoil for root extraction may account for the difference.

Table 4. 3 Tiller density (counted on 11 June 2014), crop biomass (including straw and grain which were measured after the harvest), ratio of LAI to tiller density, and maximal root length in the three plots (P1: sheltered; P2: rainfed; P3, irrigated) of the stony (F1) and silty (F2) soils.

		P1	P2	P3
Tiller density (m^{-2})	F1	228	310	370
	F2	346	380	390
Biomass (kg m^{-2})	F1	0.2951	0.6719	0.7164
	F2	0.7164	1.0659	1.2097
LAI/Tiller density (m^2)	F1	0.0050	0.0067	0.0067
	F2	0.0075	0.0074	0.0075
Maximal total root length (m m^{-2})	F1	2533.9	2941.9	3431.2
	F2	6787.4	7043.9	7024.1

As for the belowground part of the crops, RLD decreased gradually downwards for all plots of the two facilities at the beginning of the measurements (Fig. 4.3). The RLD in the shallow layers (-10 to -20 cm) was similar in the stony and silty soils, ranging from 0.12 to 0.67 cm cm^{-2}. However, larger differences in RLD between the two soils were observed at greater depths (-60 to -120 cm depth). In the stony soil, maximal root densities were observed at shallower depths (-40 cm in the sheltered and irrigated plots and -60 cm in the rainfed plot) than in the silty soil (-60 cm in the irrigated and -80 cm in the sheltered and rainfed plots). Furthermore, the maximal root length densities were considerably higher in the silty than in the stony soil (note the difference in

color scale). The root density distributions showing maximal densities at greater depths are markedly different from the root density profiles that have been observed for winter wheat using soil coring in loamy soil (Zhang et al., 2004) and in soils with seven different textures (from clay to sandy loam) (e.g., White et al., 2015; Zhang et al., 2004). This might on the one hand be due to a great amount of water stored at those depths in the silty soil but probably also nutrient distribution in the soil profile at this site, which might have promoted root development in deeper soil layers (Thorup-Kristensen et al., 2009; Yang et al., 2003). On the other hand, some studies indicated that root length densities estimated from rhizotubes may underestimate the root densities in surface soil layers due to temperature effects (Fitter et al., 1998), or roots growing parallel to the horizontal plane not intersecting the tube surface (Meyer and Barrs, 1991). We obtained root lengths ranging from 1.5 to 7.0 km m^{-2} which is within the range of the results from White et al. (2015) who investigated root development of 11 winter wheat varieties in four different soils (from clay to sandy loam) in the UK. They found an average of 9.8 km m^{-2} from the samples to 1 m depth. The lower estimate might be due to an underestimation of the root density in the upper 30 cm using the rhizotubes (Bragg et al. 1983, Samson and Sinclair, 1994).

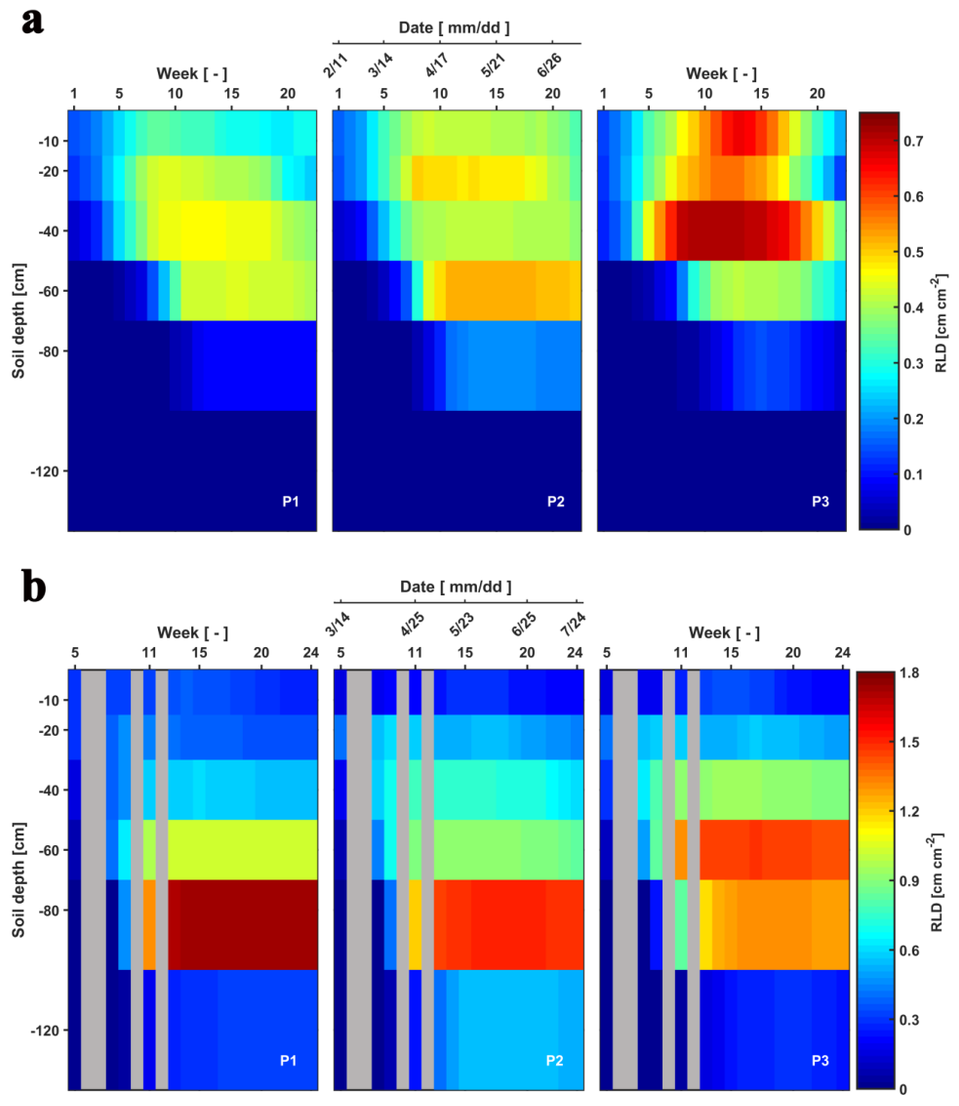

Fig. 4. 3 Depth-time distribution of root length density (RLD) in the stony (a) and silty (b) soils from 11 Feb. to 11 July 2014 and from 14 Mar. to 24 July 2014, respectively. P1: sheltered; P2: rainfed; P3, irrigated. No measurements in the gray grids.

Root senescence was observed at the end of the growing season. It started in the upper soil layers and progressively moved to deeper layers, which is more obvious in the three plots of the stony

soil after 21 May. Furthermore, root senescence in shallower layers (above 30 cm) occurred simultaneously with root development in deeper layers (below 30 cm).

The observed root development in the two different soils and for the different water treatments show opposite reactions to soil water availability. On the one hand, lower water availability in the stony soil led to a lower root density and lower total root length than in the silty soil (Table 4.3). The same behavior was observed when comparing the sheltered with the rainfed and irrigated plots in the stony soil. In the silty soil, however, an increase in root density was observed when water availability decreased. When plants experience water deficits, above shoot development is reduced by different mechanisms (e.g. reduced leaf expansion by lower turgor, enhanced respiration, stomatal closure, and reduced photosynthesis) (Bunce, 1978; Mansfield and Atkinson, 1990; Wesselius and Brouwer, 1972). The reduction in shoot growth can be counteracted with an increase in carbon allocation to the root zone as was shown in a review by Poorter et al. (2012) on environmental effects on biomass allocation. The ratio of total root length to aboveground biomass (Fig. 4.4) suggests that indeed a larger fraction of carbon was allocated to the roots in the sheltered than in the rainfed or irrigated plots both in the stony and silty soils. Although the differences in the ratio between the two soils are not so large, the total root length per kg shoot biomass was larger in the silty than in the stony soil. This seems at first sight contradictory to the lower water (and nutrient) availability in the stony than in the silty soil. This might reflect that other factors like soil mechanical strength may have stimulated root growth more in the silty than in the stony soil (Merotto Jr and Mundstock, 1999; Unger and Kaspar, 1994).

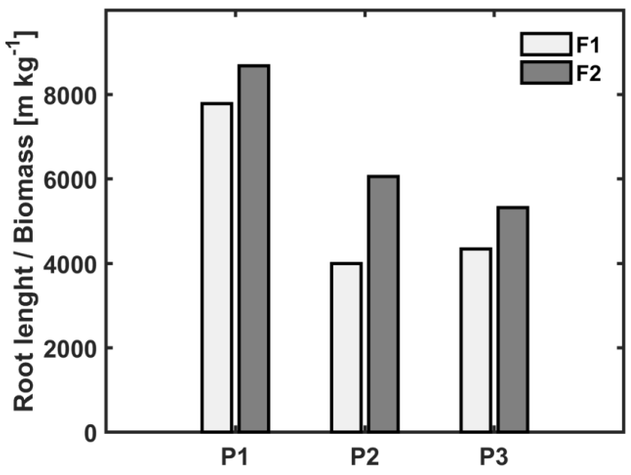

Fig. 4. 4 Ratio of root length to biomass in the three plots (P1: sheltered; P2: rainfed; P3, irrigated) of the stony (F1) and silty (F2) soils.

4.3.2 Inverse estimation of soil and root water uptake parameters of the Feddes-Jarvis and Couvreur models from soil water contents and water potential measurements

Time series of observed and simulated SWC and SWP are illustrated in Fig. 4.5 and 4.6 for the plots with different water treatments of the stony and silty soils, respectively. As expected, the irrigated plots were wetter than the rainfed and sheltered plots but in the top layers of the silty soil measured water contents and pressure heads decreased between irrigation events to similar low values as in the non-irrigated plots. For the period that measurements were carried out in both soils (from mid of May until beginning of July) the SWPs in the sheltered and rainfed plots were more negative in the stony than in the silty soil suggesting that the crop experienced more water stress in the stony soil. In both soils, the top layer dried out considerably and low SWP (-10^4 cm) was reached as a result of high evaporation and transpiration demand. In the sheltered and rainfed plots of the stony soil, such low SWP were also reached in the deeper soil layers (-60 and -80 cm) whereas SWPs stayed higher at those depths in the silty soil due to the larger water holding capacity of the silty soil.

The statistics RMSE, ME, and *d* of the SWC and SWP simulated by the two models are listed in Table S1. Since the statistics were very similar for both models, there was no notable difference between simulation accuracies of the FJ and C models. The values of RMSE for SWC in the stony soil (0.02 to 0.03 cm^3 cm^{-3}) were almost half of those in the silty soil whereas for SWP the values did not differ much between the two soils (from 0.3 to 0.9 log_{10}([-cm])). The larger RMSE of SWC in the silty soil is also due to the larger uncertainty in the measured SWC due to the variability of SWC between the four replicate TDR sensors (standard error of the sample mean reached 0.035 cm^3 cm^{-3}) (Cai et al., 2016).

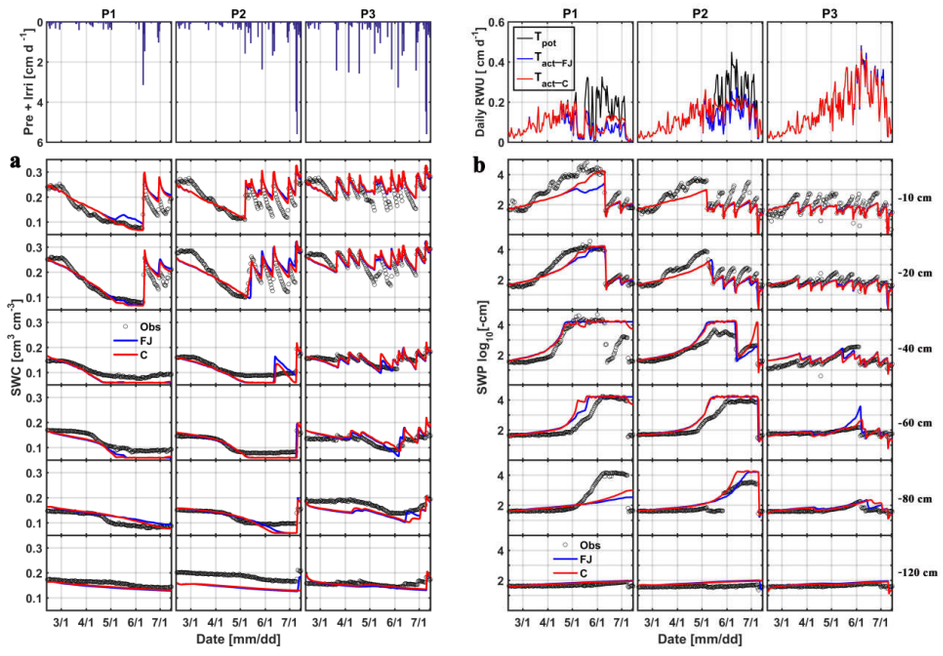

Fig. 4. 5 Comparison between observed (black) / simulated (a) soil water content (SWC) and (b) soil water pressure head (SWP) by the Feddes-Jarvis (FJ, blue) and Couvreur (C, red) models at six soil depths in the sheltered (P1), rainfed (P2), and irrigated (P3) plots of the stony soil (F1) from 11 Feb. to 14 July 2014. Time series of precipitation (right) and irrigation rates (left) and of the potential daily potential (T_{pot}) and actual transpiration (T_{act} = RWU) that were simulated by the Feddes-Jarvis (FJ) and Couvreur (C) models are given in the panels above the SWC and SWP measurements.

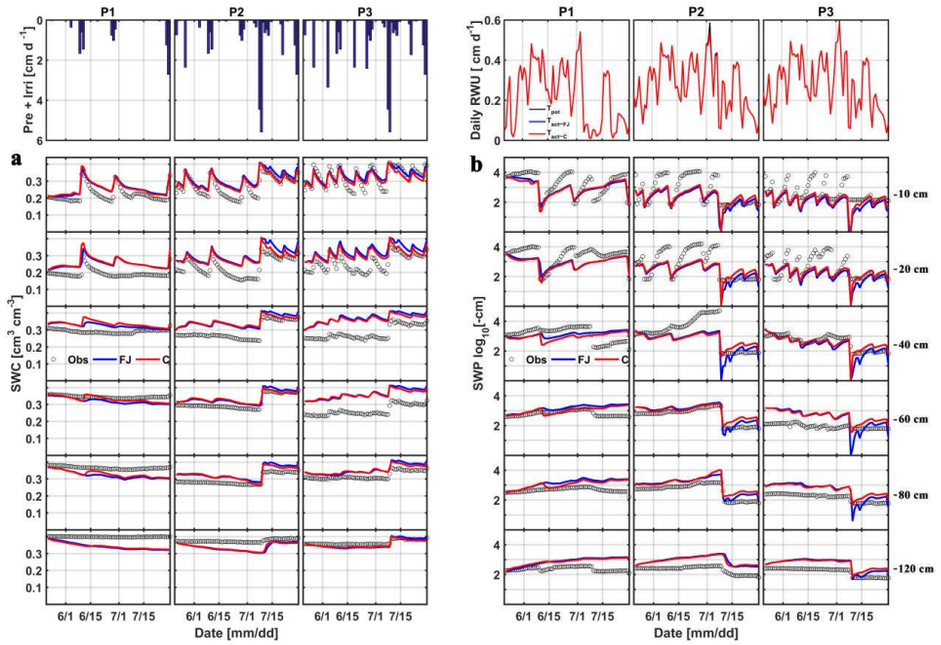

Fig. 4. 6 Same as Fig. 4. 5 but for silty soil from 22 May to 30 July 2014.

The obtained soil hydraulic parameters, parameters of the water stress function of the FJ model, and root-system parameters of the C model are listed in Table 4.4. The corresponding hydraulic conductivity curves are plotted in Fig. D1. For the stony soil, the soil hydraulic parameters estimated by the two models were comparable but larger differences between the model parameters were obtained for the subsoil layer of the silty soil. Smaller (even negative) tortuosity parameters l were obtained for silty than for the stony soil which implies that in the latter the hydraulic conductivities decrease stronger with a decrease in saturation degree. For the same water content, hydraulic conductivities were higher in the stony than in the silty soil.

Table 4. 4 The saturated hydraulic conductivity (K_s), model shape parameter (l), critical pressure head in the Feddes water stress function (h_{3h}, h_{3l}), the critical water stress threshold (ω_c), and the root system related parameters (K_{rs} and K_{comp}) estimated by the Feddes-Jarvis (FJ) and Couvreur (C) models of the stony (F1) and silty (F2) soils.

Site	Model	K_{s1} (cm h^{-1})	l_1 (-)	K_{s2} (cm h^{-1})	l_2 (-)	h_{3l} (cm)	h_{3h} (cm)	ω_c (-)	$K_{rs\_ini}^*$ (cm h^{-1})†	$K_{comp\_ini}^*$ (cm h^{-1}) †	OF
F1	FJ	0.663 (3.417) ††	4.669 (1.470)	1.581 (0.026)	3.459 (-2.797)	-694 (-1172)	-238 (-648)	0.95 (0.8)	-	-	33.42 (41.79)
	C	0.426 (3.853)	3.773 (1.472)	1.556 (0.021)	3.947 (-2.892)	-	-	-	1.20×10^{-7} (1.26×10^{-7})	3.89×10^{-8} (3.74×10^{-8})	33.40 (40.97)
F2	FJ	0.450	-1.358	0.144	-3.165	-747	-279	0.95	-	-	31.93
	C	0.417	-2.219	0.623	1.379	-	-	-	8.60×10^{-8}	4.77×10^{-9}	35.90

† $K_{rs\_ini}^*$ and $K_{comp\_ini}^*$ are K_{rs_ini} and K_{comp_ini} normalized by root length per surface area.
† † Parameters obtained using only measurements in the sheltered plot of the stony soil (Cai et al., 2017).

For the FJ model, parameters of the stress function were similar for the stony and silty plots, which implies that the estimated parameters were not sensitive to the different root density in the two different soils. It is important to note that the difference in root density between the different water treatments in one soil was not considered in the model since only one parameter set was used to simulate the different water treatments. The obtained threshold values of the stress function α_F, h_{3l} and h_{3h} in Eq. 4.8 were higher than the lowest SWPs measured and simulated in the top- and subsoil layer in the sheltered and rainfed plots of the stony soil. Consequently, the FJ model simulated a reduction in RWU due to reduced water availability in these plots (Fig. 4.5b). For the silty soil, h_{3l} and h_{3h} were also higher than the lowest SWPs measured in the topsoil layer but lower than the SWPs in the subsoil. However, despite the lower SWPs in the topsoil and the low compensatory uptake (high ω_c), no reduction in transpiration rate was simulated in the silty soil (Fig. 4.6b) as compared to the calculated potential transpiration rate. A first explanation for this observation is, that the high root density in the subsoil made that most of the water was simulated to be taken from the subsoil where SWP was high. Therefore, a reduction of uptake in the top layer where root densities were low would not affect the total uptake considerably and would require only a small compensatory uptake from the subsoil. Albasha et al. (2015) noted that compensatory water uptake could also be caused by increased root growth in soil layers where more water is available. The second explanation is, that the

simulated SWP in the topsoil layer remained higher than corresponding measured values which is another reason why no reduction in transpiration was simulated in the silty soil.

Temporal changes in root system hydraulic conductance K_{rs} of the C model is illustrated in Fig. 4.7 for the stony and silty soils. The K_{rs} values in the different plots of the same soil were calculated using the same fitted initial K_{rs_ini} and RLDs so that the difference in K_{rs} between the different plots of the same soil reflected differences in RLD. However, K_{rs_ini} was fitted independently for the two different soil types. The higher K_{rs} obtained for the silty soil with the higher root density than the stony soil supports our hypothesis that the root system hydraulic conductance increases with the RLD. Considering the root system conductance that was normalized by the root length per soil surface area, the normalized root conductance was different for the two different soils. The value of the normalized K_{rs_ini} was 1.4 times larger and normalized K_{comp_ini} 8.2 times larger in the stony than in the silty soil. This indicated that for a single root segment the root conductance and compensatory ability was higher in the stony soil than in the silty soil. This difference does not support our assumption that K_{rs} is directly proportional to the RLD. It indicates that the different development of the root system in the stony soil, in which more water stress occurred, had an impact on the root hydraulic conductance of individual root segments.

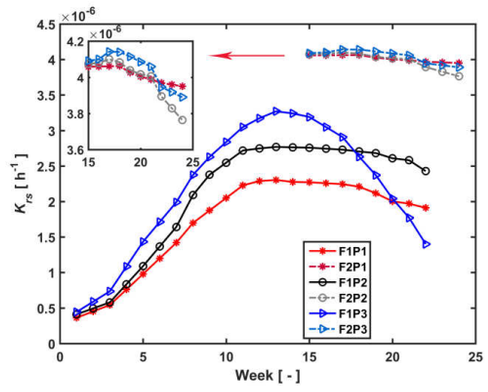

Fig. 4. 7 Estimated root hydraulic conductance (K_{rs}) in the three plots (P1: sheltered; P2: rainfed; P3: irrigated) of the stony (F1) and silty (F2) soils during the measurement period (F1: from 11 Feb. to 11 July 2014, F2: from 23 May to 24 July 2014).

To evaluate the uniqueness of the estimated parameters of the FJ and C models, response surfaces of the objective function were plotted. Selected contour plots in Fig. D2 show that the soil hydraulic parameters were identifiable. The parameters in the C model were also identifiable in both soils but K_{rs} and K_{comp} in the silty soil could be less precisely identified than in the stony soil. When RWU is not reduced and remains equal to the potential transpiration, which was the case in the silty soil (see later), Eq. 4.6 states that K_{rs} can decrease without changing the RWU by decreasing H_{leaf} until the H_{leaf} reaches the critical leaf water potential. This explains why regions with low objective function values are bound by minimally possible K_{rs} values but not by maximally possible K_{rs} values in the silty soil. When RWU is lower than the potential transpiration, there is also a maximally possible K_{rs} value so that leaf water potentials still reach the critical leaf water potential during the simulation period. In agreement with what was found by Cai et al. (2017), the response surface did not show a distinct global minimum for the water stress parameters in the FJ model.

In contrast to the current study, Cai et al. (2017) inversely estimated the soil hydraulic parameters and parameters of the FJ and C models using only observations from the sheltered plot in the stony soil. Inclusion of data from the rainfed and irrigated plots had an impact on the optimized soil hydraulic parameters (see values in parentheses in Table 4.4) whereas similar values of the root hydraulic conductances K_{rs_ini} and K_{comp_ini} were obtained. Including data that represent the hydraulic behavior of the soil under wetter conditions led to higher estimates of the hydraulic conductivity of the subsoil under wet conditions but lower estimates of hydraulic conductivities in the topsoil and in the subsoil for drier conditions (see Fig. D1). Using the parameter set obtained by Cai et al. (2017) resulted into a slightly better (e.g. for SWC, RMSE was 0.0057 and 0.0036 smaller for FJ and C models, and d was 0.0257 and 0.0129 higher for FJ and C models) estimates of SWC and SWP in the sheltered plot but to an underestimation of the SWC and SWP in the rainfed and especially in the irrigated plot (see Fig. D3). This illustrates that soil hydraulic parameters that were obtained for a certain set of boundary conditions are not always transferable to other conditions. Combining experimental datasets that represent a wider range of boundary conditions is therefore preferable.

4.3.3 Simulations of root water uptake and comparison with sap flow measurements

The cumulative ET_{pot}, T_{pot}, and RWU simulated by the FJ and C models in the three plots of stony and silty soils during the whole measurement period and during the overlapping period of measurements in both soils are shown in Fig. 4.8. The higher cumulative ET_{pot} in the stony plot than in the silty plots is simply due to the longer measurement period in the stony plot. The lower ET_{pot} in the sheltered plot results from the lower net-radiation due to sheltering as compared to the neighboring unsheltered plots. The difference in cumulative ET_{pot} between the stony and silty soils during the overlapping measurement period results from different K_c values due to different time of ripening of the crop in the two soils (Table 4.1). The ratio T_{pot}/ET_{pot} was considerably smaller in the stony soil than in the silty soil since the early crop development stage, when the crop canopy was not fully covering the soil and the LAI was low, was not covered by the measurement period in the silty soil. Differences in LAI also explain the smaller T_{pot}/ET_{pot} ratio in the sheltered plot of the stony soil compared with the rainfed and irrigated plots of this soil and the larger T_{pot}/ET_{pot} in the silty than in the stony soil during the overlapping measurement period. This illustrates that the potential water uptake by the wheat crop from the sheltered plot of the stony soil differs substantially from that of the other plots due to a different crop development and LAI. Only in the sheltered and rainfed plots of the stony soil, the simulated T_{act} or RWU was reduced compared to the T_{pot}. In the silty plot, there was no reduction in simulated T_{act} compared to T_{pot} indicating that the calculated soil water supply in the root zone in the silty soil was sufficient for meeting the atmospheric demand.

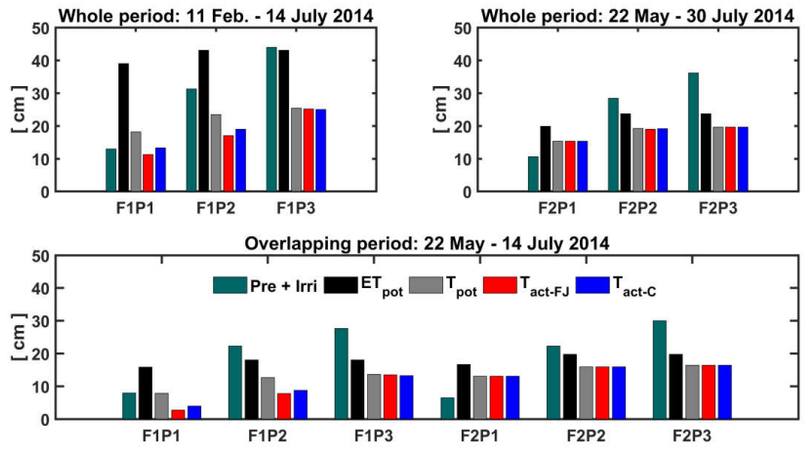

Fig. 4. 8 Potential evapotranspiration (ET_{pot}), potential transpiration (T_{pot}), and actual transpiration (T_{act} = RWU) estimated by the Feddes-Jarvis (FJ) and Couvreur (C) models in the three plots (P1: sheltered; P2: rainfed; P3: irrigated) of the stony (F1) and silty (F2) soils in the whole period (F1, from 11 Feb. to 14 July 2014; F2, from 22 May to 30 July 2014) and in the overlapping period (from 22 May to 14 July 2014).

Figure 4.9 shows potential and actual RWU simulated by the FJ and C models, and sap flow in the three plots of the stony soil and the silty soil from 23 May to 6 July 2014. When the measured sap flow was regressed against the simulated RWU by the two models, there was a good agreement between crop transpiration obtained from the sap flow measurements and model simulations with r^2 of 0.86 by the FJ model and 0.85 by the C model. But, there was a constant offset of 0.05 cm d^{-1} between the sap flow measurements and the simulated RWU (Fig. 4.10a). The observed sap flow and the simulated T_{act} were both higher in the silty than in the stony soil. In the silty soil, the sap flow measurements did not differ considerably between the different water treatments, which was consistent with the simulated T_{act} that was equal to T_{pot}. For the stony soil, the measured sap flow differed between the different water treatments which was also consistent with the differences in simulated T_{act}.

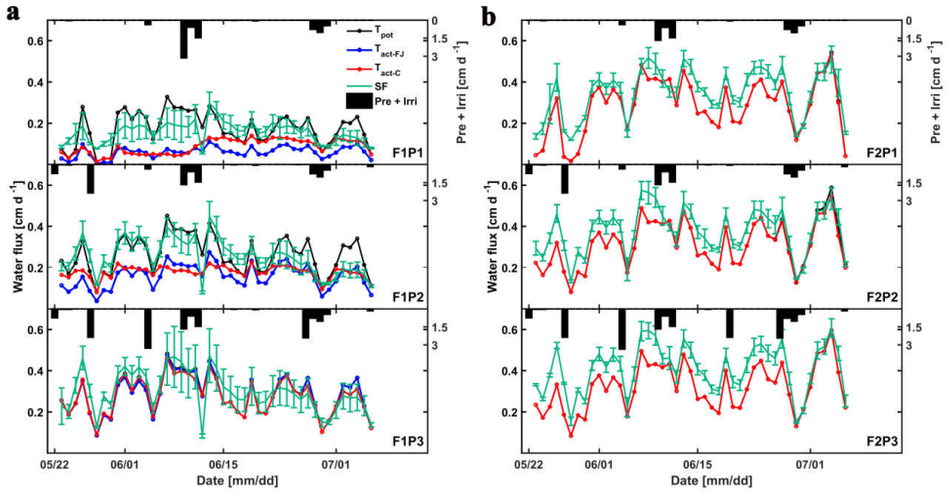

Fig. 4. 9 Daily cumulative solar radiation, potential transpiration (T_{pot}), root water uptake (T_{act} = RWU) simulated by the Feddes-Jarvis (FJ) and Couvreur (C) models, and sap flow (SF) in the three plots (P1: sheltered; P2: rainfed; P3: irrigated) of (a) the stony (F1) and (b) silty soils (F2) from 23 May to 6 July 2014. Pre: precipitation, Irri: irrigation.

There was, as far as we know, no similar comparison between sap flow and simulated RWU using field observations for wheat crop. Due to the "delicate anatomy of the walls of hollow wheat stems" (Langensiepen et al., 2014), it is challenging to install the sensors and measure the temperature variation of the thin wheat stalk with high time frequency for the field condition. Furthermore, spatial variation in environmental conditions that influence the sap flow in a single stem and variability in stem development lead to a considerable stem to stem variability in sap flow in which the average deviation from mean sap flow is quantified for the three different treatments shown in Fig. 4.9 (Chabot et al., 2005; Zhang et al., 2014). The simulated RWU was based on a chain of models linked with assumptions and preset parameterizations starting from the calculation of the potential crop evapotranspiration using the empirical FAO56 approach, its split into soil evaporation and transpiration as a function of LAI, and its reduction to actual transpiration as a function of soil water potential. The overall good correlation between simulated RWU and sap flow measured transpiration therefore gives some confidence in the used approaches.

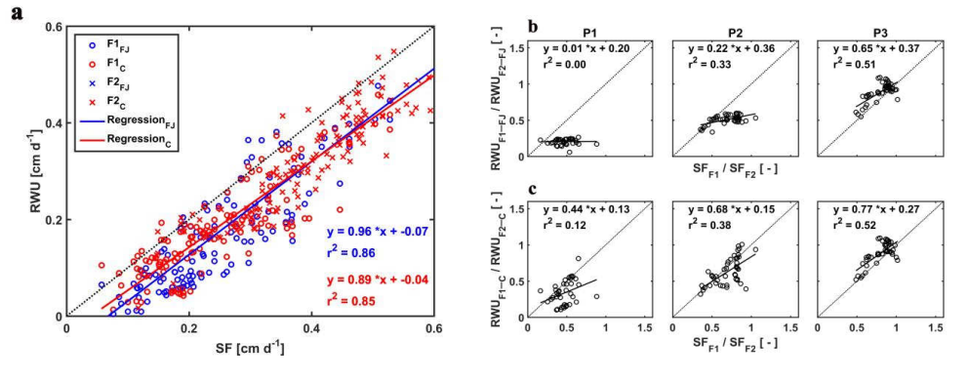

Fig. 4. 10 Correlation (a) between sap flow (SF) and root water uptake (RWU) simulated by the Feddes-Jarvis (FJ) and Couvreur (C) models of the stony (F1) and silty soil (F2). Relation between the ratio of the RWU in the stony to the RWU in the silty soil estimated by the FJ (b) and C (c) models in the three plots (P1: sheltered; P2: rainfed; P3, irrigated) versus the ratio of sap flow in the stony soil to that in the silty soil.

In order to unravel further the model's capability to calculate RWU in different soils and for different water treatments, we made plots of the ratios of the measured sap flow in the two soils versus the ratios of simulated RWU in the two soils for the different water treatments (Fig. 4. 10b and c). Ratios were used to cancel out the temporal variations due to varying meteorological conditions. The good agreement between measured and simulated ratios for the irrigated plots, in which RWU was not influenced by water availability, indicates that the differences in potential transpiration rates between the two plots due to different crop development (ripening) and LAI were adequately represented in the models. There is no difference between the FJ and C models since RWU is completely defined as a boundary condition and not dependent on the soil water status in the irrigated plots, which was discussed by Cai et al. (2017). For the rainfed and sheltered plots, the correlation between the measured and simulated ratios is smaller. These ratios represent to what extent the simulated reduction of RWU in the stony soil due to reduced water availability is consistent with the measured reduction in sap flow relative to the simulated RWU and measured sap flow in the silty plots where there was no reduction in RWU. Of note is that simulations by the C model are more consistent with the sap flow measurements than the simulations by the FJ model. First, the FJ model predicts a larger reduction in RWU than the sap flow measurements suggest (see Fig. 4.9). Secondly, the ratios of the FJ model simulations vary less than the ratios of the sap flow measurements whereas the range of ratios of the C model

simulations is more in agreement with the sap flow measurements. This indicates that the C model represents better than the FJ model how changing soil moisture and soil moisture distributions change the RWU. Furthermore, since the root hydraulic conductance in the C model depends on the root density, the model can reflect the impact of the differences in root density between the different water treatments on RWU. The FJ model did not possess this flexibility since only one set of water stress parameters was used for the different water treatments. Similar observations were made by Vandoorne et al. (2012) who optimized the water stress parameters of the FJ model for Chicory (*Cichorium intybus L.*) and found that the values of those parameters had to be adapted for different soil moisture conditions and different plant growth stages.

Sap flow per unit soil surface area was obtained by multiplying the average sap flow in the measured tillers with the number of tillers per unit soil surface area. Figure 4.11 shows the average sap flow per tiller and the sap flow per unit leaf area index. For the silty soil, the sap flow per tiller and sap flow per leaf area were very similar for the different water treatments. For the stony soil, the sap flow per tiller in the irrigated plot was similar to that in the silty soil until approximately 15 June. After that, the sap flow per tiller reduced in the irrigated plot of the stony soil because of the reduction in leaf area (the sap flow per leaf area remained similar to that in the silty soil). Water stress limited the leaf development of wheat in both longevity and quantity (Khalid et al., 2016; Zhou et al., 2015). The sap flow per tiller in the rainfed plot of the stony soil became smaller than that in the irrigated plot or in the silty soil after 11 June but recovered for a short time period to same sap flow after the rainfall on 10 June. This recovery was also observed for the sap flow in the sheltered plot of the stony soil. But, the sap flow per tiller was generally lower in this plot than in the other plots. This indicates that transpiration in this plot was reduced by both a reduced number of tillers and a lower flux per tiller. It is interesting to note that the sap flow per leaf area surface in the sheltered stony plot shortly increased to higher values than in other plots after the rainfall event on 10 June.

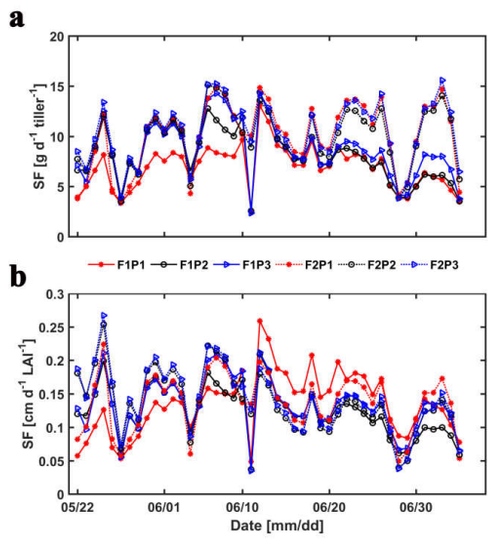

Fig. 4. 11 Measured sap flow (SF) per tiller (a) and per unit leaf area index (LAI) (b) in the three plots (P1: sheltered; P2: rainfed; P3, irrigated) of the stony (F1) and silty (F2) soils.

4.3.4 Effects of root and shoot development on simulated transpiration

The different root development in the two soils and for the different water treatments (Fig. 4.3) was related to a different parameterization of the root hydraulic conductance (Fig. 4.7). The different shoot development and different LAI values (Fig. 4.2a) affected calculations of potential transpiration rates (Fig. 4.8) that were used as boundary conditions for RWU simulations. In order to demonstrate the impact of the plant development on the RWU simulation, we conducted two sets of simulations in which the plant parameters were prescribed by measurements done in another soil and/or water treatment. In the first set of simulations, we changed the root hydraulic conductance, K_{rs}. For the stony soil, K_{rs} of all plots were rescaled by a factor of 1.78 which corresponds to the ratio of K_{rs} in the sheltered plot of the silty soil in week 15 to K_{rs} in the sheltered plot of the stony soil in the same week. This rescaling represents how RWU would change if the plants would not reduce the root hydraulic conductance in the stony soil. For the silty soil, K_{rs} was scaled by a factor of 0.56, which is the inverse of the factor used to scale the root conductance in the stony plot. The rescaling for the silty plot represents how

water uptake in the silty soil would be reduced if the root conductance was equal to that in the sheltered plot of the stony soil. For the stony plot, rescaling (i.e. increasing) the root conductance increased the cumulative water uptake only by about 2% in all plots (see Table 4.5). Increasing the root conductance therefore did not increase substantially the amount of water that could be extracted from the stony soil. For the silty soil, rescaling (i.e. decreasing) the root conductance in fact generated water stress and reduced the RWU by 9%. Therefore, the root system with higher root densities and conductance in silty soil is apparently not 'over-dimensioned' whereas increasing the root conductance in the stony soil would hardly lead to more water uptake.

Table 4. 5 Cumulative root water uptake simulated by the Couvreur model using K_{rs} obtained from the silty soil (F2) for the stony soil (F1) and using K_{rs} obtained from the stony soil for the silty soil. P1, P2, and P3 are the sheltered, rainfed, and irrigated plots. Values in parentheses are simulated RWU using the optimized parameters from measured SWC and SWP in the respective plots.

	P1	P2	P3
F1	13.55 (13.27)	19.38 (19.01)	25.40 (25.02)
F2	14.04 (15.36)	17.40 (19.12)	17.96 (19.65)

In a second set of simulations, we changed the calculated potential transpiration of the sheltered stony plot to that of the irrigated stony plot (Fig. 4.12). Only the stony soil was considered since the shoot and LAI development did not differ considerably between the different water treatments in the silty plot. Until 1 May, there was almost no difference in the LAI and T_{pot} among different plots so that there was also no big effect on the simulated T_{act}. T_{pot} in the irrigated plot started to deviate from T_{pot} in the sheltered plot from 1 May due to higher LAI in the irrigated plot (Fig. 4.2a). Increasing T_{pot} in the sheltered plot did not affect the simulated RWU by the C model. In this model, the boundary condition switches to a constant pressure head boundary condition when stress occurs so that the simulated root water becomes independent of the potential transpiration rate.

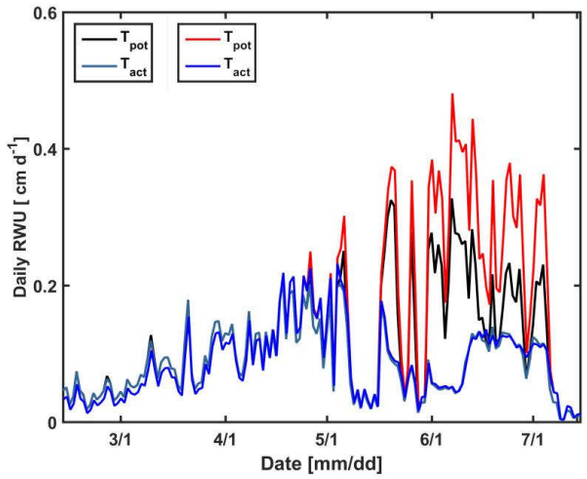

Fig. 4. 12 Daily potential (T_{pot}) and actual transpiration (T_{act} = RWU) estimated by the Couvreur model using the measured leaf area index (LAI) in the sheltered plot (black and cyan) of the stony soil and the LAI in the irrigated plot of the stony soil (red and blue).

Of interest is also the time at which water uptake starts to decrease and its effect on plant development. In the sheltered and rainfed stony plots, a slight reduction in RWU is simulated during April. This reduction in RWU was accompanied by only a slight decrease in LAI development compared to the irrigated plot (Fig. 4.2a). After mid of May, which is also the period when RWU more strongly reduced, the LAI did not increase anymore in the sheltered plots whereas in the other plots of the stony soil, it reached its maximum at the beginning of June. In the silty soil, the maximum was reached at the beginning of July. The root system reached its full development, however, earlier than the time when the LAI reaches its maximum (Fig. 4.3). The root system development in the stony plot was much stronger reduced by the lower water availability in April than the LAI development. Both leaves and roots showed reaction to environmental changes but this reaction was not simultaneous. Walter and Schurr (2005) reviewed studies of leaf and root growth of herbaceous plants and indicated that roots experienced more directly the effect of environmental factors (i.e. water stress, nutrient deficiency) compared with leaves. They also indicated that roots responded faster than leaves to the environmental conditions to optimize resource use efficiency.

4.4 Conclusions

The different crop development of winter wheat had consequences for the parameterization of RWU models. First, the different shoot development led to differences in boundary conditions such as the potential evapotranspiration (K_c factor) and the potential transpiration (LAI). Differences in root development led to differences in root density distributions, root system conductivities, and RWU stress parameters. Water stress led to smaller root system conductances in the C model and a reduction of the RWU for less negative soil water potentials in the FJ model. Such a down-regulation of the root system conductance due to drought stress has also been reported by Maurel et al. (2010), Trillo and Fernandez (2005), and Wang et al. (2013) wheat, and Matsuo et al. (2009) for rice.

The C model, which is based on a physical description of the flow in the soil-root system, represented the effect of the differences in root system development on RWU directly since it relates the root system conductance to the root length. When root parameters that were obtained from the sheltered stony plot were used to predict RWU in the silty soil, water stress was simulated in the silty soil. On the other hand, when root parameters obtained from the silty soil were used to simulate water uptake in the stony plot, the water uptake could only slightly be increased but the 'severity' of the water stress remained the same. This suggests that the root system that developed in the stony soil would be under-dimensioned for the silty soil and the opposite for the root system that developed in the silty soil.

The simulated differences in transpiration from the two different soils and the different water treatments could be confirmed by sap flow measurements. The physically-based C model predicted the ratios of the transpiration fluxes in the two soil types slightly better than the FJ model. Since the transpiration from the silty soil was close to T_{pot}, these ratios represented to what extent the transpiration was reduced due to reduced water availability in the stony soil.

This study illustrated that a combined dataset of root and shoot development, of soil water contents and soil water potentials, and of transpiration fluxes derived from sap flow measurements can be used to parameterize and validate RWU models. These models require inputs about root and shoot developments, which were observed to depend strongly on the

environmental conditions. In how far the C model can improve prediction of RWU, transpiration and soil water stock depletion in widely used crop models for different crops and climate conditions is subject of further investigations. Next to improving the description of the RWU, the C model also simulates the water potential in the root collar. In the current model formulation, the water potential in the collar is used as a control variable which is kept fixed when a critical threshold value is reached. We interpreted the reduction in transpiration when this threshold was reached as 'water stress'. However, we observed considerable reduction in aboveground biomass even when no reduction in transpiration was simulated (or observed with sap flow measurements), e.g. in the sheltered and rainfed silty soil plots. Next to transpiration, stomatal opening, and carbon assimilation, plant growth is also linked to the hydraulic status of the shoot (Tardieu et al., 2014). Improving the prediction of the shoot water potential, which is closely linked to the water potential in the root collar, is therefore also important to predict the reaction of plant growth to environmental conditions related to drought stress.

Concerning the observations of the root development using horizontally rhizotubes, it needs to be further investigated how root counts along rhizotubes can be translated to root densities. Also, the reasons for the constant offset between the simulated transpiration and the sap flow measurements need to be further investigated.

Chapter 5

Synthesis

5.1 Final conclusions

The objective of this study was to investigate the effect of soil water distribution on root development and RWU simulated by different RWU models using the measured soil moisture and root growth in the field. To answer the questions that were posed for achieving the objective, a first emphasis was put on introducing two MR facilities with horizontally installed rhizotubes that were constructed in the stony and silty soils by different methods in Chapter 2. Measurements in the facilities indicated that differences in the dynamics of root development, soil water content, soil water potential, and soil temperature can be observed between different soil types and water treatments with minimal destruction. To get a representation of the root distribution, 120 images were collected at each soil depth. The observed roots in the horizontal direction were not spatially correlated. The local soil moisture measurements within a water treatment and soil depth varied considerably between different TDR sensors and for three out of 36 soil texture-water treatment-soil depth combinations. Data measured from three sensors (72 in total) in the silty soil were identified as outliers using statistic outlier detection. SWC's measured by GPR in the rhizotubes show a similar trend but lower than the SWC measured by TDR.

Chapter 2 also offered answers to question 2. The root and shoot development of winter wheat differed considerably between the two soils (stony vs. silty) with different water holding capacity and for different water treatments. Root density was larger in the irrigated plots and in the silty soil than in the stony soil. Comparing the spatio-temporal root distribution in the two facilities indicates that plant water stress depends rather on the soil water potential than on the soil water content.

To answer question 3, inverse modeling was conducted using different dataset in Chapter 3 and 4. Using only the data from the sheltered plot in the stony soil, the three models, the Feddes (without compensation), the Feddes-Jarvis (with compensation), and the Couvreur (with compensation) models described the soil water content and water potential equally well. The soil hydraulic parameters inversely estimated by the two models considering uptake compensation were comparable, whereas the parameters obtained by the Feddes model were different. The obtained RWU parameters of the Feddes-Jarvis model and root hydraulic parameters of the Couvreur model were consistent with data reported in the literature. Response surface analysis

indicated that the root hydraulic parameter could be identified but the onset of the water stress as a function of the water stress could not be uniquely identified.

When combining the observations from the three plots of each facility, the soil hydraulic properties could be well constrained by the Feddes-Jarvis and the Couvreur models. The soil hydraulic parameters estimated by the two models were similar in each soil. But for the stony soil the values were different from the ones previously obtained from only the sheltered plot possibly due to soil heterogeneity in the whole test site, varied boundary conditions (e.g., ET_{pot}, root distribution, root hydraulic conductance), and the fact that more data from times when the soil is wet are included in the dataset which leads to different estimates of the hydraulic conductivity. Root-system related parameters of the Couvreur model could be constrained but not the parameters of the water stress function of the Feddes-Jarvis model.

The simulations conducted in Chapter 3 and 4 answered question 2 and 4. The RWU profiles simulated by the Feddes-Jarvis and the Couvreur models differed due to different water redistribution by the root system. However, there was no obvious difference between the two models in simulated total RWU and other water fluxes. The Feddes-Jarvis and the Couvreur models simulated similar root-system scale stress functions that link total RWU to the effective root zone water potential. This suggested the parameters of the two models may transferable at root-system or crop scale. Results obtained from the combined plots of each soil in Chapter 4 indicated that the water treatments and different soil textures had consequences for RWU simulation. In the stony soil, the two models simulated similar RWU which was the lowest in the sheltered plot. The RWU was also lower than the potential RWU in the non-irrigated plots. In the silty soil, RWU was equal to the potential uptake for all treatments. The variations of estimated RWU matched well with the measured sap flow for all plots of the two facilities. There was, however, a constant offset between the two approaches, which needs to be further investigated. The physically based Couvreur model predicted the ratios of the transpiration fluxes in the two soil types slightly better than the Feddes-Jarvis model. The reason for this is that the Couvreur model takes into account the effect of different absolute root density on the water uptake and its reduction when the soil water potential declines whereas the Feddes Jarvis model only uses the normalized root length densities. Using simulations with the Couvreur model, it was shown that developing higher root densities in the stony soil (similar to those in the silty soil) would hardly

reduce the water stress of the crop in the stony soil. On the opposite, lowering the root densities in the silt soil to those of the stony soil would also induce water stress in the silt soil. This indicates that an optimal root density developed depending on the soil type and water availability.

The results of using the parameters obtained from a single plot for the combined plots and the sensitivity analysis in Chapter 4 offered answers to question 5. The parameters estimated from the sheltered stony plot led to underestimation of the SWC and SWP in the two non-sheltered plots, which indicated that the model parameters obtained from a certain set of boundary conditions are not always suitable for other conditions (for instance, larger investigated area). When root parameters that were obtained from the sheltered stony plot were used to predict RWU in the silty soil, water stress was simulated in the silty soil. On the other hand, when root parameters obtained from the silty soil were used to simulate water uptake in the stony plot, the water uptake could only slightly be increased but the 'severity' of the water stress remained the same. This suggests that the root system that developed in the stony soil would be under dimensioned for the silty soil and the opposite for the root system that developed in the silty soil.

The simulation of RWU using the combined dataset of time series of soil moisture and root growth in this study also indicated that a simulation of crop development is needed for a full simulation of the soil-root-plant system, which could be explored in future research.

5.2 Outlook

MR facility is a system that provides the underground dynamics of root distribution, soil moisture, soil temperature, and aboveground variations of crop development, sap flow, leaf water potential, and canopy status *in situ*. The abundant information from the facility will not only serve for the investigation of different environmental factors on water flow in the soil-plant-atmosphere continuum and model evaluation but also provide the possibilities for coupling different models concerning water movement, root development, and crop growth at different scales. The measurements conducted in the MR facilities and RWU simulations conducted for winter wheat in this study could also be applied to other plant species.

This study indicated that soil textures largely influence the root and crop development and subsequently RWU or sap flow. Besides the soil texture, macropores (Landl et al., 2016; Pagliai

and Denobili, 1993; Valentine et al., 2012), soil structures (Gao et al., 2016; Pagenkemper et al., 2014), and soil compaction (Glab, 2007; Iijima et al., 1991) were proven to influence root growth and distribution. It will have effects on the variations of RWU. However, few studies reported the impact of those factors on RWU using both field experiments and modeling studies (Amato and Ritchie, 2002). Moreover, wetting and drying cycles could lead to variations in soil structure and soil hydraulic conductivity (Csorba et al., 2014; Lehrsch and Kincaid, 2010; Mapa et al., 1986), which was not often considered in the RWU modeling. Applying dynamic soil hydraulic conductivity in RWU models will be challenging. Considering these influences may help to improve the prediction of plant water use for different soil and water status.

Root hydraulic properties were changed due to the root development, water, and salinity stress (Colombo and Asselstine, 1989; Doussan et al., 1998; Ruggiero and Angelino, 2007; Zhao et al., 2005). The compensatory ability of roots may also differ in different growth periods and in different species. The inverse study of Vandoorne et al. (2012) indicated that the ω_c in the Feddes-Jarvis model was not unique in different growth periods. However, the relation between ω_c and crop or root development is still unknown. It could be investigated with functional-structural root models how the change in root architecture over time and the change in root hydraulic properties of root segments with aging affect the RWU distribution, its relation to root density, and compensatory RWU. In Chapter 3 and 4, the two RWU models (Feddes-Jarvis and Couvreur) predicted similar RWU and water stress function at root-system scale during the water stress period using effective soil water potential when the root hydraulic conductance did not change much. This indicated that there may be a relation between the two models and the parameters of the stress and compensation function may be transferable. To figure out this relation, a function that links the water stress parameters of the Feddes-Jarvis model to the root system parameters could be investigated. In addition, the order of magnitude of the root hydraulic conductance from the sheltered plot and combined plots of the stony soil and from the silty soil was the same with that obtained from the root architecture model, which may indicate that the root hydraulic conductance of winter wheat is a constant value or within a small range (having the order of magnitude as we obtained) in a certain growing period. This speculation may transferable for other crops in further investigation.

Based on the definition of RWU in the Couvreur model (Eq. 4.3), actual RWU was determined by root hydraulic conductivity and potential gradients between the soil-root interface and leaves of isohydric plants. As leaf water potential can be measured destructively (Boyer, 1967) and nondestructively (De Bei et al., 2011; Martinez et al., 2011), the dynamics of root hydraulic conductivity, therefore, can be obtained indirectly from sap flow, soil water potential, and leaf water potential measurements *in situ*. These measurements could help to validate the inversely estimated root hydraulic conductance. Especially under conditions that transpiration rate is not reduced by low soil water potentials, measurements of water fluxes in the soil-plant and water potentials and water contents in the soil only are not sufficient to constrain the root system conductances.

Using the shelter created water stress in the stony soil, which was indicated by the decreased SWP in the soil and reduced sap flow (or RWU) in the stem (root). For a canopy level, the leaf temperature was suggested to be an indicator of water stress (Jackson et al., 1981; Tanner, 1963) and the measurements showed good potential of crop water status estimation for irrigation scheduling (DeJonge et al., 2015; Gonzalez-Dugo et al., 2006; Moller et al., 2007). Variations of canopy temperature are also useful for investigating root plastic development response to different soil water status. A thermodynamic based RWU model (Hildebrandt et al., 2016) using canopy temperature was developed to study the effect of soil moisture heterogeneity from an energy perspective. Therefore, continuous measurements of canopy temperature from the leaves will offer additional information to better understand the RWU process in the water stress periods and evaluate the effect of heterogeneity of soil water distribution on plant growth and RWU from the aboveground.

Appendix

Appendix A

Grubbs' test is based on the differences between the sample mean and the extreme data considering the standard deviation of the whole sample. The suspected data is an outlier if Grubbs' value (G)

$$G > G_{crit} \quad \text{A1}$$

$$\text{where } G = \frac{|x_{sus} - \overline{x}|}{\sigma} \quad \text{A2}$$

$$G_{crit} = \frac{(N-1)}{N}\sqrt{\frac{(t_{a/(N),\ N-2})^2}{N-2+(t_{a/(N),\ N-2})^2}} \quad \text{A3}$$

G_{crit} is the critical value, x_{sus} the suspected value (max or min), $\overline{x}$ the mean value, σ the standard deviation, N the sample number, $t_{a/(N),\ N-2}$ the critical value of the t distribution with the significance level of a/N ($a/2N$ for two-sided tests) and a degree of freedom of $N-2$ for one-sided tests. The Dixon test is based on the differences between the two closest data points at the head or tail of the data set, which is defined as:

$$Q = \begin{cases} (x_2 - x_{sus})/(x_N - x_1), & \text{when } x_{sus} \text{ is the minimum} \\ (x_{sus} - x_{N-1})/(x_N - x_1), & \text{when } x_{sus} \text{ is the maximum} \end{cases} \quad \text{A4}$$

where Q is the Dixon value, details of the calculation of Q_{crit} can be found in Rorabacher (1991). As an alternative, the median is considered to deal with the outliers due to the insensitivity to the presence of the suspected data. In the MAD approach, the null hypothesis of outliers is rejected if:

$$|x_{sus} - M| < 2.5MAD, \text{ where } MAD = bM_{new}, \quad \text{A5}$$

where M is the median of the sample, M_{new} the median of the absolute difference between each sample data (x_i) and the median of the sample (M), and b a constant (usually equals 1.4826) disregarding the abnormality which was induced by outliers (Rousseeuw and Croux, 1993). A factor 2.5 is proposed to calculate the threshold from the MAD by (Leys et al. (2013)).

Appendix B

Table B 1 The analysis of variance (ANOVA) for the influence of different factors on root development (P<0.001*, P<0.01**, P<0.05*).**

Source	SS¶	DF	MS	F	Prob>F
Soil texture	272.19	1	272.185	517.48	<0.001***
Water treatment	11.22	2	5.611	10.67	<0.001***
Soil depth	324.1	5	64.82	123.23	<0.001***
Replicate (soil texture, water treatment, and soil depth)	743.74	1414	0.526	0.95	0.8859
Soil texture * Water treatment	1.6	2	0.799	1.52	0.2195
Soil texture * Soil depth	328.48	5	65.696	124.9	<0.001***
Water treatment * Soil depth	35.35	10	3.535	6.72	<0.001***
Error	1601.72	2880	0.556		
Total	3318.39	4319			

¶SS: sum of squares, DF: degree of freedom, MS: mean sum of squares, F: F-statistic value.

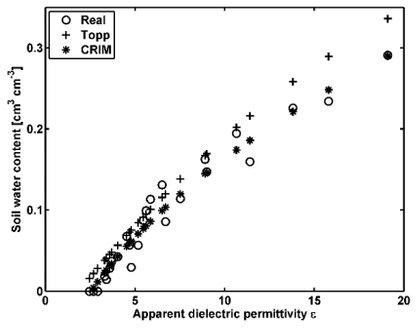

Fig. B 1 Relation between the dielectric permittivity measured by TDR, SWC added in the calibration (Real), and SWC calculated by (i) Topp's equation (Topp) and (ii) CRIM model (CRIM) in the calibration. For the calculation by Topp, RMSE = 0.0271, r^2 = 0.8825; for the calculation by CRIM, RMSE = 0.0154, r^2 =0.9623. In CRIM: $\theta = 0.1045\sqrt{\varepsilon} - 0.1671$. θ: the SWC, Ɛ: the relative dielectric permittivity.

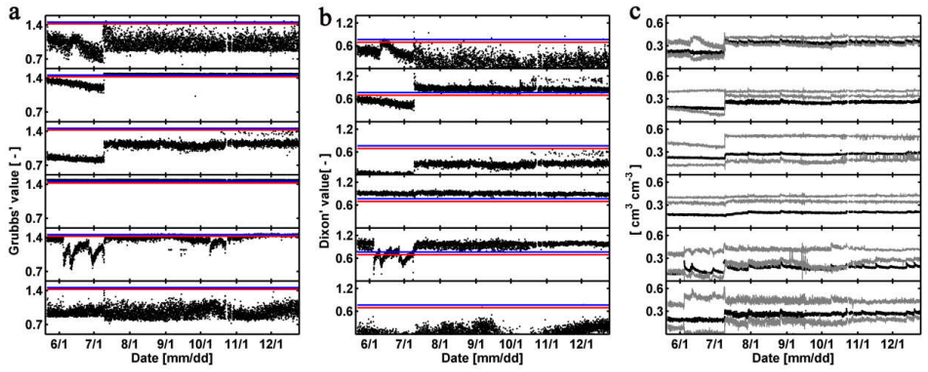

Fig. B 2 Outlier test for the SWC measured by suspected sensor at 40, 60, 80, and 120 cm in the rainfed plot, 40 cm, and 60 cm in the irrigated plot from the top to the bottom from 21 May to 24 Dec. 2014 by Grubbs (a), Dixon (b), and the median absolute deviation (c) approaches in the lower facility. In a and b, red and blue lines denote the common threshold values of 0.10 and 0.05, respectively. In c, black points are the suspected SWC; the gray curves are the upper and lower bounds of the Med approach.

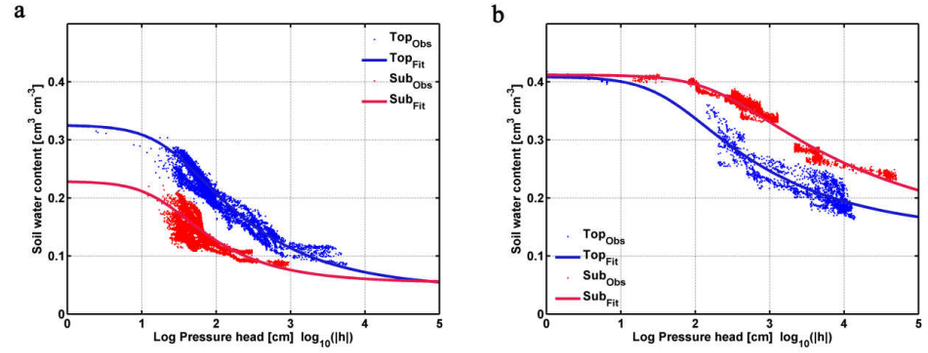

Fig. B 3 The water retention curves fitted from the measurements in the top- (0-30 cm) and subsoil (30-120 cm) of the upper (a, data points: 6562 for topsoil, 16153 subsoil) and the lower (b, data points: 3276 for topsoil, 7558 subsoil) facility. Pressure head was converted from the soil water potential. The RMSE and r^2 for the top- and subsoil of the two facilities were: 0.015, 0.021, 0.017, 0.010, 0.89, 0.35, 0.86, and 0.95 respectively.

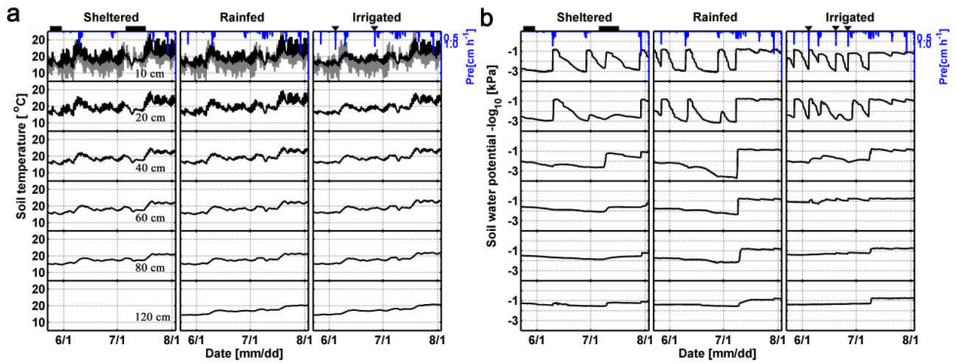

Fig. B 4 Time series soil temperature at six soil depths in the sheltered, rainfed, and irrigated plots of the upper (a) and lower (b) facilities. Gray curves: air temperature measured 2 m above the ground. ■: sheltered period, ▼: irrigation, Pre: precipitation. There was no data at 120 cm in the sheltered plot of the upper facility due to the malfunction of the MPS-2.

Appendix C

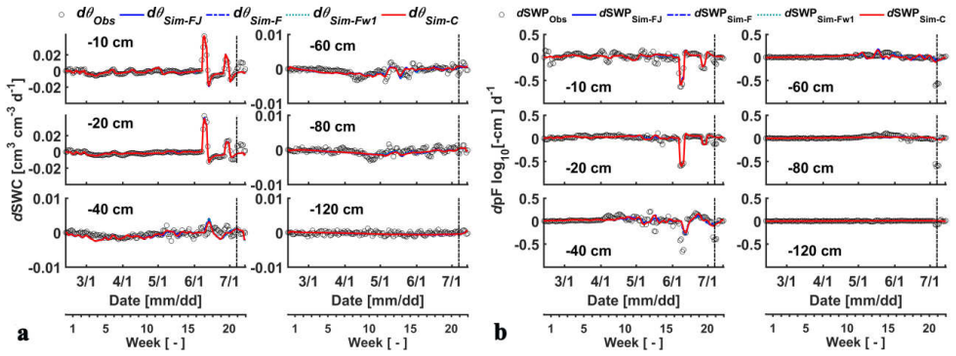

Fig. C 1 Comparison of the difference of SWC (a) and the difference of SWP (b) at six soil depths between observation ($d\theta_{obs}$, $d\mathrm{SWP}_{obs}$) and simulation ($d\theta_{Sim}$, $d\mathrm{SWP}_{Sim}$) by the Feddes model with and without compensation, and by the Couvreur model. FJ: Feddes-Jarvis, F: Feddes without compensation, F_{w1}: Feddes-Jarvis but $\omega_c = 1$, C: Couvreur.

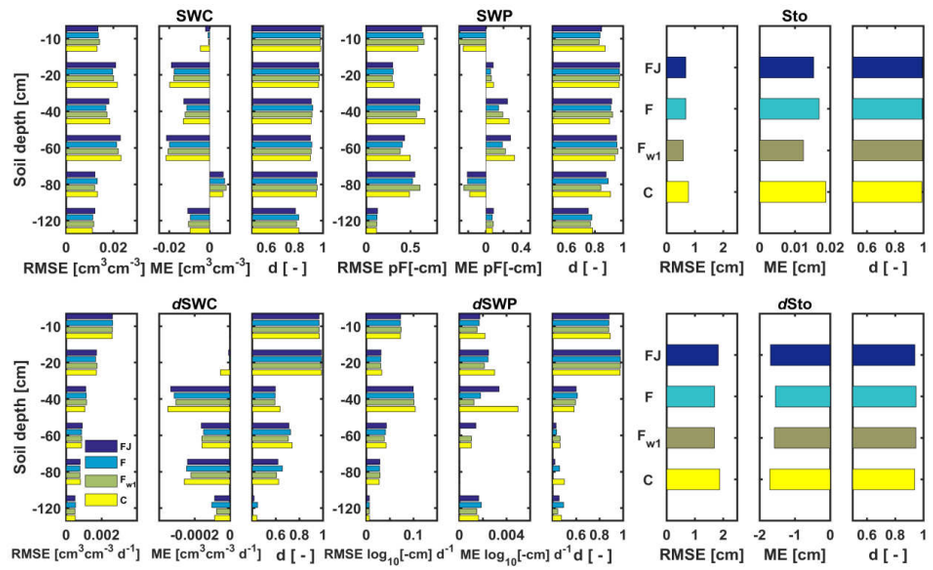

Fig. C 2 Statistical analysis of simulated results at six depths by the Feddes (FJ, F, and F_{w1}) and the Couvreur (C) models.

Appendix D

Table D 1 RMSE, MB and *d* (see Eq. 4.14, 15 and 16) for the Feddes-Jarvis (FJ) and Couvreur (C) models of the stony (F1) and silty (F2) soils. P1: sheltered; P2: rainfed; P3, irrigated.

		SWC						SWP					
		P1		P2		P3		P1		P2		P3	
		FJ	C	FJ	C	FJ	C	FJ	C	FJ	C	FJ	C
		$cm^3\ cm^{-3}$						$\log_{10}([-cm])$					
	RMSE	0.0241	0.0226	0.0324	0.0301	0.0238	0.0246	0.7315	0.6740	0.4874	0.5159	0.3162	0.3131
F1	MB	-0.0017	-0.0036	-0.0074	-0.0087	-0.0019	0.0012	-0.0014	0.0491	0.0607	0.0994	0.0312	-0.0040
	d	0.9330	0.9440	0.9121	0.9248	0.9398	0.9357	0.8453	0.8770	0.9011	0.8943	0.6530	0.6300
	RMSE	0.0460	0.0471	0.0490	0.0457	0.0654	0.0606	0.5451	0.5354	0.6378	0.6403	0.6656	0.6171
F2	MB	0.0001	0.0058	0.0311	0.0261	0.0476	0.0404	0.1017	0.0262	-0.0397	0.0474	0.0405	0.1712
	d	0.8502	0.8479	0.7843	0.8027	0.6120	0.6329	0.6145	0.6069	0.7630	0.7078	0.5421	0.5073

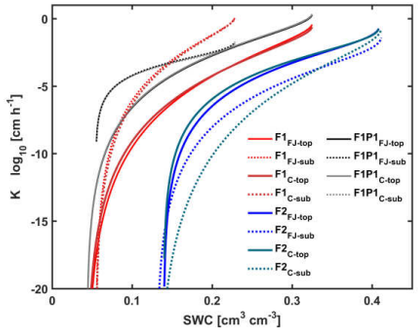

Fig. D 1 Relation between soil water content (SWC) and soil hydraulic conductivity (*K*) that was obtained by the Feddes-Jarvis (FJ) and Couvreur (C) models in the top- and subsoil of the stony (F1), the sheltered plot of the stony soil (F1P1), and silty (F2) soils.

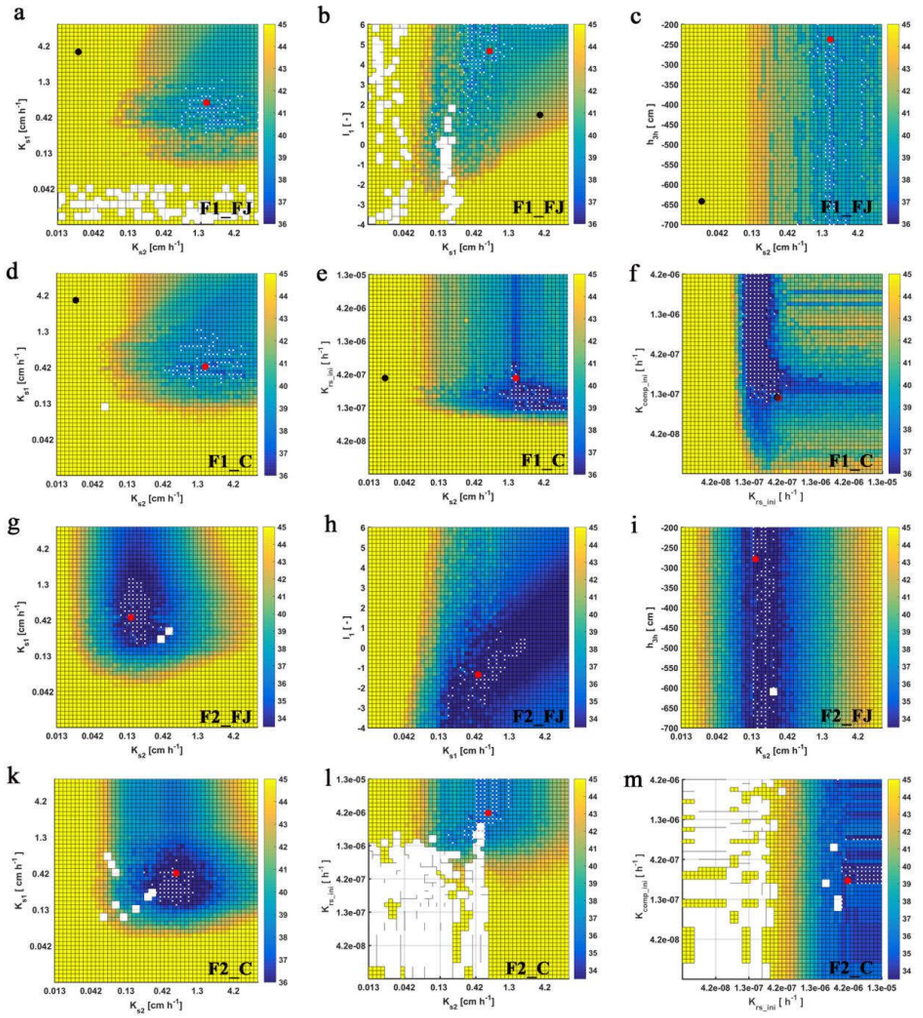

Fig. D 2 Response surface for $K_{s2} - K_{s1}$ (FJ, Feddes-Couvreur model), $K_{sl} - l_1$ (FJ), $K_{s2} - h_{3h}$ (FJ), $K_{s2} - K_{s1}$ (C, Couvreur model), $K_{s2} - K_{rs\_ini}$ (C), and $K_{rs\_ini} - K_{comp\_ini}$ (C) parameter planes of the stony (F1) and silty (F2) soils. Color bar: range of the objective function; white dot: area within 0.5% range of OF minimum; red dot: optimum value obtained from the inverse modeling; black dot: optimum value obtained from the sheltered plot of the stony soil. K_s, saturated conductivity; l, empirical model parameter; 1, 2: top- and subsoil; K_{rs}, equivalent conductance of the root system; K_{comp}, compensatory RWU conductance; h_{3h}, water potential at high transpiration.

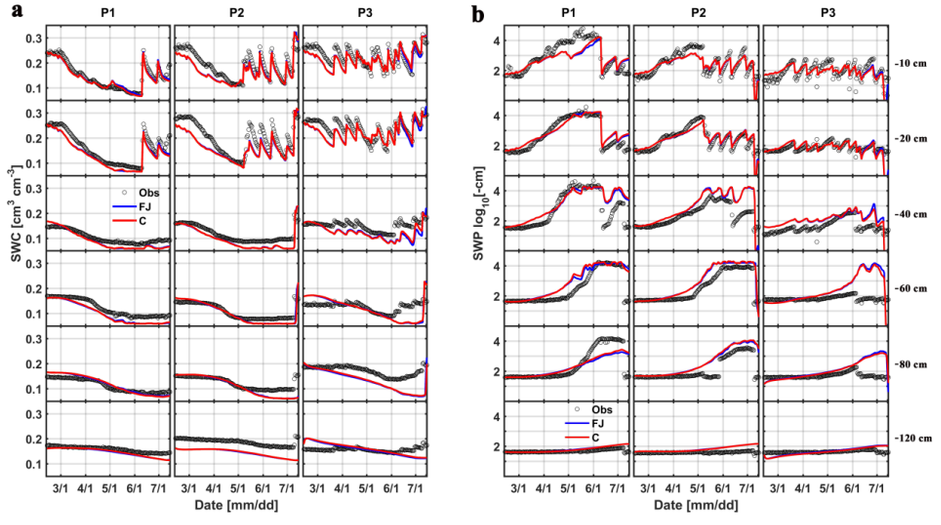

Fig. D 3 Simulated soil water content (SWC, a) and soil water pressure head (SWP, b) by the Feddes-Jarvis (FJ, blue) and Couvreur (C, red) models at different depths in depths in the sheltered (P1), rainfed (P2), and irrigated (P3) plots of the stony soil using the parameters that were obtained from the sheltered plot of the stony soil.

Acknowledgements

Doing a PhD is not just gaining the knowledge on a special area but also the cooperation between the people around. This work will not be finished without their contributions. First, I would like to express my special appreciation for my supervisor, Prof. Jan Vanderborght. He gave me countless ideas, advice, and support for both the field and paper work. He dragged me out of the confusion with patient narration and explanation. I am thankful to Prof. Harry Vereecken for accepting me as a PhD candidate in this great institute, offering the valuable suggestions on the reports and papers, and giving the possibilities in the work.

My sincere gratitude is extended to TR32 that supported the project both in finance and research training.

I would like to thank Cho Miltin Mboh for guiding me to start programming from the very beginning and helping me to set up the modeling. I still remembered that he spent weekends to solve my problems of the inverse modeling. I am grateful to Valentin Couvreur for offering the codes, solutions, and giving the fruitful suggestions and discussions for the modeling and writing.

I thank Joschka Neuman and Normen Hermes for the help to fix the problems in the measurements and maintenance of the rhizotron facilities. I also thank Horst Hardelauf for the cluster use and Thomas Schuster for resolving the computer problems. Many thanks to Werner Küpper for organizing the tools for taking soil samples.

I am grateful to Wei Qu, Michael Stockinger, Miaoyue Zhang, Xiaoqiang Jiang, Biya Cai, Qi Tang, Roland Baatz, Dorina Baatz, Maria Wolff, Anusuriya Devaraju, Ali Muhanmud, Asta Kunkel, Magdalena Landl, Amirpasha Mozaffari, Yan Liang, and Canlan Jiang for the hospitality and also to Katrin Huber, Anja Klotzsche, and Inge Wiekenkamp for enjoying the nice time together. I am thankful to Wolfgang Kurz who took me to Bonn, Aachen, and Cologne for TR32 meetings. I thank Joanna Makselon for lending the lab stuff to finish the lab experiment. I am very grateful to Robert Koller, Anna Galinski, and Esther Breuer from IBG-2 for helping with root sample treatments and scanning. I thank Cheng Sheng for the help with the field experiments, Tao Liu for the ideas to improve the program running, and Jihuan Wang for sharing his personal computer for running the inverse modeling. A lot of other colleagues in IBG-3 and TR32 also offered their kindness and help to me during the past years. Many thanks!

I am thankful to Shehan Morandage and Miriam Zöner since we had spent a lot a time working together for the measurements and solving the problems of the rhizotron facilities in the field. Thanks to Miriam's help, the German version of the summary was nicely translated. I also thank Huu Thuy Nguyen, Hubert Hüging, and Mathias Langensiepen for managing the crops and fertilizers, and sharing the data that was obtained from the same field.

I thank my family for the encouragement and the care via video calls every week. I own special thanks to my wife, Shurong Liu, for her companion and help both in life and work. We have experienced quite a lot and enjoyed the wonderful time in Germany. I am so excited and proud that our son, Leo (Junlin), came to our life at the end of my PhD.

References

Abdou, H. and M. Flury. 2004. Simulation of water flow and solute transport in free-drainage lysimeters and field soils with heterogeneous structures. Eur. J. Soil Sci. 55: 229-241.

Adiku, S., C. Rose, R. Braddock and H. Ozier-Lafontaine. 2000. On the simulation of root water extraction: examination of a minimum energy hypothesis. Soil Sci. 165: 226-236. doi:10.1097/00010694-200003000-00005

Albasha, R., J.-C. Mailhol and B. Cheviron. 2015. Compensatory uptake functions in empirical macroscopic root water uptake models – Experimental and numerical analysis. Agric. Water Manage. 155: 22-39. doi:10.1016/j.agwat.2015.03.010

Allen, R.G., M.E. Jensen, J.L. Wright and R.D. Burman. 1989. Operational estimates of reference evapotranspiration. Agron J. 81: 650-662.

Allen, R.G., L.S. Pereira, D. Raes and M. Smith. 1998. Crop evapotranspiration-Guidelines for computing crop water requirements-FAO Irrigation and drainage paper 56. FAO, Rome 300.

Alony, A. and R. Linker. 2013. Development of a laser-induced fluorescence imaging system for root activity and rhizosphere visualisation. Biosystems Eng. 114: 466-473.

Amato, M. and J.T. Ritchie. 2002. Spatial distribution of roots and water uptake of maize (Zea mays L.) as affected by soil structure. Crop Sci. 42: 773-780.

Amenu, G.G. and P. Kumar. 2008. A model for hydraulic redistribution incorporating coupled soil-root moisture transport. Hydrol. Earth Syst. Sci. 12: 55-74.

Asbjornsen, H., G. Mora and M.J. Helmers. 2007. Variation in water uptake dynamics among contrasting agricultural and native plant communities in the Midwestern US. Agric. Ecosyst. Environ. 121: 343-356. doi:10.1016/j.agee.2006.11.009.

Asseng, S., J. Ritchie, A. Smucker and M. Robertson. 1998. Root growth and water uptake during water deficit and recovering in wheat. Plant Soil 201: 265-273. doi:10.1023/A:1004317523264.

Assouline, S., D. Russo, A. Silber and D. Or. 2015. Balancing water scarcity and quality for sustainable irrigated agriculture. Water Resour. Res. 51: 3419-3436.

Baldocchi, D., E. Falge, L.H. Gu, R. Olson, D. Hollinger, S. Running, et al. 2001. FLUXNET: A new tool to study the temporal and spatial variability of ecosystem-scale carbon dioxide, water vapor, and energy flux densities. Bull. Amer. Meteor. Soc. 82: 2415-2434. doi:10.1175/1520-0477(2001)082<2415:fantts>2.3.co;2.

Baram, S., V. Couvreur, T. Harter, M. Read, P. Brown, M. Kandelous, et al. 2016. Estimating nitrate leaching to groundwater from orchards: comparing crop nitrogen excess, deep vadose zone data-driven estimates, and HYDRUS modeling. Vadose Zone J. 15. doi:10.2136/vzj2016.07.0061

Bechmann, M., C. Schneider, A. Carminati, D. Vetterlein, S. Attinger and A. Hildebrandt. 2014. Effect of parameter choice in root water uptake models - the arrangement of root hydraulic properties within the root architecture affects dynamics and efficiency of root water uptake. Hydrol. Earth Syst. Sci. 18: 4189-4206. doi:10.5194/hess-18-4189-2014.

Bleby, T.M., A.J. Mcelrone and R.B. Jackson. 2010. Water uptake and hydraulic redistribution across large woody root systems to 20 m depth. Plant Cell Environ. 33: 2132-2148. doi:10.1111/j.1365-3040.2010.02212.x

Blonquist, J., S.B. Jones and D. Robinson. 2006. Precise irrigation scheduling for turfgrass using a subsurface electromagnetic soil moisture sensor. Agric. Water Manage. 84: 153-165.

Borg, H. and D. Grimes. 1986. Depth development of roots with time: an empirical description. Trans. ASAE. doi:10.13031/2013.30125

Borrell, A.K., J.E. Mullet, B. George-Jaeggli, E.J. van Oosterom, G.L. Hammer, P.E. Klein, et al. 2014. Drought adaptation of stay-green sorghum is associated with canopy development, leaf anatomy, root growth, and water uptake. J. Exp. Bot. : eru232.

Box, J. and E. Ramsuer. 1993. Minirhizotron wheat root data: Comparisons to soil core root data. Agron J. 85: 1058-1060.
Boyer, J.S. 1967. Leaf water potentials measured with a pressure chamber. Plant Physiol. 42: 133-&. doi:10.1104/pp.42.1.133.
Bragg, P., G. Govi and R. Cannell. 1983. A comparison of methods, including angled and vertical minirhizotrons, for studying root growth and distribution in a spring oat crop. Plant Soil 73: 435-440.
Brandyk, T. and J.G. Wesseling. 1985. Steady state capillary rise in some soil profiles Z. Pflanzenernahr. Bodenk. 148: 54-65. doi:10.1002/jpln.19851480107.
Brooksbank, K., E.J. Veneklaas, D.A. White and J.L. Carter. 2011. The fate of hydraulically redistributed water in a semi-arid zone eucalyptus species. Tree Physiol. 31: 649-658.
Brown, A.L., F.P. Day and D.B. Stover. 2009. Fine root biomass estimates from minirhizotron imagery in a shrub ecosystem exposed to elevated CO2. Plant Soil 317: 145-153.
Brown, J. and G. Johnson. 1989. High resolution magnetic resonance microscopy of plant roots. J. Magn. Reson. 83: 608-616.
Brown, R.A. and N.J. Rosenberg. 1997. Sensitivity of crop yield and water use to change in a range of climatic factors and CO2 concentrations: A simulation study applying EPIC to the central USA. Agric. For. Meteorol. 83: 171-203. doi:10.1016/s0168-1923(96)02352-0.
Bunce, J.A. 1978. Effects of water stress on leaf expansion, net photosynthesis, and vegetative growth of soybeans and cotton. Can. J. Bot. 56: 1492-1498.
Busch, S., J. Van der Kruk and H. Vereecken. 2014. Improved characterization of fine-texture soils using on-ground GPR full-waveform inversion. IEEE Trans. Geosci. Remote Sens. 52: 3947-3958.
Cai, G., J. Vanderborght, V. Couvreur, C.M. Mboh and H. Vereecken. 2017. Parameterization of root water uptake models considering dynamic root distributions and water uptake compensation. Vadose Zone J. doi:10.2136/vzj2016.12.0125.
Cai, G., J. Vanderborght, A. Klotzsche, J. van der Kruk, J. Neumann, N. Hermes, et al. 2016. Construction of Minirhizotron Facilities for Investigating Root Zone Processes. Vadose Zone J. 15. doi:10.2136/vzj2016.05.0043
Caldwell, M.M., T.E. Dawson and J.H. Richards. 1998. Hydraulic lift: consequences of water efflux from the roots of plants. Oecologia 113: 151-161. doi:10.1007/s004420050363
Carminati, A., D. Vetterlein, U. Weller, H.-J. Vogel and S.E. Oswald. 2009. When roots lose contact. Vadose Zone J. 8: 805-809. doi:10.2136/vzj2008.0147
Carsel, R.F. and R.S. Parrish. 1988. Developing joint probability distributions of soil water retention characteristics. Water Resour. Res. 24: 755-769. doi:10.1029/wr024i005p00755
Cermak, J., J. Kucera and N. Nadezhdina. 2004. Sap flow measurements with some thermodynamic methods, flow integration within trees and scaling up from sample trees to entire forest stands. Trees Struct. Funct. 18: 529-546. doi:10.1007/s00468-004-0339-6.
Chabot, R., S. Bouarfa, D. Zimmer, C. Chaumont and S. Moreau. 2005. Evaluation of the sap flow determined with a heat balance method to measure the transpiration of a sugarcane canopy. Agric. Water Manage. 75: 10-24. doi:10.1016/j.agwat.2004.12.010.
Coelho, E.F. and D. Or. 1999. Root distribution and water uptake patterns of corn under surface and subsurface drip irrigation. Plant Soil 206: 123-136.
Cohen, Y., M.G. Huck, J.D. Hesketh and J.R. Frederick. 1990. Sap flow in the stem of water stressed soybean and maize plants. Irrigation Sci. 11: 45-50. doi:10.1007/bf00189994
Cohen, Y. and Y. Li. 1996. Validating sap flow measurement in field-grown sunflower and corn. J. Exp. Bot. 47: 1699-1707. doi:10.1093/jxb/47.11.1699.
Cohen, Y., S. Takeuchi, J. Nozaka and T. Yano. 1993. Accuracy of sap flow measurement using heat-balance and heat pulse methods. Agron J. 85: 1080-1086.
Cohen, Y., S. Takeuchi, J. Nozaka and T. Yano. 1993. Accuracy of sap flow measurement using heat balance and heat pulse methods. Agron J. 85: 1080-1086.

Colombo, S. and M. Asselstine. 1989. Root hydraulic conductivity and root growth capacity of black spruce (Picea mariana) seedlings. Tree Physiol. 5: 73-81. doi:10.1093/treephys/5.1.73
Communar, G. and S.P. Friedman. 2010. Relative Water Uptake Rate as a Criterion for Trickle Irrigation System Design: III. Subsurface Trickle Irrigation. Soil Sci. Soc. Am. J. 74: 1518-1525. doi:10.2136/sssaj2009.0340.
Couvreur, V., J. Vanderborght, L. Beff and M. Javaux. 2014b. Horizontal soil water potential heterogeneity: simplifying approaches for crop water dynamics models. Hydrol. Earth Syst. Sci. 18: 1723-1743. doi:10.5194/hess-18-1723-2014
Couvreur, V., J. Vanderborght, X. Draye and M. Javaux. 2014a. Dynamic aspects of soil water availability for isohydric plants: Focus on root hydraulic resistances. Water Resour. Res. 50: 8891-8906. doi:10.1002/2014wr015608
Couvreur, V., J. Vanderborght and M. Javaux. 2012. A simple three-dimensional macroscopic root water uptake model based on the hydraulic architecture approach. Hydrol. Earth Syst. Sci. 16: 2957-2971. doi:10.5194/hessd-9-4943-2012
Csorba, S., A. Raveloson, E. Toth, V. Nagy and C. Farkas. 2014. Modelling soil water content variations under drought stress on soil column cropped with winter wheat. J. Hydrol. Hydromech. 62: 269-276. doi:10.2478/johh-2014-0036.
De Bei, R., D. Cozzolino, W. Sullivan, W. Cynkar, S. Fuentes, R. Dambergs, et al. 2011. Non-destructive measurement of grapevine water potential using near infrared spectroscopy. Aust. J. Grape Wine Res. 17: 62-71. doi:10.1111/j.1755-0238.2010.00117.x.
De Faria, R., C. Madramootoo, J. Boisvert and S. Prasher. 1994. Comparison of the versatile soil moisture budget and SWACROP models for a wheat crop in Brazil. Can. Agr. Eng. 36: 57.
De Jong Van Lier, Q., J. Van Dam, K. Metselaar, R. De Jong and W. Duijnisveld. 2008. Macroscopic root water uptake distribution using a matric flux potential approach. Vadose Zone J. 7: 1065-1078. doi:10.2136/vzj2007.0083
de Jong van Lier, Q., J.C. van Dam, A. Durigon, M.A. Dos Santos and K. Metselaar. 2013. Modeling water potentials and flows in the soil–plant system comparing hydraulic resistances and transpiration reduction functions. Vadose Zone J. 12. doi:10.2136/vzj2013.02.0039
De Ruijter, F., B. Veen and M. Van Oijen. 1996. A comparison of soil core sampling and minirhizotrons to quantify root development of field-grown potatoes. Plant Soil 182: 301-312.
de Willigen, P., J.C. van Dam, M. Javaux and M. Heinen. 2012. Root Water Uptake as Simulated by Three Soil Water Flow Models. Vadose Zone J. 11. doi:10.2136/vzj2012.0018.
Deb, S.K., M.K. Shukla and J.G. Mexal. 2011. Numerical modeling of water fluxes in the root zone of a mature pecan orchard. Soil Sci. Soc. Am. J. 75: 1667-1680. doi:10.2136/sssaj2011.0086
Decagon Devices, I. 2016. MPS-2 & MPS-6 Dielectric Water Potential Sensors Operator's Manual. Decagon Devices, Inc., Washington, USA. p. 27.
DeJonge, K.C., S. Taghvaeian, T.J. Trout and L.H. Comas. 2015. Comparison of canopy temperature-based water stress indices for maize. Agric. Water Manage. 156: 51-62. doi:10.1016/j.agwat.2015.03.023.
Denmead, O. and R.H. Shaw. 1962. Availability of soil water to plants as affected by soil moisture content and meteorological conditions. Agron J. 54: 385-390.
Dixon, W.J. 1950. Analysis of extreme values. Ann. Math. Stat.: 488-506.
Dodd, I.C., G. Egea and W.J. Davies. 2008. Abscisic acid signalling when soil moisture is heterogeneous: decreased photoperiod sap flow from drying roots limits abscisic acid export to the shoots. Plant Cell Environ. 31: 1263-1274. doi:10.1111/j.1365-3040.2008.01831.x
Dong, X., B.D. Patton, A.C. Nyren, P.E. Nyren and L.D. Prunty. 2010. Quantifying root water extraction by rangeland plants through soil water modeling. Plant Soil 335: 181-198. doi:10.1007/s11104-010-0401-7
dos Santos, M.A., Q.D. van Lier, J.C. van Dam and A.H.F. Bezerra. 2017. Benchmarking test of empirical root water uptake models. Hydrol. Earth Syst. Sci. 21: 473-493. doi:10.5194/hess-21-473-2017.

Doussan, C., L. Pagès and G. Vercambre. 1998. Modelling of the hydraulic architecture of root systems: an integrated approach to water absorption—model description. Ann. Bot. 81: 213-223. doi:10.1006/anbo.1997.0540
Doussan, C., A. Pierret, E. Garrigues and L. Pagès. 2006. Water uptake by plant roots: II–modelling of water transfer in the soil root-system with explicit account of flow within the root system–comparison with experiments. Plant Soil 283: 99-117. doi:10.1007/s11104-004-7904-z
Dubach, M. and M.P. Russelle. 1995. Reducing the cost of estimating root turnover with horizontally installed minirhizotrons. Agron J. 87: 258-263.
Dynamax. 2009. Dynagage Sap Flow Sensor User Manual. Accessed on 29.06.2017. http://dynamax.com/images/uploads/papers/Dynagage_Manual.pdf.
Eamus, D. 2006. Ecohydrology: vegetation function, water and resource managementCsiro Publishing.
Ehleringer, J. and T. Dawson. 1992. Water uptake by plants: perspectives from stable isotope composition. Plant Cell Environ. 15: 1073-1082.
Ephrath, J., M. Silberbush and P. Berliner. 1999. Calibration of minirhizotron readings against root length density data obtained from soil cores. Plant Soil 209: 201-208.
Feddes, R.A., E. Bresler and S.P. Neuman. 1974. Field test of a modified numerical model for water uptake by root systems. Water Resour. Res. 10: 1199-1206. doi:10.1029/wr010i006p01199
Feddes, R.A., H. Hoff, M. Bruen, T. Dawson, P. de Rosnay, P. Dirmeyer, et al. 2001. Modeling root water uptake in hydrological and climate models. Bull. Amer. Meteor. Soc. 82: 2797-2809. doi:10.1175/1520-0477(2001)082<2797:mrwuih>2.3.co;2
Feddes, R.A., P. Kowalik, K. Kolinskamalinka and H. Zaradny. 1976. Simulation of field water uptake by plants using a soil water dependent root extraction function. J. Hydrol. 31: 13-26. doi:10.1016/0022-1694(76)90017-2.
Feddes, R.A., P.J. Kowalik and H. Zaradny. 1978. Simulation of field water use and crop yieldCentre for Agricultural Publishing and Documentation.
Fehrenbacher, J. and J. Alexander. 1955. A method for studying corn root distribution using a soil-core sampling machine and shaker-type washer. Agron J. 47: 468-472.
Fernandez, J., B. Clothier and M. van Noordwijk. 2000. Water uptake. Root methods. Springer. p. 461-507.
Fitter, A.H., J.D. Graves, G.K. Self, T.K. Brown, D.S. Bogie and K. Taylor. 1998. Root production, turnover and respiration under two grassland types along an altitudinal gradient: influence of temperature and solar radiation. Oecologia 114: 20-30. doi:10.1007/s004420050415.
Ford, C.R., R.M. Hubbard, B.D. Kloeppel and J.M. Vose. 2007. A comparison of sap flux-based evapotranspiration estimates with catchment-scale water balance. Agric. For. Meteorol. 145: 176-185. doi:10.1016/j.agrformet.2007.04.010.
Freundl, E., E. Steudle and W. Hartung. 1998. Water uptake by roots of maize and sunflower affects the radial transport of abscisic acid and its concentration in the xylem. Planta 207: 8-19. doi:10.1007/s004250050450
Fu, S., L. Sun and Y. Luo. 2016. Combining sap flow measurements and modelling to assess water needs in an oasis farmland shelterbelt of Populus simonii Carr in Northwest China. Agric. Water Manage. 177: 172-180. doi:10.1016/j.agwat.2016.07.015.
Fujimaki, H., Y. Ando, Y.B. Cui and M. Inoue. 2008. Parameter estimation of a root water uptake model under salinity stress. Vadose Zone J. 7: 31-38. doi:10.2136/vzj2007.0025.
Gao, W., L. Hodgkinson, K. Jin, C.W. Watts, R.W. Ashton, J. Shen, et al. 2016. Deep roots and soil structure. Plant Cell Environ. 39: 1662-1668. doi:10.1111/pce.12684.
Garré, S., M. Javaux, J. Vanderborght and H. Vereecken. 2011. Three-dimensional electrical resistivity tomography to monitor root zone water dynamics. Vadose Zone J. 10: 412-424. doi:10.2136/vzj2010.0079
Garré, S., E. Laloy, M. Javaux and H. Vereecken. 2012. Parameterizing a dynamic architectural model of the root system of spring barley from minirhizotron data. Vadose Zone J. 11. doi:10.2136/vzj2011.0179

Glab, T. 2007. Effect of soil compaction on root system development and yields of tall fescue. Int. Agrophys. 21: 233-239.
Gong, D., S. Kang, L. Zhang, T. Du and L. Yao. 2006. A two-dimensional model of root water uptake for single apple trees and its verification with sap flow and soil water content measurements. Agric. Water Manage. 83: 119-129. doi:10.1016/j.agwat.2005.10.005.
Gonzalez-Dugo, M.P., M.S. Moran, L. Mateos and R. Bryant. 2006. Canopy temperature variability as an indicator of crop water stress severity. Irrigation Sci. 24: 233-240. doi:10.1007/s00271-005-0022-8.
Granier, A., R. Huc and S. Barigah. 1996. Transpiration of natural rain forest and its dependence on climatic factors. Agric. For. Meteorol. 78: 19-29. doi:10.1016/0168-1923(95)02252-x
Grant, O.M., M.J. Davies, H. Longbottom and C.J. Atkinson. 2009. Irrigation scheduling and irrigation systems: optimising irrigation efficiency for container ornamental shrubs. Irrigation Sci. 27: 139-153.
Grebet, P. and R.H. Cuenca. 1991. History of lysimeter design and effects of environmental disturbances. Lysimeters for Evapotranspiration and Environmental Measurements:, ASCE.
Green, S. and B. Clothier. 1998. The root zone dynamics of water uptake by a mature apple tree. Plant Soil 206: 61-77. doi:10.1023/a:1004368906698.
Green, S., B. Clothier and B. Jardine. 2003. Theory and practical application of heat pulse to measure sap flow. Agron J. 95: 1371-1379.
Groh, J., J. Vanderborght, T. Pütz and H. Vereecken. 2016. How to Control the Lysimeter Bottom Boundary to Investigate the Effect of Climate Change on Soil Processes? Vadose Zone J. 15. doi:10.2136/vzj2015.08.0113
Grubbs, F.E. 1950. Sample criteria for testing outlying observations. Ann. Math. Stat.: 27-58.
Guderle, M. and A. Hildebrandt. 2015. Using measured soil water contents to estimate evapotranspiration and root water uptake profiles–a comparative study. Hydrol. Earth Syst. Sci. 19: 409-425. doi:10.5194/hessd-11-10859-2014
Haub, C. and T. Kaneda. 2013. 2013, World Population Data Sheet, Population Reference Bureau, 1875 Connecticut Ave. NW Suite 520: 20009-25728.
He, W., J.Y. Yang, W. Zhou, C.F. Drury, X.M. Yang, W.D. Reynolds, et al. 2016. Sensitivity analysis of crop yields, soil water contents and nitrogen leaching to precipitation, management practices and soil hydraulic properties in semi-arid and humid regions of Canada using the DSSAT model. Nutr. Cycl. Agroecosys. 106: 201-215. doi:10.1007/s10705-016-9800-3.
Heeraman, D.A., J.W. Hopmans and V. Clausnitzer. 1997. Three dimensional imaging of plant roots in situ with X-ray computed tomography. Plant Soil 189: 167-179.
Heinen, M. 2001. FUSSIM2: brief description of the simulation model and application to fertigation scenarios. Agronomie 21: 285-296. doi:10.1051/agro:2001124
Heinen, M. 2014. Compensation in root water uptake models combined with three-dimensional root length density distribution. Vadose Zone J. 13. doi:10.2136/vzj2013.08.0149
Heinen, M. and P. De Willigen. 1998. FUSSIM2. A two-dimensional simulation model for water flow, solute transport, and root uptake of water and nutrients in partly unsaturated porous media. AB-DLO [etc.].
Hendrick, R.L. and K.S. Pregitzer. 1992. The demography of fine roots in a northern hardwood forest. Ecology: 1094-1104.
Herkelrath, W., S. Hamburg and F. Murphy. 1991. Automatic, real-time monitoring of soil moisture in a remote field area with time domain reflectometry. Water Resour. Res. 27: 857-864.
Hildebrandt, A., A. Kleidon and M. Bechmann. 2016. A thermodynamic formulation of root water uptake. Hydrol. Earth Syst. Sci. 20: 3441-3454. doi:10.5194/hess-20-3441-2016.
Hilton, R., D. Bhar and G. Mason. 1969. A rhizotron for in situ root growth studies. Can. J. Plant. Sci. 49: 101-104.
Hoffman, G.J. and M.T. Van Genuchten. 1983. Soil properties and efficient water use: water management for salinity control. Limitations to efficient water use in crop production: 73-85.

Horst, T.W. and J.C. Weil. 1992. Footprint estimation for scalar flux measurements in the atmospheric surface layer. Boundary-Layer Meteorology 59: 279-296. doi:10.1007/bf00119817.
Hossain, M.A., H. Araki and T. Takahashi. 2011. Poor grain filling induced by waterlogging is similar to that in abnormal early ripening in wheat in Western Japan. Field Crops Res. 123: 100-108.
Howard, S., C. Ong, C. Black and A. Khan. 1996. Using sap flow gauges to quantify water uptake by tree roots from beneath the crop rooting zone in agroforestry systems. Agrofor. Syst. 35: 15-29. doi:10.1007/bf02345326
Howell, T.A., A.D. Schneider and M.E. Jensen. 1991. History of lysimeter design and use for evapotranspiration measurements.
Huang, B., R. Duncan and R. Carrow. 1997. Drought-resistance mechanisms of seven warm-season turfgrasses under surface soil drying: II. Root aspects. Crop Sci. 37: 1863-1869. doi:10.2135/cropsci1997.0011183x003700060033x
Huang, B.G. and P.S. Nobel. 1994. Root hydraulic conductivity and its components, with emphasis on desert succulents. Agron J. 86: 767-774. doi:10.2134/agronj1994.00021962008600050005x
Huber, B. 1932. Beobachtung und Messung pflanzlicher Saftströme. Ber Dt Bot Ges 50: 89-109.
Huber, K., J. Vanderborght, M. Javaux, N. Schröder, I.C. Dodd and H. Vereecken. 2014. Modelling the impact of heterogeneous rootzone water distribution on the regulation of transpiration by hormone transport and/or hydraulic pressures. Plant Soil 384: 93-112. doi:10.1007/s11104-014-2188-4
Huber, K., J. Vanderborght, M. Javaux and H. Vereecken. 2015. Simulating transpiration and leaf water relations in response to heterogeneous soil moisture and different stomatal control mechanisms. Plant Soil 394: 109-126. doi:10.1007/s11104-015-2502-9.
Huisman, J., S. Hubbard, J. Redman and A. Annan. 2003. Measuring soil water content with ground penetrating radar. Vadose Zone J. 2: 476-491.
Hultine, K.R., R. Scott, W. Cable, D. Goodrich and D. Williams. 2004. Hydraulic redistribution by a dominant, warm-desert phreatophyte: Seasonal patterns and response to precipitation pulses. Funct. Ecol. 18: 530-538.
Hummel, J., M. Levan and K. Sudduth. 1989. Minirhizotron installation in heavy soils. Trans. ASAE 32: 770-776.
Hupet, F., S. Lambot, R. Feddes, J. Van Dam and M. Vanclooster. 2003. Estimation of root water uptake parameters by inverse modeling with soil water content data. Water Resour. Res. 39. doi:10.1029/2003wr002046
Hupet, F., S. Lambot, M. Javaux and M. Vanclooster. 2002. On the identification of macroscopic root water uptake parameters from soil water content observations. Water Resour. Res. 38. doi:10.1029/2002wr001556
Iijima, M., Y. Kono, A. Yamauchi and J.R. Pardales. 1991. Effects of soil compaction on the development of rice and maize root systems. Environ. Exp. Bot. 31: 333-342. doi:10.1016/0098-8472(91)90058-v.
Ikeda, K., T. Kume, H. Tabuo, N. Yoshida and S. Izumi. 1994. Occurrence of abnormal early ripening of wheat and its control in Kagoshima prefecture [Japan], 2: Root activity of wheat in infected soil. Kyushu Agricultural Research (Japan).
Ines, A.V.M. and P. Droogers. 2002. Inverse modelling in estimating soil hydraulic functions: a Genetic Algorithm approach. Hydrol. Earth Syst. Sci. 6: 49-65.
Iversen, C.M., M.T. Murphy, M.F. Allen, J. Childs, D.M. Eissenstat, E.A. Lilleskov, et al. 2012. Advancing the use of minirhizotrons in wetlands. Plant Soil 352: 23-39.
Jackson, R.D., S.B. Idso, R.J. Reginato and P.J. Pinter. 1981. Canopy temperature as a crop water stress indicator. Water Resour. Res. 17: 1133-1138. doi:10.1029/WR017i004p01133.
Jaeger, L. and A. Kessler. 1997. Twenty years of heat and water balance climatology at the Hartheim pine forest, Germany. Agric. For. Meteorol. 84: 25-36. doi:10.1016/s0168-1923(96)02372-6

Jara, J., C.O. Stockle and J. Kjelgaard. 1998. Measurement of evapotranspiration and its components in a corn (Zea Mays L.) field. Agric. For. Meteorol. 92: 131-145. doi:10.1016/s0168-1923(98)00083-5.

Jarvis, N. 1989. A simple empirical model of root water uptake. J. Hydrol. 107: 57-72. doi:10.1016/0022-1694(89)90050-4

Javaux, M., V. Couvreur, J. Vanderborght and H. Vereecken. 2013. Root water uptake: from three-dimensional biophysical processes to macroscopic modeling approaches. Vadose Zone J. 12. doi:10.2136/vzj2013.02.0042

Javaux, M., T. Schröder, J. Vanderborght and H. Vereecken. 2008. Use of a three-dimensional detailed modeling approach for predicting root water uptake. Vadose Zone J. 7: 1079-1088. doi:10.2136/vzj2007.0115

Johnson, M., D. Tingey, D. Phillips and M. Storm. 2001. Advancing fine root research with minirhizotrons. Environ. Exp. Bot. 45: 263-289. doi:10.1016/s0098-8472(01)00077-6

Jones, C.A. 1983. Effect of soil texture on critical bulk densities for root growth. Soil Sci. Soc. Am. J. 47: 1208-1211.

Judd, L.A., B.E. Jackson, W.C. Fonteno and J.-C. Domec. 2016. Measuring root hydraulic parameters of container-grown herbaceous and woody plants using the hydraulic conductance flow meter. HortScience 51: 192-196.

Kandelous, M.M., T. Kamai, J.A. Vrugt, J. Simunek, B. Hanson and J.W. Hopmans. 2012. Evaluation of subsurface drip irrigation design and management parameters for alfalfa. Agric. Water Manage. 109: 81-93. doi:10.1016/j.agwat.2012.02.009.

Khalid, M., F. Afzal, A. Gul, M.A. Ahanger and P. Ahmad. 2016. Analysis of novel haplotype variation at TaDREB-D1 and TaCwi-D1 genes influencing drought tolerance in bread/synthetic wheat derivatives. Water Stress and Crop Plants. John Wiley & Sons, Ltd. p. 206-226.

Klotzsche, A., J. van der Kruk, J. Bradford and H. Vereecken. 2014. Detection of spatially limited high-porosity layers using crosshole GPR signal analysis and full-waveform inversion. Water Resour. Res. 50: 6966-6985.

Knaps, A. 2016. Klimastatistik: Jahresmittelwerte von 1961-2015. 2016. 26 Oct. http://www.fz-juelich.de/gs/DE/UeberUns/Organisation/S-U/Meteorologie/klima/statistik_tabelle.html.

Kropff, M.J. and H. Van Laar. 1993. Modelling crop-weed interactionsInt. Rice Res. Inst.

Krounbi, L. and N. Lazarovitch. 2011. Soil hydraulic properties affecting root water uptake. Encyclopedia of Agrophysics. Springer. p. 748-754.

Kuchenbrod, E., M. Landeck, F. Thurmer, A. Haase and U. Zimmermann. 1996. Measurement of water flow in the xylem vessels of intact maize plants using flow-sensitive NMR imaging. Bot. Acta 109: 184-186.

Kuhlmann, A., I. Neuweiler, S. Zee and R. Helmig. 2012. Influence of soil structure and root water uptake strategy on unsaturated flow in heterogeneous media. Water Resour. Res. 48. doi:10.1029/2011wr010651

Kumar, R., V. Shankar and M.K. Jat. 2014. Evaluation of root water uptake models–a review. ISH J. Hydraul. Eng.: 1-10. doi:10.1080/09715010.2014.981955

Lambot, S., M. Javaux, F. Hupet and M. Vanclooster. 2002. A global multilevel coordinate search procedure for estimating the unsaturated soil hydraulic properties. Water Resour. Res. 38. doi:10.1029/2001wr001224

Landl, M., K. Huber, A. Schnepf, J. Vanderborght, M. Javaux, A.G. Bengough, et al. 2016. A new model for root growth in soil with macropores. Plant Soil: 1-18. doi:10.1007/s11104-016-3144-2.

Langensiepen, M., M. Kupisch, A. Graf, M. Schmidt and F. Ewert. 2014. Improving the stem heat balance method for determining sap-flow in wheat. Agric. For. Meteorol. 186: 34-42. doi:10.1016/j.agrformet.2015.08.132

Ledieu, J., P. De Ridder, P. De Clerck and S. Dautrebande. 1986. A method of measuring soil moisture by time-domain reflectometry. J. Hydrol. 88: 319-328.

Leffler, A.J., M.S. Peek, R.J. Ryel, C.Y. Ivans and M.M. Caldwell. 2005. Hydraulic redistribution through the root systems of senesced plants. Ecology 86: 633-642. doi:10.1890/04-0854
Lehrsch, G.A. and D.C. Kincaid. 2010. Sprinkler irrigation effects on infiltration and near-surface unsaturated hydraulic conductivity. Trans. ASABE 53: 397-404.
Leitner, D., S. Klepsch, G. Bodner and A. Schnepf. 2010. A dynamic root system growth model based on L-Systems. Plant Soil 332: 177-192.
Letey, J. 1958. Relationship between soil physical properties and crop production. Adv. Soil Sci. Springer. p. 277-294.
Leys, C., C. Ley, O. Klein, P. Bernard and L. Licata. 2013. Detecting outliers: do not use standard deviation around the mean, use absolute deviation around the median. J. Exp. Soc. Psychol 49: 764-766.
Li, K., R. De Jong and J. Boisvert. 2001. An exponential root-water-uptake model with water stress compensation. J. Hydrol. 252: 189-204. doi:10.1016/s0022-1694(01)00456-5
Liao, R., P. Yang, W. Wu and S. Ren. 2016. An Inverse Method to Estimate the Root Water Uptake Source-Sink Term in Soil Water Transport Equation under the Effect of Superabsorbent Polymer. PloS one 11: e0159936.
Linsenmeier, A., R. Lehnart, O. Löhnertz and H. Michel. 2010. Investigation of grapevine root distribution by in situ minirhizotron observation. Vitis 49: 1-6.
Lobet, G., V. Couvreur, F. Meunier, M. Javaux and X. Draye. 2014. Plant water uptake in drying soils. Plant Physiol. 164: 1619-1627. doi:10.1104/pp.113.233486
Lobet, G. and X. Draye. 2013. Novel scanning procedure enabling the vectorization of entire rhizotron-grown root systems. Plant Methods 9: 1. doi:10.1186/1746-4811-9-1
Lobet, G., M.P. Pound, J. Diener, C. Pradal, X. Draye, C. Godin, et al. 2015. Root system markup language: toward a unified root architecture description language. Plant Physiol. 167: 617-627.
Logsdon, S.D., J.W. Singer, J.H. Prueger and J.L. Hatfield. 2014. Comparison of Corn Transpiration, Eddy Covariance, and Soil Water Loss. Soil Sci. Soc. Am. J. 78: 1214-1223. doi:10.2136/sssaj2014.01.0044.
López-Bucio, J., A. Cruz-Ramırez and L. Herrera-Estrella. 2003. The role of nutrient availability in regulating root architecture. Curr. Opin. Plant Biol. 6: 280-287.
Luo, Y., Z. OuYang, G. Yuan, D. Tang and X. Xie. 2003. Evaluation of macroscopic root water uptake models using lysimeter data. Trans. ASAE 46: 625-634.
Luster, J., A. Göttlein, B. Nowack and G. Sarret. 2009. Sampling, defining, characterising and modeling the rhizosphere—the soil science tool box. Plant Soil 321: 457-482.
Lynch, J.P. 2013. Steep, cheap and deep: an ideotype to optimize water and N acquisition by maize root systems. Ann. Bot. 112: 347-357. doi:10.1093/aob/mcs293
MacFall, J., G. Johnson and P. Kramer. 1991. Comparative water uptake by roots of different ages in seedlings of loblolly pine (Pinus taeda L.). New Phytol. 119: 551-560.
Machado, R.M., M. do Rosário and G. Oliveira. 2003. Comparison of tomato root distributions by minirhizotron and destructive sampling. Roots: The Dynamic Interface between Plants and the Earth. Springer. p. 375-385.
Madi, H. and P. Kangas. 1997. Demography of fine roots in response to nutrient applications in a Norway spruce stand in southwestern Sweden.
Mansfield, T.A. and C.J. Atkinson. 1990. Stomatal behavior in water stressed plants. Alscher, R. G. And J. R. Cumming. p. 241-264.
Mapa, R., R. Green and L. Santo. 1986. Temporal variability of soil hydraulic properties with wetting and drying subsequent to tillage. Soil Sci. Soc. Am. J. 50: 1133-1138.
Martinez, E.M., J.J. Cancela, T.S. Cuesta and X.X. Neira. 2011. Review. Use of psychrometers in field measurements of plant material: accuracy and handling difficulties. Span. J. Agric. Res. 9: 313-328.

Massai, R. and D. Remorini. 2000. Estimation of water requirements in a young peach orchard under irrigated and stressed conditions. In: M. I. Ferreira and H. G. Jones, editors, Proceedings of the Third International Symposium on Irrigation of Horticultural Crops, Vols 1 and 2. p. 77-86.
MathWorks. 2015. Matlab 2015b and statistics toolbox. The MathWorks, Inc., Natick, Massachusetts, United States.
Matsuo, N., K. Ozawa and T. Mochizuki. 2009. Genotypic differences in root hydraulic conductance of rice (Oryza sativa L.) in response to water regimes. Plant Soil 316: 25-34. doi:10.1007/s11104-008-9755-5.
Maurel, C., T. Simonneau and M. Sutka. 2010. The significance of roots as hydraulic rheostats. J. Exp. Bot. 61: 3191-3198. doi:10.1093/jxb/erq150.
Meier, I.C. and C. Leuschner. 2008. Genotypic variation and phenotypic plasticity in the drought response of fine roots of European beech. Tree Physiol. 28: 297-309.
Merotto Jr, A. and C. Mundstock. 1999. Wheat root growth as affected by soil strength. Revista Brasileira de Ciência do Solo 23: 197-202.
Meunier, F., Y. Rothfuss, T. Bariac, P. Biron, P. Richard, J.-L. Durand, et al. 2017. Measuring and Modeling Hydraulic Lift of Using Stable Water Isotopes. Vadose Zone J. doi:10.2136/vzj2016.12.0134.
Meyer, W.S. and H.D. Barrs. 1991. Roots in irrigated clay soils: Measurement techniques and responses to rootzone conditions. Irrigation Sci. 12: 125-134.
Milchunas, D.G. 2011. Potnetial biases, problems, and advantages of minirhizotron. In: S. Mancuso, editor Measuring roots: an updated approach. Springer Science & Business Media. p. 316.
Minasny, B., A.B. McBratney and B.M. Whelan. 2005. VESPER version 1.62. Australian Centre for Precision Agriculture, McMillan Building A05, The University of Sydney, NSW.
Miyamoto, N., E. Steudle, T. Hirasawa and R. Lafitte. 2001. Hydraulic conductivity of rice roots. J. Exp. Bot. 52: 1835-1846. doi:10.1093/jexbot/52.362.1835
Mo, X. and S. Liu. 2001. Simulating evapotranspiration and photosynthesis of winter wheat over the growing season. Agric. For. Meteorol. 109: 203-222. doi:10.1016/s0168-1923(01)00266-0
Moller, M., V. Alchanatis, Y. Cohen, M. Meron, J. Tsipris, A. Naor, et al. 2007. Use of thermal and visible imagery for estimating crop water status of irrigated grapevine. J. Exp. Bot. 58: 827-838. doi:10.1093/jxb/erl115.
Molz, F.J. 1981. Models of water transport in the soil-plant system: A review. Water Resour. Res. 17: 1245-1260. doi:10.1029/wr017i005p01245
Mooney, S.J., T.P. Pridmore, J. Helliwell and M.J. Bennett. 2012. Developing X-ray computed tomography to non-invasively image 3-D root systems architecture in soil. Plant and soil 352: 1-22.
Moreira, M.Z., L.D.L. Sternberg and D.C. Nepstad. 2000. Vertical patterns of soil water uptake by plants in a primary forest and an abandoned pasture in the eastern Amazon: an isotopic approach. Plant Soil 222: 95-107. doi:10.1023/a:1004773217189.
Moreno, F., J.E. Fernandez, B.E. Clothier and S.R. Green. 1996. Transpiration and root water uptake by olive trees. Plant Soil 184: 85-96. doi:10.1007/bf00029277.
Mualem, Y. 1976. A new model for predicting the hydraulic conductivity of unsaturated porous media. Water Resour. Res. 12: 513-522. doi:10.1029/wr012i003p00513.
Musick, J.T. and D.A. Dusek. 1980. Planting date and water deficit effects on development and yield of irrigated winter wheat. Agron J. 72: 45-52.
Musters, P. and W. Bouten. 1999. Assessing rooting depths of an Austrian pine stand by inverse modeling soil water content maps. Water Resour. Res. 35: 3041-3048. doi:10.1029/1999wr900173
Musters, P. and W. Bouten. 2000. A method for identifying optimum strategies of measuring soil water contents for calibrating a root water uptake model. J. Hydrol. 227: 273-286. doi:10.1016/s0022-1694(99)00187-0.

Nelsen, C.E., G.R. Safir and A.D. Hanson. 1978. Water Potential in Excised Leaf Tissue Comparison of a Commercial Dew Point Hygrometer and a Thermocouple Psychrometer on Soybean, Wheat, and Barley. Plant Physiol. 61: 131-133.
Neumann, R.B. and Z.G. Cardon. 2012. The magnitude of hydraulic redistribution by plant roots: a review and synthesis of empirical and modeling studies. New Phytol. 194: 337-352. doi:10.1111/j.1469-8137.2012.04088.x
Nimah, M. and R. Hanks. 1973. Model for estimating soil water, plant, and atmospheric interrelations: I. Description and sensitivity. Soil Sci. Soc. Am. J. 37: 522-527. doi:10.2136/sssaj1973.03615995003700040018x.
Nobel, P.S., P.M. Miller and E.A. Graham. 1992. Influence of rocks on soil temperature, soil water potential, and rooting patterns for desert succulents. Oecologia 92: 90-96.
North, G.B. and P.S. Nobel. 1995. Hydraulic conductivity of concentric root tissues of Agave deserti Engelm. under wet and drying conditions. New Phytol. 130: 47-57. doi:10.1111/j.1469-8137.1995.tb01813.x.
Novák, V., K. Kňava and J. Šimůnek. 2011. Determining the influence of stones on hydraulic conductivity of saturated soils using numerical method. Geoderma 161: 177-181. doi:10.1016/j.geoderma.2010.12.016
O'Toole, J. and T. Moya. 1981. Water deficits and yield in upland rice. Field Crops Res. 4: 247-259.
Oberröhrmann, M., A. Klotzsche, H. Vereecken and J. van der Kruk. 2013. Optimization of acquisition setup for cross-hole GPR full-waveform inversion using checkerboard analysis. Near Surf. Geophys. 11: 197-209.
Oleson, K., G.Y. Niu, Z.L. Yang, D. Lawrence, P. Thornton, P. Lawrence, et al. 2008. Improvements to the community land model and their impact on the hydrological cycle. J. Geophys. Res. Biogeosci. 113. doi:10.1029/2007jg000563
Orellana, F., P. Verma, S.P. Loheide and E. Daly. 2012. Monitoring and modeling water-vegetation interactions in groundwater-dependent ecosystems. Rev. Geophys. 50.
Pagenkemper, S.K., D.U. Puschmann, S. Peth and R. Horn. 2014. Investigation of time dependent development of soil structure and formation of macropore networks as affected by various precrop species. International soil and water conservation research 2: 51-66.
Pagès, L. 2011. Links between root developmental traits and foraging performance. Plant, Cell and Environment 34: 1749-1760. doi:10.1111/j.1365-3040.2011.02371.x
Pagès, L., D. Moreau, V. Sarlikioti, H. Boukcim and C. Nguyen. 2012. ArchiSimple: a parsimonious model of the root system architecture. Plant Growth Modeling, Simulation, Visualization and Applications (PMA), 2012 IEEE Fourth International Symposium on, IEEE.
Pagès, L., G. Vercambre, J.-L. Drouet, F. Lecompte, C. Collet and J. Le Bot. 2004. Root Typ: a generic model to depict and analyse the root system architecture. Plant Soil 258: 103-119. doi:10.1023/b:plso.0000016540.47134.03
Pagliai, M. and M. Denobili. 1993. Relationships between soil porosity, root development and soil enzyme activity in cultivated soils. Geoderma 56: 243-256. doi:10.1016/0016-7061(93)90114-z.
Pang, L., M.E. Close, J.P. Watt and K.W. Vincent. 2000. Simulation of picloram, atrazine, and simazine leaching through two New Zealand soils and into groundwater using HYDRUS-2D. J. Contam. Hydrol. 44: 19-46. doi:10.1016/s0169-7722(00)00091-7
Pang, X. and J. Letey. 1998. Development and evaluation of ENVIRO-GRO, an integrated water, salinity, and nitrogen model. Soil Sci. Soc. Am. J. 62: 1418-1427. doi:10.2136/sssaj1998.03615995006200050039x
Peters, A., W. Durner and S.C. Iden. 2017. Modified Feddes type stress reduction function for modeling root water uptake: Accounting for limited aeration and low water potential. Agric. Water Manage. 185: 126-136. doi:10.1016/j.agwat.2017.02.010.
Petropoulos, G.P. 2013. Remote sensing of energy fluxes and soil moisture contentCRC Press.

Phillips, D.L., M.G. Johnson, D.T. Tingey, C. Biggart, R.S. Nowak and J.C. Newsom. 2000. Minirhizotron installation in sandy, rocky soils with minimal soil disturbance. Soil Sci. Soc. Am. J. 64: 761-764.
Pierret, A., C. Doussan and L. Pages. 2006. Spatio-temporal variations in axial conductance of primary and first-order lateral roots of a maize crop as predicted by a model of the hydraulic architecture of root systems. Plant Soil 282: 117-126. doi:10.1007/s11104-005-5373-7
Pohlmeier, A., M. Javaux, H. Vereecken and S. Haber-Pohlmeier. 2013. Magnetic resonance imaging techniques for visualization of root growth and root water uptake processes. Soil–Water–Root Processes: Advances in Tomography and Imaging: 137-156.
Poorter, H., K.J. Niklas, P.B. Reich, J. Oleksyn, P. Poot and L. Mommer. 2012. Biomass allocation to leaves, stems and roots: meta-analyses of interspecific variation and environmental control. New Phytol. 193: 30-50. doi:10.1111/j.1469-8137.2011.03952.x.
Porter, J.R. and M.A. Semenov. 2005. Crop responses to climatic variation. Philosophical Transactions of the Royal Society B-Biological Sciences 360: 2021-2035. doi:10.1098/rstb.2005.1752.
Raich, J., R. Riley and P. Vitousek. 1994. Use of root-ingrowth cores to assess nutrient limitations in forest ecosystems. Can. J. For. Res. 24: 2135-2138.
Rana, G. and N. Katerji. 2000. Measurement and estimation of actual evapotranspiration in the field under Mediterranean climate: a review. Eur. J. Agron. 13: 125-153.
Ray, D.K., N.D. Mueller, P.C. West and J.A. Foley. 2013. Yield trends are insufficient to double global crop production by 2050. PloS one 8: e66428.
Rewald, B. and J.E. Ephrath. 2012. Minirhizotron technique. Plant roots: the hidden half, 4th edn. CRC Press, New York. doi:10.1201/b14500-50.
Richards, J.H. and M.M. Caldwell. 1987. Hydraulic lift: substantial nocturnal water transport between soil layers by Artemisia tridentata roots. Oecologia 73: 486-489. doi:10.1007/bf00379405
Ritter, A., F. Hupet, R. Muñoz-Carpena, S. Lambot and M. Vanclooster. 2003. Using inverse methods for estimating soil hydraulic properties from field data as an alternative to direct methods. Agric. Water Manage. 59: 77-96. doi:10.1016/s0378-3774(02)00160-9
Roncucci, N., N.N.O. Di Nasso, E. Bonari and G. Ragaglini. 2015. Influence of soil texture and crop management on the productivity of miscanthus (Miscanthus x giganteus Greef et Deu.) in the Mediterranean. Glob. Change Biol. Bioenergy 7: 998-1008. doi:10.1111/gcbb.12202.
Rorabacher, D.B. 1991. Statistical treatment for rejection of deviant values: critical values of Dixon's" Q" parameter and related subrange ratios at the 95% confidence level. Analytical Chemistry 63: 139-146.
Rost, S., D. Gerten, A. Bondeau, W. Lucht, J. Rohwer and S. Schaphoff. 2008. Agricultural green and blue water consumption and its influence on the global water system. Water Resour. Res. 44.
Rothfuss, Y., P. Biron, I. Braud, L. Canale, J.L. Durand, J.P. Gaudet, et al. 2010. Partitioning evapotranspiration fluxes into soil evaporation and plant transpiration using water stable isotopes under controlled conditions. Hydrol. Processes 24: 3177-3194.
Rothfuss, Y. and M. Javaux. 2016. Isotopic approaches to quantifying root water uptake and redistribution: a review and comparison of methods. Biogeosciences Discuss 2016: 1.
Rothfuss, Y. and M. Javaux. 2017. Reviews and syntheses: Isotopic approaches to quantify root water uptake: a review and comparison of methods. Biogeosciences 14: 2199-2224.
Rousseeuw, P.J. and C. Croux. 1993. Alternatives to the median absolute deviation. J. Am. Stat. Assoc. 88: 1273-1283.
Rudolph, S., J. van der Kruk, C. Von Hebel, M. Ali, M. Herbst, C. Montzka, et al. 2015. Linking satellite derived LAI patterns with subsoil heterogeneity using large-scale ground-based electromagnetic induction measurements. Geoderma 241: 262-271.
Ruggiero, C. and G. Angelino. 2007. Changes of root hydraulic conductivity and root/shoot ratio of durum wheat and barley in relation to nitrogen availability and mercury exposure. Ital. J. Agron. 2: 281-290.

Sakuratani, T. 1981. A heat balance method for measuring water flux in the stem of intact plants. J. Agric. Meteorol. 37: 9-17. doi:10.2480/agrmet.37.9

Schaap, M.G. and F.J. Leij. 2000. Improved prediction of unsaturated hydraulic conductivity with the Mualem-van Genuchten model. Soil Sci. Soc. Am. J. 64: 843-851. doi:10.2136/sssaj2000.643843x

Scharnagl, B., J. Vrugt, H. Vereecken and M. Herbst. 2011. Inverse modelling of in situ soil water dynamics: Investigating the effect of different prior distributions of the soil hydraulic parameters. Hydrol. Earth Syst. Sci. 15.

Schneider, C., S. Attinger, J.-O. Delfs and A. Hildebrandt. 2010. Implementing small scale processes at the soil-plant interface–the role of root architectures for calculating root water uptake profiles. Hydrol. Earth Syst. Sci. 14: 279-289.

Schneider, S., D. Jacques and D. Mallants. 2013. Inverse modelling with a genetic algorithm to derive hydraulic properties of a multi-layered forest soil. Soil Res. 51: 372-389. doi:10.1071/sr13144.

Schroth, G. and D. Kolbe. 1994. A method of processing soil core samples for root studies by subsampling. Biol. Fertil. Soils 18: 60-62.

Senock, R.S., J.M. Ham, T.M. Loughin, B.A. Kimball, D.J. Hunsaker, P.J. Pinter, et al. 1996. Sap flow in wheat under free-air CO2 enrichment. Plant Cell Environ. 19: 147-158. doi:10.1111/j.1365-3040.1996.tb00236.x.

Shen, J., W.D. Batchelor, J.W. Jones, J.T. Ritchie, R.S. Kanwar and C.W. Mize. 1998. Incorporation of a subsurface tile drainage component into a soybean growth model. Trans. ASAE 41: 1305-1313. doi:10.13031/2013.17303

Shen, Y., Y. Zhang and S. Li. 2011. Nutrient effects on diurnal variation and magnitude of hydraulic lift in winter wheat. Agric. Water Manage. 98: 1589-1594. doi:10.1016/j.agwat.2011.05.012

Shimshi, D. 1979. Leaf permeability as an index of water relations, CO2 uptake and yield of irrigated wheat. Irrigation Sci. 1: 107-117.

Šimůnek, J. and J.W. Hopmans. 2009. Modeling compensated root water and nutrient uptake. Ecol. Model. 220: 505-521. doi:10.1016/j.ecolmodel.2008.11.004

Simunek, J., M. Sejna, H. Saito, M. Sakai and M. Van Genuchten. 2013. The HYDRUS-1D Software Package for Simulating the Movement of Water, Heat, and Multiple Solutes in Variably Saturated Media, Version 4.16, HYDRUS Software Series 3. Department of Environmental Sciences, University of California, Riverside, CA.

Simunek, J., M. Sejna, H. Saito, M. Sakai and M. van Genuchten. 2013. The HYDRUS-1D Software Package for Simulating the One-Dimensional Movement of Water, Heat and Multiple Solutes in Variably-Saturated Media. Department of Environmental Sciences, University of California Riverside, Riverside, California, US.

Šimůnek, J. and D.L. Suarez. 1993. Modeling of carbon dioxide transport and production in soil: 1. Model development. Water Resour. Res. 29: 487-497. doi:10.1029/92wr02225

Šimůnek, J., M.T. van Genuchten and M. Šejna. 2016. Recent developments and applications of the HYDRUS computer software packages. Vadose Zone J. 15. doi:10.2136/vzj2016.04.0033.

Simunek, J. and M.T. vanGenuchten. 1996. Estimating unsaturated soil hydraulic properties from tension disc infiltrometer data by numerical inversion. Water Resour. Res. 32: 2683-2696. doi:10.1029/96wr01525.

Simunek, J., O. Wendroth and M.T. van Genuchten. 1998. Parameter estimation analysis of the evaporation method for determining soil hydraulic properties. Soil Sci. Soc. Am. J. 62: 894-905.

Skaggs, T.H., M.T. van Genuchten, P.J. Shouse and J.A. Poss. 2006. Macroscopic approaches to root water uptake as a function of water and salinity stress. Agric. Water Manage. 86: 140-149. doi:10.1016/j.agwat.2006.06.005

Smit, A.L., J. Groenwold and J. Vos. 1994. The Wageningen Rhizolab — a facility to study soil-root-shoot-atmosphere interactions in crops. II. Methods of root observations. Plant Soil 161: 289-298. doi:10.1007/bf00046400.

Smith, C.K., M.R. Coyea and A.D. Munson. 2005. Response of fine roots to fertilized ingrowth cores in burned and harvested black spruce ecosystems. Commun. Soil Sci. Plant Anal. 36: 1361-1372.
Smith, D., P. Jarvis and J. Odongo. 1998. Management of windbreaks in the Sahel: the strategic implications of tree water use. Agrofor. Syst. 40: 83-96.
Smith, D.M. and S.J. Allen. 1996. Measurement of sap flow in plant stems. J. Exp. Bot. 47: 1833-1844. doi:10.1093/jxb/47.12.1833.
Smith, M. 2000. The application of climatic data for planning and management of sustainable rainfed and irrigated crop production. Agric. For. Meteorol. 103: 99-108.
Smucker, A. 1993. Soil environmental modifications of root dynamics and measurement. Annu. Rev. Phytopathol. 31: 191-218.
Smucker, A., J. Ferguson, W. DeBruyn, R. Belford and J. Ritchie. 1987. Image analysis of video-recorded plant root systems. Minirhizotron Observation Tubes: Methods and Applications for Measuring Rhizosphere Dynamics: 67-80. doi:10.2134/asaspecpub50
Somma, F., J. Hopmans and V. Clausnitzer. 1998. Transient three-dimensional modeling of soil water and solute transport with simultaneous root growth, root water and nutrient uptake. Plant Soil 202: 281-293.
Sonnleitner, M.A., K.C. Abbaspour and R. Schulin. 2003. Hydraulic and transport properties of the plant-soil system estimated by inverse modelling. Eur. J. Soil Sci. 54: 127-138. doi:10.1046/j.1365-2389.2002.00491.x.
Stadler, A., S. Rudolph, M. Kupisch, M. Langensiepen, J. van der Kruk and F. Ewert. 2015. Quantifying the effects of soil variability on crop growth using apparent soil electrical conductivity measurements. Eur. J. Agron. 64: 8-20.
Stadnyk, C.N. 2010. Root dynamics and carbon accumulation of six willow clones in Saskatchewan. University of Saskatchewan Saskatoon, Canada.
Steele, S.J., S.T. Gower, J.G. Vogel and J.M. Norman. 1997. Root mass, net primary production and turnover in aspen, jack pine and black spruce forests in Saskatchewan and Manitoba, Canada. Tree Physiol. 17: 577-587. doi:10.1093/treephys/17.8-9.577
Steelman, C.M. and A.L. Endres. 2011. Comparison of petrophysical relationships for soil moisture estimation using GPR ground waves. Vadose Zone J. 10: 270-285.
Steudle, E. 2000. Water uptake by roots: effects of water deficit. Journal of Experimental Botany 51: 1531-1542. doi:10.1093/jexbot/51.350.1531.
Steudle, E., R. Oren and E.-D. Schulze. 1987. Water transport in maize roots measurement of hydraulic conductivity, solute permeability, and of reflection coefficients of excised roots using the root pressure probe. Plant Physiol. 84: 1220-1232. doi:10.1104/pp.84.4.1220
Steudle, E. and C.A. Peterson. 1998. How does water get through roots? J. Exp. Bot. 49: 775-788. doi:10.1093/jexbot/49.322.775
Sutanto, S.J., J. Wenninger, A.M.J. Coenders-Gerrits and S. Uhlenbrook. 2012. Partitioning of evaporation into transpiration, soil evaporation and interception: a comparison between isotope measurements and a HYDRUS-1D model. Hydrol. Earth Syst. Sci. 16: 2605-2616. doi:10.5194/hess-16-2605-2012.
Tanner, C.B. 1963. Plant temperatures. Agron J. 55: 210-&.
Tardieu, F., B. Parent, C.F. Caldeira and C. Welcker. 2014. Genetic and Physiological Controls of Growth under Water Deficit. Plant Physiol. 164: 1628-1635. doi:10.1104/pp.113.233353.
Tardieu, F. and T. Simonneau. 1998. Variability among species of stomatal control under fluctuating soil water status and evaporative demand: modelling isohydric and anisohydric behaviours. J. Exp. Bot. 49: 419-432. doi:10.1093/jxb/49.special_issue.419
Taylor, H.M. 1969. Rhizotron at Auburn, Alabama: a plant root observation laboratory.
Thoma, M.J., W. Barrash, M. Cardiff, J. Bradford and J. Mead. 2014. Estimating unsaturated hydraulic functions for coarse sediment from a field-scale infiltration experiment. Vadose Zone J. 13. doi:10.2136/vzj2013.05.0096

Thorup-Kristensen, K., M.S. Cortasa and R. Loges. 2009. Winter wheat roots grow twice as deep as spring wheat roots, is this important for N uptake and N leaching losses? Plant Soil 322: 101-114. doi:10.1007/s11104-009-9898-z.
Toorman, A.F., P.J. Wierenga and R.G. Hills. 1992. Parameter estimation of hydraulic properties from one-step outflow data. Water Resour. Res. 28: 3021-3028. doi:10.1029/92wr01272.
Topp, G., J. Davis and A.P. Annan. 1980. Electromagnetic determination of soil water content: Measurements in coaxial transmission lines. Water Resour. Res. 16: 574-582.
Trillo, N. and R.J. Fernandez. 2005. Wheat plant hydraulic properties under prolonged experimental drought: Stronger decline in root-system conductance than in leaf area. Plant Soil 277: 277-284. doi:10.1007/s11104-005-7493-5.
Twine, T.E., W. Kustas, J. Norman, D. Cook, P. Houser, T. Meyers, et al. 2000. Correcting eddy-covariance flux underestimates over a grassland. Agric. For. Meteorol. 103: 279-300. doi:10.1016/s0168-1923(00)00123-4
Tyree, M.T., S. Patiño, J. Bennink and J. Alexander. 1995. Dynamic measurements of roots hydraulic conductance using a high-pressure flowmeter in the laboratory and field. J. Exp. Bot. 46: 83-94. doi:10.1093/jxb/46.1.83
UMS. 2011. Pressure Transducer Tensiometer T4/T4e: user manual. UMS GmbH München, München, Germany. p. 37.
Unger, P.W. and T.C. Kaspar. 1994. Soil compaction and root growth - A review. Agron J. 86: 759-766.
Upchurch, D.R. 1987. Conversion of minirhizotron-root intersections to root length density. Minirhizotron Observation Tubes: Methods and Applications for Measuring Rhizosphere Dynamics. Ed. HM Taylor 50: 143. doi:10.2134/asaspecpub50.c5
Vadez, V. 2014. Root hydraulics: The forgotten side of roots in drought adaptation. Field Crops Res. 165: 15-24. doi:10.1016/j.fcr.2014.03.017.
Valentine, T.A., P.D. Hallett, K. Binnie, M.W. Young, G.R. Squire, C. Hawes, et al. 2012. Soil strength and macropore volume limit root elongation rates in many UK agricultural soils. Ann. Bot. 110: 259-270. doi:10.1093/aob/mcs118.
Vamerali, T., M. Bandiera and G. Mosca. 2012. Minirhizotrons in modern root studies. Measuring Roots. Springer. p. 341-361.
van Dam, J.C., P. Groenendijk, R.F. Hendriks and J.G. Kroes. 2008. Advances of modeling water flow in variably saturated soils with SWAP. Vadose Zone J. 7: 640-653.
Van de Geijn, S.C., J. Vos, J. Groenwold, J. Goudriaan and P.A. Leffelaar. 1994. The Wageningen Rhizolab—a facility to study soil-root-shoot-atmosphere interactions in crops. I. Description of main functions. Plant Soil 161: 275-287.
Van den Honert, T. 1948. Water transport in plants as a catenary process. Discussions of the Faraday Society 3: 146-153. doi:10.1039/df9480300146
Van Genuchten, M.T. 1980. A closed-form equation for predicting the hydraulic conductivity of unsaturated soils. Soil Sci. Soc. Am. J. 44: 892-898.
van Noordwijk, M., G. Brouwer, F. Meijboom, M.d.R.G. Oliveira and A. Bengough. 2000. Trench profile techniques and core break methods. Root methods. Springer. p. 211-233.
Vanderborght, J., A. Graf, C. Steenpass, B. Scharnagl, N. Prolingheuer, M. Herbst, et al. 2010. Within-field variability of bare soil evaporation derived from eddy covariance measurements special section: patterns. Vadose Zone J. 9: 943-954. doi:10.2136/vzj2009.0159
Vandoorne, B., L. Beff, S. Lutts and M. Javaux. 2012. Root water uptake dynamics of cichorium intybus var. sativum under water-limited conditions. Vadose Zone J. 11. doi:10.2136/vzj2012.0005
Vansteenkiste, J., J. Van Loon, S. Garré, L. Pagès, E. Schrevens and J. Diels. 2014. Estimating the parameters of a 3-D root distribution function from root observations with the trench profile method: case study with simulated and field-observed root data. Plant Soil 375: 75-88. doi:10.1007/s11104-013-1942-3
Vepraskas, M. and G. Hoyt. 1988. Comparison of the trench-profile and core methods for evaluating root distributions in tillage studies. Agron J. 80: 166-172.

Vereecken, H., J.A. Huisman, H.J. Hendricks Franssen, N. Brüggemann, H.R. Bogena, S. Kollet, et al. 2015. Soil hydrology: Recent methodological advances, challenges, and perspectives. Water Resour. Res. 51: 2616-2633. doi:10.1002/2014wr016852

Vereecken, H., A. Schnepf, J.W. Hopmans, M. Javaux, D. Or, D.O.T. Roose, et al. 2016. Modeling soil processes: review, key Challenges, and new perspectives. Vadose Zone J. 15. doi:10.2136/vzj2015.09.0131.

Vereecken, H., M. Weynants, M. Javaux, Y. Pachepsky, M. Schaap and M.T. Genuchten. 2010. Using pedotransfer functions to estimate the van Genuchten–Mualem soil hydraulic properties: a review. Vadose Zone J. 9: 795-820. doi:10.2136/vzj2010.0045

Volkmar, K. 1993. A comparison of minirhizotron techniques for estimating root length density in soils of different bulk densities. Plant Soil 157: 239-245. doi:10.1007/bf00011052

von Hebel, C., S. Rudolph, A. Mester, J.A. Huisman, P. Kumbhar, H. Vereecken, et al. 2014. Three-dimensional imaging of subsurface structural patterns using quantitative large-scale multiconfiguration electromagnetic induction data. Water Resour. Res. 50: 2732-2748.

Vrugt, J.A., J.W. Hopmans and J. Šimunek. 2001a. Calibration of a two-dimensional root water uptake model. Soil Sci. Soc. Am. J. 65: 1027-1037. doi:10.2136/sssaj2001.6541027x

Vrugt, J.A. and C. Ter Braak. 2011. DREAM (D): an adaptive Markov Chain Monte Carlo simulation algorithm to solve discrete, noncontinuous, and combinatorial posterior parameter estimation problems. Hydrol. Earth Syst. Sci. 15. doi:10.5194/hessd-8-4025-2011

Vrugt, J.A., M.T. van Wijk, J.W. Hopmans and J. Simunek. 2001b. One-, two-, and three-dimensional root water uptake functions for transient modeling. Water Resour. Res. 37: 2457-2470. doi:10.1029/2000wr000027.

Walter, A. and U. Schurr. 2005. Dynamics of leaf and root growth: Endogenous control versus environmental impact. Ann. Bot. 95: 891-900. doi:10.1093/aob/mci103.

Wang, M., Q.S. Zheng, Q.R. Shen and S.W. Guo. 2013. The Critical Role of Potassium in Plant Stress Response. Int. J. Mol. Sci. 14: 7370-7390. doi:10.3390/ijms14047370.

Wang, P., X. Song, D. Han, Y. Zhang and X. Liu. 2010. A study of root water uptake of crops indicated by hydrogen and oxygen stable isotopes: A case in Shanxi Province, China. Agric. Water Manage. 97: 475-482. doi:10.1016/j.agwat.2009.11.008.

Water, U. 2012. Managing water under uncertainty and risk, The United Nations world water development report 4, UN Water Reports, World Water Assessment Programme. UNESCO, Paris, France.

Weaver, J.E. and J.W. Voigt. 1950. Monolith method of root-sampling in studies on succession and degeneration. Botanical Gazette: 286-299.

Wegehenkel, M. and H.H. Gerke. 2013. Comparison of real evapotranspiration measured by weighing lysimeters with simulations based on the Penman formula and a crop growth model. J. Hydrol. Hydromech. 61: 161-172. doi:10.2478/johh-2013-0021.

Weihermüller, L., J. Huisman, S. Lambot, M. Herbst and H. Vereecken. 2007. Mapping the spatial variation of soil water content at the field scale with different ground penetrating radar techniques. J. Hydrol. 340: 205-216.

Weihermuller, L., J.A. Huisman, N. Hermes, S. Pickel and H. Vereecken. 2013. A new TDR multiplexing system for reliable electrical conductivity and soil water content measurements. Vadose Zone J. 12: 11. doi:10.2136/vzj2012.0194.

Wells, C. and S. Birchfield. 2009. Rootfly: Software for minirhizotron image analysis. Clemson University, Kingstree, SC.

Wesseling, J. 1991. Meerjarige simulaties van grondwateronttrekking voor verschillende bodemprofielen, grondwatertrappen en gewassen met het model SWATRE. SC-DLO report 152.

Wesseling, J. and T. Brandyk. 1985. Introduction of the occurrence of high groundwater levels and surface water storage in computer program SWATRE. ICW.

Wesseling, J., J. Elbers, P. Kabat and B. van den Broek. 1991. SWATRE: Instructions for Input. Internal Note, Winand Staring Centre, Wageningen, The Netherlands. International Waterlogging and Salinity Research Institute, Lahore, Pakistan.
Wesselius, J.C. and R. Brouwer. 1972. Influence of water stress on photosynthesis, respiration and leaf growth of Zea mais L. Mededelingen Landbouwhogeschool Wageningen 72: 1-15.
White, C.A., R. Sylvester-Bradley and P.M. Berry. 2015. Root length densities of UK wheat and oilseed rape crops with implications for water capture and yield. J. Exp. Bot. 66: 2293-2303. doi:10.1093/jxb/erv077.
Willmott, C.J., S.G. Ackleson, R.E. Davis, J.J. Feddema, K.M. Klink, D.R. Legates, et al. 1985. Statistics for the evaluation and comparison of models. J. Geophys. Res. Oceans 90: 8995-9005. doi:10.1029/JC090iC05p08995.
Wilson, K.B., P.J. Hanson, P.J. Mulholland, D.D. Baldocchi and S.D. Wullschleger. 2001. A comparison of methods for determining forest evapotranspiration and its components: sap-flow, soil water budget, eddy covariance and catchment water balance. Agric. For. Meteorol. 106: 153-168. doi:10.1016/s0168-1923(00)00199-4
Withington, J.M., A.D. Elkin, B. Bułaj, J. Olesiński, K.N. Tracy, T.J. Bouma, et al. 2003. The impact of material used for minirhizotron tubes for root research. New Phytol. 160: 533-544.
Wöhling, T., S. Gayler, E. Priesack, J. Ingwersen, H.D. Wizemann, P. Högy, et al. 2013. Multiresponse, multiobjective calibration as a diagnostic tool to compare accuracy and structural limitations of five coupled soil-plant models and CLM3. 5. Water Resour. Res. 49: 8200-8221. doi:10.1002/2013wr014536
Wu, J., R. Zhang and S. Gui. 1999. Modeling soil water movement with water uptake by roots. Plant Soil 215: 7-17. doi:10.1023/A:1004702807951.
Yang, D., T. Zhang, K. Zhang, D.J. Greenwood, J.P. Hammond and P.J. White. 2009. An easily implemented agro-hydrological procedure with dynamic root simulation for water transfer in the crop–soil system: validation and application. J. Hydrol. 370: 177-190. doi:10.1016/j.jhydrol.2009.03.005
Yang, J., R.D. Hammer and R.W. Blanchar. 2003. Minirhizotron quantification of soybean root growth as affected by reduced - A horizon in soil. J. Plant Nutr. Soil Sci. 166: 708-711. doi:10.1002/jpln.200321193.
Yates, S.R., M.T. Vangenuchten, A.W. Warrick and F.J. Leij. 1992. Analysis of measured, predicted, and estimated hydraulic conductivity using the RETC computer program. Soil Sci. Soc. Am. J. 56: 347-354.
Young, M.H., P.J. Wierenga and C.F. Mancino. 1996. Large weighing lysimeters for water use and deep percolation studies. Soil Sci. 161: 491-501. doi:10.1097/00010694-199608000-00004.
Zacharias, S., H. Bogena, L. Samaniego, M. Mauder, R. Fuß, T. Pütz, et al. 2011. A network of terrestrial environmental observatories in Germany. Vadose Zone J. 10: 955-973.
Zarebanadkouki, M., Y.X. Kim and A. Carminati. 2013. Where do roots take up water? Neutron radiography of water flow into the roots of transpiring plants growing in soil. New Phytol. 199: 1034-1044. doi:10.1111/nph.12330.
Zarebanadkouki, M., F. Meunier, V. Couvreur, J. Cesar, M. Javaux and A. Carminati. 2016. Estimation of the hydraulic conductivities of lupine roots by inverse modelling of high-resolution measurements of root water uptake. Ann. Bot. 118: 853-864. doi:10.1093/aob/mcw154
Zegada-Lizarazu, W. and M. Iijima. 2004. Hydrogen stable isotope analysis of water acquisition ability of deep roots and hydraulic lift in sixteen food crop species. Plant Prod. Sci. 7: 427-434. doi:10.1626/pps.7.427
Zhang, X.Y., D. Pei and S.Y. Chen. 2004. Root growth and soil water utilization of winter wheat in the North China Plain. Hydrol. Processes 18: 2275-2287. doi:10.1002/hyp.5533.
Zhang, Z., F. Tian, H. Hu and P. Yang. 2014. A comparison of methods for determining field evapotranspiration: photosynthesis system, sap flow, and eddy covariance. Hydrol. Earth Syst. Sci. 18: 1053-1072. doi:10.5194/hess-18-1053-2014.

Zhao, C.X., X.P. Deng, L. Shan, E. Steudle, S.Q. Zhang and Q. Ye. 2005. Changes in root hydraulic conductivity during wheat evolution. J. Integr. Plant Biol. 47: 302-310. doi:10.1111/j.1744-7909.2005.00043.x.

Zhou, S., Y.Y. Han, Y.H. Chen, X.Z. Kong and W. Wang. 2015. The involvement of expansins in response to water stress during leaf development in wheat. J. Plant Physiol. 183: 64-74. doi:10.1016/j.jplph.2015.05.012.

Zuo, Q., L. Meng and R.D. Zhang. 2004. Simulating soil water flow with root-water-uptake applying an inverse method. Soil Sci. 169: 13-24. doi:10.1097/01.ss.0000112018.97541.85.

Band / Volume 397
Mixed-phase and ice cloud observations with NIXE-CAPS
A. Costa (2017), xviii, 117 pp
ISBN: 978-3-95806-273-3

Band / Volume 398
Deposition Mechanisms of Thermal Barrier Coatings (TBCs) Manufactured by Plasma Spray-Physical Vapor Deposition (PS-PVD)
W. He (2017), ix, 162 pp
ISBN: 978-3-95806-275-7

Band / Volume 399
Carbonyl Sulfide in the Stratosphere: airborne instrument development and satellite based data analysis
C. Kloss (2017), vi, 84, 1-14 pp
ISBN: 978-3-95806-276-4

Band / Volume 400
Lagrangian transport of trace gases in the upper troposphere and lower stratosphere (UTLS)
P. Konopka (2017), 70 pp
ISBN: 978-3-95806-279-5

Band / Volume 401
Numerical Simulation of Plasma Spray-Physical Vapor Deposition
P. Wang (2017), IX, 127 pp
ISBN: 978-3-95806-282-5

Band / Volume 402
The Selective Separation of Am(III) from Highly Radioactive PUREX Raffinate
P. Kaufholz (2017), IV, 173 pp
ISBN: 978-3-95806-284-9

Band / Volume 403
Spatio-Temporal Estimation and Validation of Remotely Sensed Vegetation and Hydrological Fluxes in the Rur Catchment, Germany
M. Ali (2018), xvi, 116 pp
ISBN: 978-3-95806-287-0

Band / Volume 404
Thermomechanical Characterization of Advanced Ceramic Membrane Materials
Y. Zou (2018), xvi, 168 pp
ISBN: 978-3-95806-288-7

Schriften des Forschungszentrums Jülich
Reihe Energie & Umwelt / Energy & Environment

Band / Volume 405
Betrachtung der Kristallinitätsentwicklung in mikrokristallinem Dünnschicht-Silizium mit in-situ Raman-Spektroskopie
T. Fink (2018), XI, 166 pp
ISBN: 978-3-95806-289-4

Band / Volume 406
Institute of Energy and Climate Research
IEK-6: Nuclear Waste Management
Report 2015 / 2016
Material Science for Nuclear Waste Management
S. Neumeier, H. Tietze-Jaensch, D. Bosbach (Eds.)
(2018), 221 pp
ISBN: 978-3-95806-293-1

Band / Volume 407
Reduction properties of a model ceria catalyst at the microscopic scale
J. Hackl (2018), VIII, 98 pp
ISBN: 978-3-95806-294-8

Band / Volume 408
Comparative Analysis of Infrastructures: Hydrogen Fueling and Electric Charging of Vehicles
M. Robinius, J. Linßen, T. Grube, M. Reuß, P. Stenzel, K. Syranidis, P. Kuckertz and D. Stolten (2018), VII, 108 pp
ISBN: 978-3-95806-295-5

Band / Volume 409
Reactions between nitrite and soil organic matter and their role in nitrogen trace gas emissions and nitrogen retention in soil
J. Wei (2018), XXII, 160 pp
ISBN: 978-3-95806-299-3

Band / Volume 410
The impact of soil water distribution on root development and root water uptake of winter wheat
G. Cai (2018), xviii, 143 pp
ISBN: 978-3-95806-303-7

Energie & Umwelt / Energy & Environment
Band / Volume 410
ISBN 978-3-95806-303-7

Mitglied der Helmholtz-Gemeinschaft

JÜLICH Forschungszentrum

Estimate of root water uptake using root dynamics

Energie & Umwelt
Energy & Environment

410

Gaochao Cai

The impact of soil water distribution on root development and root water uptake of winter wheat

Gaochao Cai

Energie & Umwelt / Energy & Environment
Band / Volume 410
ISBN 978-3-95806-303-7

JÜLICH Forschungszentrum

Mitglied der Helmholtz-Gemeinschaft

JÜLICH Forschungszentrum